Multichromophoric Perylene Bisimide Dyes

Abimbola Ololade Aleshinloye

Submitted to the
Institute of Graduate Studies and Research
in partial fulfillment of the requirements for the Degree of

Master of Science
in
Chemistry

Eastern Mediterranean University
March 2009, Gazimağusa
North Cyprus

ABSTRACT

Chromophores are responsible for the color of matter. The control of molecular interactions in multichromophores lead to functional dyes with novel properties. Furthermore, tailor-made spectroscopic properties could be achieved, which are a prerequisite for applications that require dyes with absorption and emission in a specific region of the visible spectrum. With this special interest, we targeted to synthesize a multichromophoric macromolecule containing two different chromophores – a perylene and naphthalene.

We have designed a molecular architecture of, and synthesized a novel multichromphoric macromolecule, N,N'-bis-{N-(3-[4-(3-amino-propyl)-piperazin-1-yl]-propyl)-N'-[1-dehdroabiety]- 1,4,5,8-naphthalenetetracarboxydiimidly}-3,4,9,10 perylenebis(dicarboximide)bisimides (NPM) which was carried out in three consecutive steps. Our focus was also to enlarge both the absorption and emission ranges of the macromolecule and to investigate consequent optical properties.

The first step includes the synthesis of a perylene dye, N-N'-bis-{3-[4-(3-amino-propyl)-piperazin-1-yl]-propyl}-3,4,9,10-perylenebis(dicarboximide) (PDI) where as in the second step, a naphthalene monoimide, N-(1-dehydroabietyl)-1,4,5,8-naphthalenetetracarboxylic-1,8-anhydride-4,5-imide (NMI) was synthesized. Finally, the designed macromolecule dye (NPM) was synthesized by using the above synthesized compounds, PDI and NMI. All the synthesized compounds were characterized in detail by IR, MS, NMR, UV-vis, DSC and TGA measurements.

A much enlarged absorption (325 nm – 550 nm) and emission (375 nm – 700 nm) ranges were achieved by the synthesized macromolecule dye which was appreciably soluble in most of the commercial organic solvents. All the three synthesized compounds were photochemically and thermally stable and found no glass transition temperature in the DSC runs until 300 ^{o}C. The fluorescence quantum yields of the compounds were measured and PDI was reported high quantum yield among the three synthesized compounds. Several optical parameters were also calculated and reported.

ÖZET

Madelere rengini veren gruplar kromoforlardır. Çok kromoforlu yapılarda moleküler etkileşimlerin kontrolü, yaratılan özellikler ile fonksiyonel boyalarda yeni ufuklar açmaktadır. Bununla birlikte, görünür bölge absorpsiyon ve emisyon özelliklerinin önemli olduğu uygulamalarda özel olarak tasarlanmış spektroskopik özellikler sağlanabilmektedir. Bu çalışmada perilen ve naftalin kromoforlarını içeren çok kromoforlu bir makromolekül sentezlenmiştir.

Tez kapsamında yeni bir çok kromoforlu makromolekül olan N,N'-bis-{N-(3-[4-(3-amino-propil)-piperazin-1-yl]-propil)-N'-[1-dehidroabietil]-1,4,5,8-naftalintetrakarboksidiimid}-3,4,9,10 perilenbis(dikarboksiimid)bisimid (NPM) üç basamakta sentezlenmiştir. Böylelikle sentezlenen makromolekülün absorpsiyon ve emisyon aralığı genişletilmiş ve optik özellikleri araştırılmıştır.

İlk basamakda bir perilen diimid, N,N'-bis-{3-[4-(3-amino-propil)-piperazin-1-yl]-propil}-3,4,9,10-perilenbis(dikarboksiimid) (PDI), ikinci basamakta ise bir naftalin monoimid, N-[1-dehidroabietil]-1,4,5,8-naftalintetrakarboksilik-1,8-anhidrid-4,5-imid (NMI) sentezlenmiştir. Son basamakta ise sentezlenmiş olan PDI ve NMI kullanılarak makromolekül boya (NPM) sentezlenmiştir. Sentezlenen tüm bileşikler IR, MS, NMR, UV-vis, DSC ve TGA ölçümleri ile karakterize edilmişlerdir.

Sentezlenen makromolekül, birçok organik çözücüde çözünürlüğe sahip olup geniş absorpsiyon (325 nm – 550 nm) ve emisyon (375 nm – 700 nm) aralıkları sağlanmıştır.

Sentezlenmiş olan üç bileşik de fotokimyasal ve termal kararlılığa sahip olup DSC ölçümlerinde 300 ^{o}C sıcaklığa kadar camsı geçiş sıcaklığı gözlemlenmemiştir. Bileşiklerin floresans kuantum verimleri ölçülmüş ve PDI en yüksek floresans kuantum verimine sahip bileşik olarak bulunmuştur. Diğer optik özellikler de hesaplanmıştır ve yorumlanmıştır.

ACKNOWLEDGMENTS

Now that "my fearful trip is done," it is time to weigh anchor and set sail for the ocean…

All glory and honor be to **ALMIGHTY GOD** for his faithfulness is from everlasting to everlasting.

I would like to say a 'big thank' you to my supervisor **Prof. Dr. HURİYE İCİL** for allowing me to work in her group and for giving me the opportunity and resources to work on this interesting topic. I also wish to point out her great knowledge and experience not only in organic chemistry, but also, in life general, her great ability for teaching, telling motivating stories and of great sense to give rise of someone's interest in chemistry, especially the organic aspect.

I am extremely grateful to Jagadeesh Babu Bodapati (JBB) for his understanding, patience, tolerance, assistance and some many others that can't be expressed during my research work. He is indeed the best person to work with.

I am also grateful to everyone in the research group, Süleyman Aşır, Hürmüs Refiker, Duygu Uzun, Nur Paşaoğulları Aydınlık, Devrim Özdal, Sayeh Shahmohammadi and İlke Yücekan for their assistance and friendship.

I am also grateful for the graduate research assistantship given to me by the physics department and especially Çilem Aydıntan, the secretary for her help always.

To crown it all, my grate gratitude goes to my hubby, Kayode who helped me in adding more quality to my life. Also to my "Jewels", Daniella and Chelsea, i love you both. To my mum, thanks for giving me the basics of life. My siblings, u are always in my heart. My mother-law, uncles, aunties and friends, thank you for all your prayers and support.

To

ALMIGTHY JEHOVAH

&

Dare Aleshinloye

TABLE OF CONTENTS

Page

LIST OF FIGURES

List of Schemes

ABBREVIATIONS

Å	Armstrong
cm	centimeter
^{o}C	Degree celcius
$\Delta\nu_{1/2}$	Half-width of the selected absorption
ε_{max}	Maximum extinction coefficient
E_s	Singlet state
eV	Electron volt
h	Hour
hν	Irradiation
Hz	Hertz
i	Current
J	Coupling constant
K	Kelvin
kcal	kilocalorie
k_f	Fluorescence rate constant
λ_{exc}	Excitation wavelength
λ_{max}	Absorption wavelength maximum
M^+	Molecular ion peak
µ	micro
M	Molar concentration
MHz	Mega hertz
min	minute
mmol	millimole
nm	nanometer

ns	nanosecond
δ	Chemical shift (ppm)
τ_o	Theoretical radiative lifetime
τ_f	Fluorescence lifetime
t	time
ν	wavenumber
V	Volt

A	Acceptor
A	Absorption
AU	Arbitrary Unit
c	Concentration
C	Carbon
calcd	Calculated
$CDCl_3$	Deutero-Chloroform
$CHCl_3$	Chloroform
CV	Cyclic Voltammetry
DC	Dielectric Constant
DMF	N,N'-dimethylformamide
DMSO	Dimethylsulfoxide
DSC	Differential Scanning Calorimetry
DCSPSCs	Dye-Sensitized Photovoltaic Solar Cells
DSSC	Dyesensitized Solar Cell

NMI	N-(1-dehydroabietyl)-1,4,5,8-naphthalenetetracarboxylic-1,8-anhydride-4,5-imide
NPM	N,N'-bis-{N-(3-[4-(3-amino-propyl)-piperazin-1-yl]-propyl)-N'-[1-dehdroabiety]-1,4,5,8-naphthalenetetracarboxydiimidly}-3,4,9,10-perylenebis(dicarboximide)
PDI	N-N'-bis-{3-[4-(3-amino-propyl)-piperazin-1-yl]-propyl}-3,4,9,10-perylenebis(dicarboximide)
Fig.	Figure
Figs.	Figures
FTIR	Fourier Transform Infrared Spectroscopy
LC	Liquid Chromatography
H	Hydrogen
H_3PO_4	Phosphoric acid
HRMS	High Resonance Mass Spectroscopy
IC	Integrated
IR	Infrared Spectroscopy
KBr	Potassium bromide
KOH	Potassium hydroxide
LB	Langmuir-Blodgett
MS	Mass Spectroscopy
NDA	Naphthalene 1,4,5,8-tetracarboxylic dianhydride
NMR	Nuclear Magnetic Resonance
O	Oxygen
PDA	Perylene 3,4,9,10- tetracarboxylic dianhydride
PET	Photoinduced Electron Transfer

PV	Photovoltaic
Φ_f	Fluorescence Quantum Yield
std	Standard
SWV	Square Wave Voltammetry
TGA	Thermogravimetric Analysis
TiO_2	Titanium dioxide
u	Unknown
UV-vis	Ultraviolet Visible Absorption Spectroscopy

CHAPTER 1

INTRODUCTION

Perylene is made up of a conjugated planar molecule with five fused phenyl rings leading to a very strong intermolecular π-π interactions.

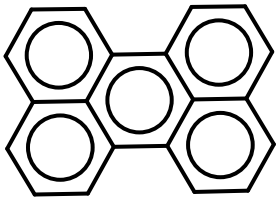

Perylene dyes, perylene-3,4,9,10-tetrecarboxylic bisimides such as figure 1.1 are known for their high chemical, thermal, photochemical stabilities and high quantum yield of fluorescence (Pasaogullari N, Icil H, et al. 2005).

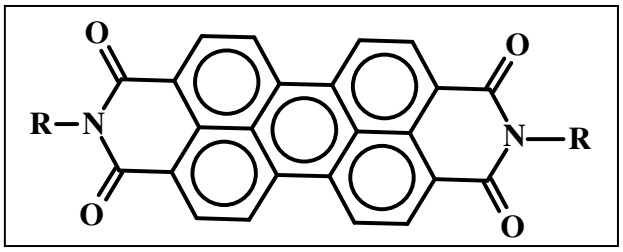

Figure 1.1 A general structure of perylene diimide

Perylene dyes were first discovered by Kardos in 1913 and have been used for various applications including textiles, general paints and plastics. Due to their poor solubility caused by the strong π-π stacking interactions, the highly fluorescence

nature of perylene bisimide was not revealed until 1959 by Geissler and Remy. Since then, varieties of different structures with improved solubility and processibility have been synthesized.

Novel researches show that perylene dyes are used as indicators of relative humidity in optical sensors (Posch H.E, Wolfbeis O. S 1998) and the rapid precipitation and quantitative of trace amount of DNA (Liu Z, Rill R. L. 1996).

Naphthalene diimides such as figure 1.2 are well known dyes due to their effectiveness in biological and medical areas as in supramolecular chemistry. The uses of these compounds in chemotherapy and as fluorescent labeling systems are new findings. On the other hand, they are used as optical brighteners, laser dyes, electrophotography, conducting materials, metallomacrocycles, intercalators for DNA and models for photosynthetic reaction center. (Ozser M.E, Uzun D. et al. 2002).

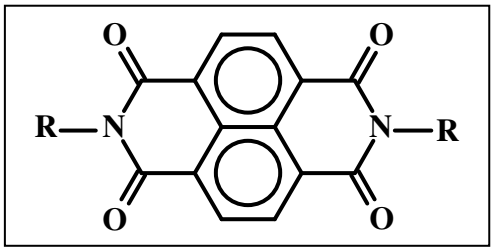

Figure 1.2 A general structure of naphthalene diimide

The control of spatial organization of functional π-systems is important for their application in molecular electronic, optoelectronics, photonics, sensor design and other areas of nanotechnology. Researchers have found that naphthalene and perylene bisimide dyes are of great interest because they combine favorable functional and structural properties. From the functional point of view, these dyes are highly promising candidates for organic field effect transistors and solar cells due

to their well known electron affinities and favorable packing properties. From the structural point of view, the imide positions are highly suited to direct organization of these dyes by hydrogen bonding or metal-ligand coordination. Furthermore, that macromolecular order is governed by means of hydrogen bonding between the imide units (Thalacker C, Miura A et al. 2005).

Since perylene and naphthalene bisimides are of great interest to tailor defined materials with improved properties, a novel macromolecule; N,N'-bis-{N-(3-[4-(3-amino-propyl)-piperazin-1-yl]-propyl)-N'-[1-dehdroabiety]-1,4,5,8-naphthalenetetracarboxydiimidly}-3,4,9,10-perylenebis(dicarboximide),(NPM) with an enlarged range of absorption has been synthesized from perylene bisimide and naphthalene monoimide dyes in order to determine its optical and thermal properties.

The structures and the properties of the synthesized compounds were proved by FT-IR, UV-vis, NMR, emission, elemental analysis, TGA, DSC and Mass spectroscopy.

CHAPTER 2

THEORETICAL

2.1 Perylene Bisimide Dyes

Perylene bisimide is a short form of perylene tetracarboxylic acid bisimide. Due to their favorable thermal stability and chemical inertness, light and weather fastness, combination of insolubility and migrational stability as well as high color intensity ranging from red to violet and even black shades, perylene bisimide(s) were found to have high grade application industrially, most especially in automobile finishes several decades ago (Würthner 2004). But nowadays, due to the improved properties such as optical, photochemical, electrochemical, thermal stabilities etc., the applications are vast in areas of organic solar cells production, photovoltaic devices, dye lasers, electrophotography and in biochemistry, medicine, photonic technology.

With all the properties mentioned above, different perylene bisimide dyes have been synthesized with optical and thermal stabilities (Icil H, Uzun D et al. 1998; lcil H, Arslan E 2001).

2.1.1 Structural Properties

Perylene bisimide is one of the most applicable n-type organic semiconductors and is an excellent candidate for creating self-organized molecular electronic materials due to its strong, well studied π-π interaction which could be used to direct self organization (Lan Ying Yang et al. 2008). Perylene bisimides exhibit flat π- systems proved by X-ray diffractions analysis of several single crystals, molecular modeling and NMR studies. It was observed from the bond length of these crystals shown in figure 2.1, that perylene bisimides can be regarded as being composed of two naphthalene half units, each of which is attached to an imide unit and connected to the other naphthalene unit by Csp^2-Csp^2 single bonds.

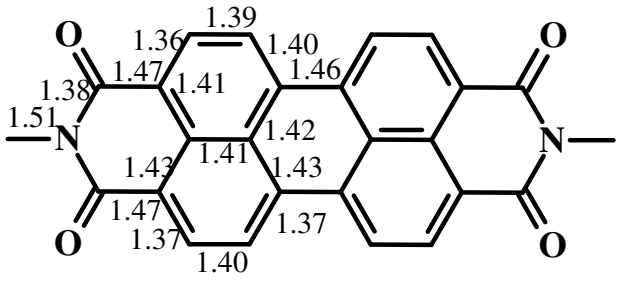

Fig.2.1 Bond length of a perylene bisimide compound in the crystal.

If the connecting bonds between the two half units are considered as single bonds, then the sterical strain in the bay-area can lead to a propeller-like twisting of the two naphthalene half units.

The distortion of the π-system has a significant impact on the intermolecular π-π-stacking energy of these compounds in the solid state as well as the molecular aggregate. The advantage of this distortion is that it can afford better soluble dyes. There is increase in solubility of very pronounced tetraphenoxy-substituents since the solubility of the substituents benefits additionally by entropic reasons as the motional

freedom of the four phenoxy arms has to be frozen upon packing in the solid state (Würthner F 2004; Würthner F 2006).

2.2 Naphthalene Dyes

Naphthalene dyes are stable aromatic molecules which have become increasingly important in the past few years, due to their use in a series of applications, ranging from the biomedical area to the science of materials. Naphthalene diimides are very useful in macromolecular chemistry and are very attractive for the information of charge transfer complexes, as enzymes mimics, organic hosts and thermal molecular sensors if assembled as cyclophanes (Ozser M.E, Uzun D et al. 2002). Chemical or electrochemical reduction of 1,4,5,8-naphthalene diimides gives rise to a stable anion radical, making them very attractive for the construction of conducting materials and for artificial photosynthesis (Rodrigues M. A, Petri D.F et al. 2000).

2.3 Macromolecules

Organic syntheses have being improved to an extent of obtaining very complex structures, combining multiple rings with heteroatoms. These kinds of structures are called **macromolecules** which are made up of atoms ranging from hundreds to thousands leading to a very high molecular mass with distinctive properties when compared with their monomers. This word is mostly used in polymer chemistry when talking about polysaccharides, proteins and nucleic acids due to their high molecular weight.

Different types of reactions as well as varieties of molecules have been used to prepare macromolecules. Self-assembly is said to be one approach to the formation of well defined macromolecular structures. In this novel research, the macromolecule comprises of one perylene bisimide and two naphthalene monoimide molecules leading to formation of a supramolecule. Supramolecular assemblies constitute a state of matter that is just in between pigment particles and dissolved dyes. A reasonable approach to obtain supramolecular perylene bisimide assemblies is the modification of these chromophores in such a way that structural growth (or self-assembly) becomes possible only in one or two dimensions, while intermolecular interaction in the third dimension leading to crystalline solid is prevented by attaching appropriate substituents in the molecules. It is considered that a moderate intermolecular interaction, meaning a balance between molecular stacking and solubility, is crucial for processing the self-assembly of perylene bisimide molecules into ordered structures. If the molecular interaction is too strong, the solubility will be insufficient for processing self-assembly from individual molecules. On the reverse, with too weak interaction the π-π stacking of perylene backbones will be hindered thus prevents the effective packing of perylene bisimide molecules (Lan Ying Yang 2008, Würthner 2004).

2.3.1 Multichromophoric Dye

Well defined **multichromophoric dyes** are receiving increasing attention due to their control over energy and electron transfer processes. The formation of these dyes can be accomplished by either covalent coupling of chromophores into a single molecule or by assembly of interacting mono-chromophoric molecules. Emil

Fischer in 1894, acknowledge the relevance of selective interactions between molecules when he introduced the “lock and key” principle. Nature demonstrates, for example with the photosynthesis reaction center and the flower pigments, how special properties can be obtained by such interactions. In today’s chemistry, there is increase in complexity of molecules giving rise to the formation of supramolecules and multi-molecular assemblies. These are held together by relatively weak non-covalent interactions like hydrogen-bonds, van der Waals interactions, electrostatic interactions, metal ion coordination and donor-acceptor interactions or π-stacking. The combined strength of these relatively weak intermolecular interactions, possessing different degrees of strength, directionality and dependence on distance and angles, determines the final architecture of the assembly (Langhals H 2005).

2.3.2 Photonic Application

Photonics is the science and technology of generation, manipulation and detection of photons. Photonics is an analogue of electronics, it describes the technology in which photons (instead of electrons) are used to acquire, store, transmit and process information. Lasing, waveguiding emission, ability to alter the frequency or color of light and ability to amplify switch or alter transmission characteristics through a medium of one source of light with another are some potentially useful of linear and nonlinear optical processes which provide key function for photonics (Ruland G. E 1997). In the last few years, rationally designed dye assemblies proved to be successful in the fields of organic electronic and photonics where dye-dye interactions in the bulk state and at interfaces are of crucial

importance for the desired functionalities of charge and energy transport (Würthner F).

There are several important applications of photonics. One of them is sensor protection; the use of light-intensity dependent transmission properties of materials can protect human eyes or optoelectronic sensors from unwanted or stray sources of laser radiation. Second area involves frequency shifting to generate multiwavelength laser sources and modulators for remote communication and sensing. The possibility of multiwavelength usage minimizes the threat of countermeasure (interference) against a single wave length. The third area is optical telecommunication which is another technology that involves photonics. Lastly, optical processing and optical data storage of information is also of great importance to technology where high speed modulators and demodulators are needed. These methods will allow parallel processing with enhanced speed (Burzynski R, Prasad P.N 1994).

2.4 Solar cells

Typical solar cells (photovoltaic cells) are a special class of semiconductors that convert sunlight into electricity without any pollution. The solar cells on calculators and satellites are photovoltaic cells or modules (modules are simply a group of cells electrically connected and packaged in one frame). Photovoltaic is a combination of two words (photo = light, voltaic = electricity), convert sunlight into electricity. Once used almost exclusively in space, photovoltaics are used more in less exotic ways.

Solar cells as shown in figure 2.2 or photovoltaic (**PV**) cells are made of special materials called semiconductors such as silicon, which is currently the most commonly used.

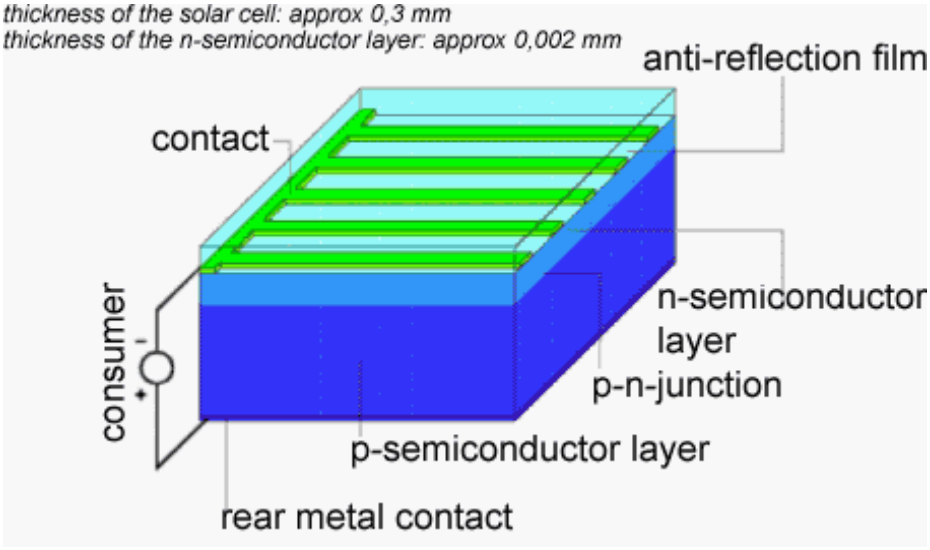

Fig.2.2 Model of a crystalline solar cell

Basically, when light strikes the cells, a certain portion of it is absorbed within the semiconductor material. This means that the energy of the absorbed light is transferred to the semiconductor. The energy knocks electrons loose, allowing them to flow freely. **PV** cells also have one or more electric fields that act to force electrons freed by light absorption to flow in a certain direction. This flow of electrons is a current and by placing metal contacts on the top and bottom of the **PV** cell, we can draw that current off to use externally. For example, the current can power a calculator. This current, together with the cell's voltage (which is a result of its built-in electric field or fields) defines the power (voltage) that the solar cell can produce.

When light, in the form of photons, hits solar cell, its energy frees electron-hole pairs. Each photon with enough energy will normally free exactly one electron

and result in a free hole as well. If this occur close enough to the electric field, or if free electron and free hole happen to wander into its range of influence, the field will send the electron to the N side and the hole to the P side, this causes further disruption of electrical neutrality and if we provide an external current path, electrons will flow through the path to their original side (P side) to unite with holes that the electric field sent there, doing work along the way. The electron flow provides the current and the cell's electric field causes a voltage. With both current and voltage, there is power, which is the product of the two.

However, owing to the high production cost of silicon-based semiconductors, there has been an increasing demand for affordable **PV** cells. This has led to much attention being focused on polymer solar cells, which use much cheaper polymeric materials in comparison to silicon-based semiconductors.

2.4.1 Dye Synthesized Photonic Solar Cells (DSPV)

In an entirely different historical background, photography, using dyes with silver halide grains was discovered in 1873 by Vogel. Since then, many scientists have been attracted towards photoelectric molecules. The first observation of injecting electrons by a dye molecule into the conduction band of the semiconductor substrate was reported in 1960s'. From then on, the concept of dye sensitization developed gradually. Highly efficient sensitization of titanium dioxide (TiO_2) by a Ruthenium dye was first published in 1985, which led to the development of a new concept of generating electricity from sunlight. This approach has many advantages over silicon solar cell technology. The **DSPV** cells are much cheaper to manufacture compared to crystalline solar cells. They can be made in transparent modules to

integrate into windows and sunroofs. They maintain their performance even in shaded conditions and higher temperatures unlike silicon solar cells. Through various other wide band gap semiconductors such as SnO_2, ZnO, Nb_2O_5, WO_3, $SrTiO_3$ etc. were studied, TiO_2 based **DSPSC**s are more used as it has many advantages including long term thermal and photo-stability. It is cheap, abundant, non-toxic, biocompatible and widely used in health care products. In 1988, Michael Gratzel and others discovered that TiO_2 is the best suited semiconductors for chemisorbing the dyes for efficient light harvesting and energy conservation. In recent times, organic dye sensitized TiO_2 solar cells have made great progress and highest overall yield of solar cells sensitized by pure organic dyes has exceeded 6.3% (New J. Chem. 2003).

2.5 Photochemistry of Dyes

Photochemistry is the part of chemistry that study reaction taking place under the influence light. All photochemical processes depend on light which is a small part of the electromagnetic spectrum ranging from 400-700 nm. But for some reasons, this range is brought down to 290 nm in the ultraviolet region and up to 850 nm in the near infrared.

Light, which is a form of electromagnetic radiation propagates through space in wave form, obeying the relationship $c = \lambda\nu$; (c = velocity of light, i.e, 2.9979 x 10^8 m $sec^{-}1$, ν = frequency; and λ = wavelength). Matter absorbs or emits radiation in discrete quanta (photons), however, whose energy $E = hc / \lambda$ (h = plank's constant). (JK Sugden 2004). The basic principle of photochemistry is that, upon absorption of a photon of suitable energy, an excited state is formed.

$$\mathbf{E} + \lambda\nu \rightarrow \mathbf{E}^{*} \qquad \textbf{(2.1)}$$

The electronic distribution of ground and excited states differ from each other which leads to their differences both in chemical and physical properties (i.e. bond distances, bond angels, geometry, magnetic properties, redox potentials, acid-base properties etc)(Pasaogullari N 2005). Reactions that are unfavorable thermodynamically when the reactants are in ground state i.e. $E_o \rightarrow \mathbf{F}$ may occur when the reactants are in the excited state i.e. $E^{*} \rightarrow \mathbf{F}$. In particular, an excited specie can give rise to high energy products such as radicals, biradicals or strained ring compounds, which are not readily formed from the ground state.

2.5.1 Photochemical Reactions

Photochemical reactions are any chemical reactions in which light is produced or light initiates the reaction. Light can initiate reactions by exciting atoms of molecules and making them more reactive and colon; the light energy becomes converted to chemical energy. Many photochemical reactions set up a chain reaction and produce free radicals.

In photochemical reactions, thermal equilibrium between excited state, intermediate(s) and product(s) is rarely achieved, because of the magnitude of some of the energy changes involved and because of the high rate constants for many of the individual steps.

For a photochemical reaction to be readily observable, the rate constant for the initial photochemical step involving the excited state must be high (typically 10^6 - 10^9 s^{-1}). This is because the excited state is short-lived, decaying to the ground state

very rapidly and efficient photochemical reaction must complete successfully with these very rapid photophysical processes.

2.5.2 Excited State of Molecules

Excited electronic states usually occur by the absorption of radiation of correct frequency are almost always singlet states. This is due to the fact that all molecules in organic chemistry have a singlet ground state and the selection rules for the absorption strongly favor conservation of spin during the absorption process.

The electronic excited state contains two unpaired electron in the different orbitals and these can be of the same (parallel) spin or of different (opposed) spin. Such states are triplet and singlet state respectively and the two are distinct species, with different physical and chemical properties. A triplet state has a lower energy than the corresponding singlet state.

The magnitude of the difference in the energy varies according to the degree of overlap between the orbital involved.

There are several processes by which an excited state molecule can return back to its ground state. The singlet and triplet states are ranged in order of increasing energy and numbered in the same order as S_o, S_1, S_2, S_n……. and T_1, T_2……respectively. A diagram known as Jablonski diagram is commonly used to describe these processes (Fig.2.3).

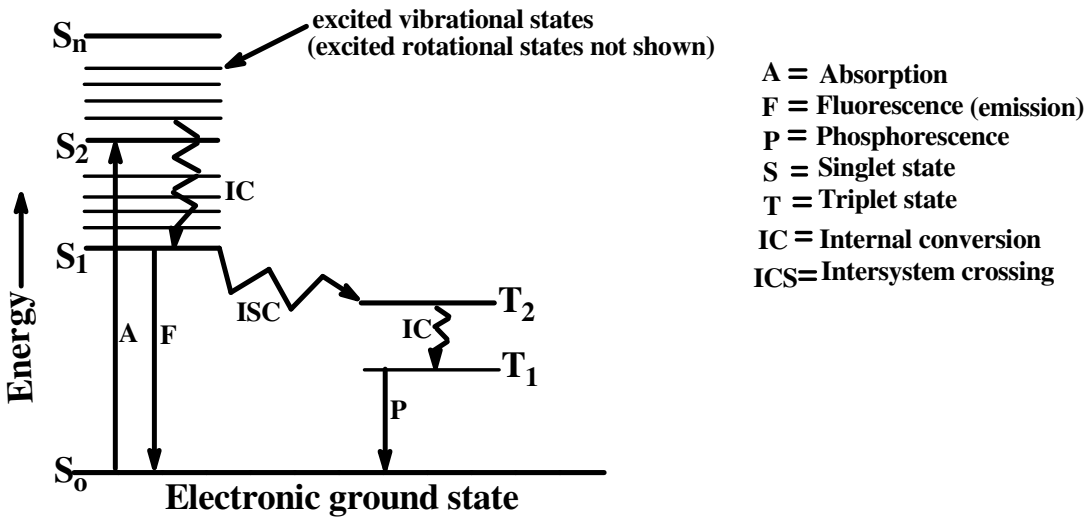

Fig. 2.3 Jablonski Diagram.

In Jablonski diagram above, states represented by horizontal lines are grouped into vertical columns according to their multiplicity. The individual processes are indicated by arrows **(radiative processes = straight arrows, non-radiative processes = wavy arrows)**. The energy difference between the ground state (S_o), singlet (S_1, S_2), and triplet (T_1, T_2) states is progressively lower at higher vibronic states.

The term **fluorescence** is a spontaneous spin-allowed emission of radiation with lifetime ~ 10^{-8}s within vibronic states of the same multiplicity; usually form the thermally relaxed S_1 to S_o states. **Phosphorescence** is the spin forbidden emission of the radiation between vibronic states of different multiplicity, generally from T_1 to S_0 states. The vibrational structure of a phosphorescence spectrum is a mirror image of the phosphorescence excitation spectrum (S_0 to T_1). Since the T_1 state always lies below the S_1 state, this band occurs at longer wavelengths than that of fluorescence. The lifetime is relatively long ~10^{-4}s.

There are two non-radiative deactivation processes shown in the diagram namely; **Internal conversion (IC)** which is the radiationless transition between

energy states of the same spin and **Intersystem crossing (ISC)** is a radiationless transition between different spin states.

2.5.3 Photoinduced Electron Transfer (PET)

This is a branch of photochemistry that exploits the ability of certain photoexcited molecules to act as strong oxidizing or reducing species and induce a permanent chemical change in a ground state molecule through an electron transfer mechanism. After being oxidized or reduced by a photosensitizer, an organic substrate is transformed into a reactive intermediate that is capable of undergoing a variety of reactions. As shown in Figure 2.4, an example of a ground state redox reaction where electron transfer occurs between a donor and an acceptor molecule. In the ground state the free energy change for the electron transfer process is the difference in the redox potentials of the donor and acceptor. Because of the large HOMO-LUMO gap in the ground state of organic molecules, electrons transfer would be a large endothermic process.

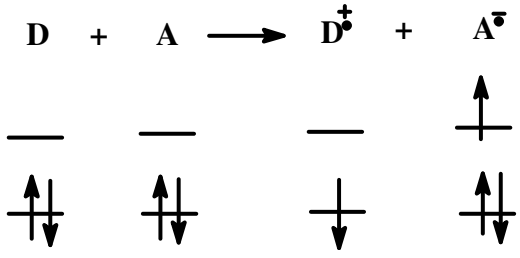

Fig. 2.4 Ground state redox reactions.

In addition to a donor (D) and an acceptor (A), PET reactions require an electronic excitation source (light). In PET, the electronically excited species serves

as the oxidizing or reducing species, as shown in Figure 2.5. Here, the free energy change associated with electron transfer, which includes the redox potentials of the donor and acceptor, is made more negative by an addition term corresponding to the excitation energy. Electronic excitation exploits the large HOMO (Highest Occupied Molecular Orbital)-LUMO (Lowest Unoccupied Molecular Orbital) gap, making electron transfer energetically more favorable process.

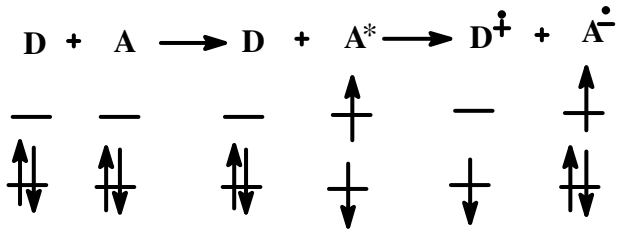

Fig. 2.5 Photoinitiated electron transfer.

The Rehm-Weller equation provides a useful expression for calculating the free energy change associated with PET reactions. For most PET reactions the number of electrons transferred, represented by *n*, is usually one and the charge associated with the transfer of one mole of electron, the unit of Faraday, is represented by *F*. For most electron transfer processes this quantity, *nF*, is approximately equal tone and can be disregarded in the calculations. The oxidation potential of the donor (OP_D),the reduction potential of the acceptor (OP_R) and the equilibrium excitation energy (ΔG_{00}), based on the wavelength of excitation, factor into the thermodynamic condition for spontaneous electron transfer. The work term $w_{p,}$ describes the coulombic attraction between ions generated by electron transfer. Below is the Rehm- Weller equation (Aubele 2004).

$$\Delta G_{ET} = nF[OP_D - OP_R - \Delta G_{00} - w_P] \qquad (2.2)$$

2.5.4 Energy Transfer

The simultaneous emission of an excited molecule, donor and the absorption to an excited state by an acceptor molecule is simply known as energy transfer or resonant energy transfer (RET).

Resonant energy transfer (RET) by dipolar coupling is regarded as occurring via two distinct mechanisms. One called radiative mechanism or "trivial" because of its simplicity, in which a photon is emitted by the donor molecule and is subsequently absorbed by an acceptor molecule.

$$\mathbf{D^* \longrightarrow D + h\nu} \qquad \textbf{(2.3)}$$

$$\mathbf{A + h\nu \longrightarrow A^*} \qquad \textbf{(2.4)}$$

The other mechanism is radiationless coulombic intermolecular interaction. While both the radiation and radiationless mechanisms require an overlap between emission spectrum of donor and absorption spectrum of acceptor, distinctions are usually drawn between other mechanistic features. The rate constant of energy is given by the Forster equation **(equation 2.5).**

$$\kappa_{ENT} = \frac{0.529\kappa^2\phi_D}{n^4 \mathrm{N}\tau_D \Re^6} J \qquad \textbf{(2.5)}$$

where ***k*** is the orientational factor, $\mathbf{\Phi_D}$ is the quantum yield of the fluorescence of the donor, ***n*** is the dielectric constant of the medium, ***N*** is the Avogadro's number, $\mathbf{\tau_D}$ is the excited state of the life time of the donor in the absence of energy transfer, ***R*** is the distance between chromophores and ***J*** is the overlap integral.

The electronic interaction between two molecule species can be approximated as the sum of two terms, coulombic and exchange. The two terms have different dependencies on various parameters and each can become predominant depending on the specific systems and experimental situation. The rate and efficiency of any actual system depend on the donor-acceptor pair with regard to the transfer energetic, the spin charactactistics of the overall transfer, the distance of the separation and the occurrence of molecule diffusion and/or energy migration.

The coulombic "resonance or Forster-type" mechanism is considered a long-range mechanism that occurs "through space", i.e. does not require physical contact between donor and acceptor. The most important term within the coulombic interaction is the dipole-dipole transition of the two partners. That is to say, the basic mechanism involves the induction of a dipole oscillation in A by D^*. So, coulombic energy transfer is expected to be efficient in systems in which the radiative transitions connecting ground and excited states of each molecule to have high oscillator strength. A typical example of an efficient coulombic mechanism is the singlet-singlet energy transfer between large aromatic molecules.

The exchange "Dexter-type" mechanism is considered a short-range mechanism that requires finite orbital overlap between donor and acceptor, hence physical contact. The exchange interaction can be visualized as simultaneous exchange of two electrons between donor and acceptor via LUMOs and HOMOs. The orbital for the two mechanisms are schematically represented below in Fig. 2.6

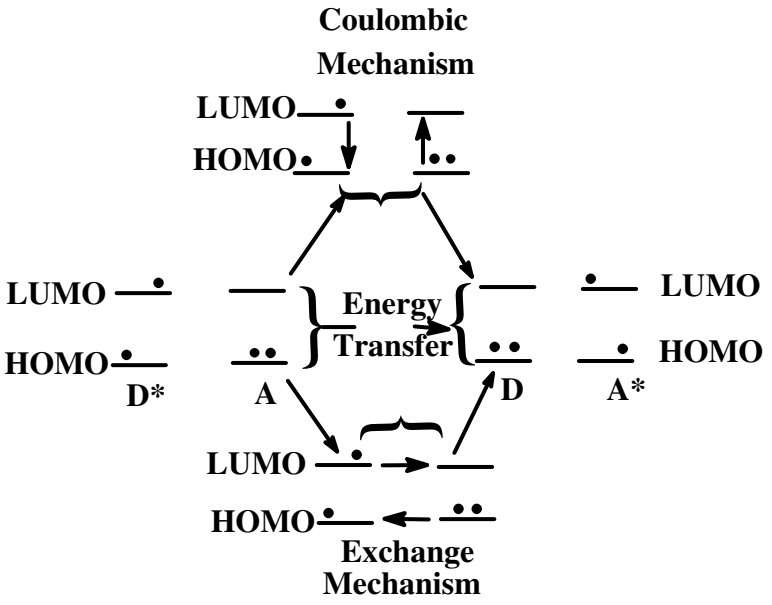

Fig.2.6 Coulombic Mechanism

The spin selection rules for the exchange mechanism arise from the need to obey spin conservation in the reacting pair as a whole. This allows the mechanism to be operative in many cases in which the excited states involved as spin-forbidden in the usual spectroscopic sense. Energy transfer by an exchange can happen in one or several steps – concerted exchange, charge transfer exchange and chemical or covalent bonding exchange of electrons. So, the typical example of an efficient exchange mechanism in organic photochemistry is triplet- triplet energy transfer, a process used for photosensitization of triplet reactions or for selective quenching of triplets (Prevost 2001, Straight 2007).

2.6 Optical and Electronic Functionalities

2.6.1 Optical Properties

The optical properties of perylene bisimide dyes are usually investigated by UV-vis and fluorescence spectroscopy. Quite a number of these dyes have been synthesized for their application as standard for fluorescent spectrometers, in fluorescent light collectors or as laser dyes since the intense yellow-green photoluminescence of the main structure of perylene bisimide has been discovered. It has been proved by various researchers that such applications are advantageous that the imide substituents has a negligible influence on the absorption emission properties of perylene bisimides which can be explained on the basis of quantum-chemical calculations because of the nodes or very low atomic coefficients of the HOMO and LUMO orbitals at the N-atoms. Therefore, perylene bisimides can be regarded as a closed chromophoric system with an S_0-S_1 (polarized along the extended molecular axis) whose intensity and position remain unaltered by the respective imide substituents. More so, the color characteristics of these dyes are rarely dependent upon the environment i.e. little solvatochromism is observed for these dyes. Accordingly, imide substituents are well placed to tailor application-directed properties like solubility and to prevent aggregation that has pronounced influence on the optical spectra (Langhals 2005, Würthner 2004).

2.6.2 Electrochemistry

Electrochemistry is concerned with transfer of electrons between species which brings about oxidation-reduction (redox) reaction. Loss of electrons by specie is referred as oxidation and gain of electrons is referred to as reduction. There is

release of chemical energy by spontaneous redox reaction, for instance in electrochemical cell like battery (voltaic cell). The non-spontaneous redox reaction can be found in an electrolytic cell using external electric energy. The oxidation reaction occurs at the anode, the reduction reaction occurs at the cathode and the energy transfer reactions occur at the electrode.

2.6.3 Cyclic Voltammetry

Cyclic Voltammetry (CV) is a very useful electrochemical measurement due to its simplicity and qualitative information. It is rarely used for quantitative determinations, but it is widely used for the study of redox processes, for understanding reaction intermediates and for obtaining stability of reaction products.

CV consists of scanning linearly the potential of a stationary working electrode, using a triangular potential waveform as shown in figure 2.7. Depending on the information sought, single or multiple cycles can be used. During the potential sweep, the potentiostat measures the current resulting from the applied potential. The current versus potential is termed a cyclic voltammogram. The cyclic Voltammetry is a complicated, time-dependent function of a large number of physical and chemical parameters.

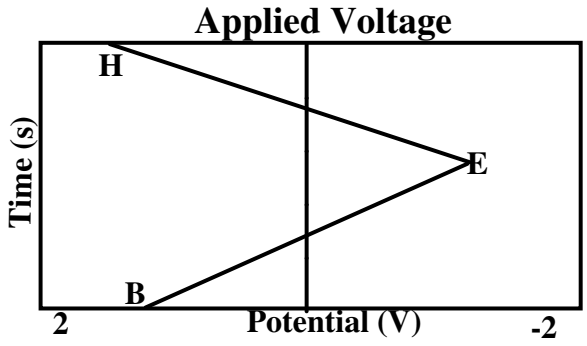

Fig.2.7 Triangle potential waveform.

The figure below illustrates the expected response of a reversible redox couple during a single potential cycle. Here it is assumed that only the oxidized form **O** is present initially. Thus, a negative-going potential scan is chosen for the first half cycle, starting from a value where no reduction occurs. As the applied potential approaches the characteristic E^o for the redox process, a cathodic current begin to increase, until a peak is reached. After traversing the potential region in which the reduction process takes place, the direction of the potential sweep is reversed.

$$\mathbf{O} + e^- \longrightarrow \mathbf{R} \qquad \textbf{(2.6)}$$

During the reverse scan, R molecules (generated the forward cycle and accumulated near the surface) are reoxidized back to **O** and an anodic peak results.

$$\mathbf{R} \longrightarrow \mathbf{O} + e^- \qquad \textbf{(2.7)}$$

The characteristic peak in the cyclic voltammogram is caused by the formation of the diffusion layer near the electrode surface. These can be best understood by carefully examining the concentration profile during the potential sweep. For example, the figure below demonstrate four concentration gradients for reactants and products during different times corresponding to (B) the initial potential value, (D) and (G) to the formal potential of the couple (during the forward and the reverse scan respectively) and (C) to the achievement of a zero reactant surface concentration. Note the continuous change in the surface concentration is coupled with an expansion of the diffusion layer thickness (as expected in quiescent solutions). The resulting current peaks thus reflect the continuous change of the

concentration gradient with the time. Hence, the increase to the peak current corresponds to the achievement of diffusion control, while the current drop (beyond the peak) exhibits a $t^{-1/2}$ dependence (independent of the applied potential). For the above reasons, the reversal current has the same shape as the forward one. The use of ultramicroelectrodes for which the mass transport process is dominated by radical (rather than linear) diffusion results in a sigmoidal-shape cyclic voltammogram.

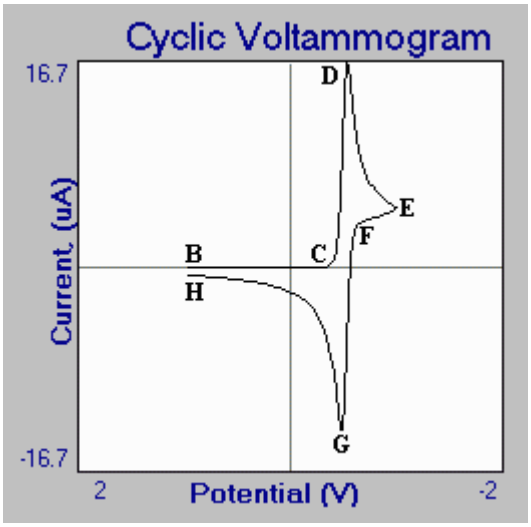

Fig.2.8 An example of cyclic voltammogram

The cyclic voltammogram in fig.2.8 is characterized by several important parameters. Four of these observables, the two peak currents and two peak potentials, provide the basis for the diagnostics developed by Nicholson and Shain, 1964 for analyzing the cyclic voltammetric response. The peak current for a reversible couple (at 25°C), is given by the Randles-Sevcik equation:

$$i_p = (2.69 \times 10^5)\, n^{3/2} A C D^{1/2} v^{1/2} \qquad \textbf{(2.8)}$$

where n is the number of electrons, A the electrode area (in cm^2),C the concentration (in mol/cm^3), D the diffusion coefficient (in cm^2/s), and v the scan rate (in V/s).

Accordingly, the current is directly proportional to concentration and increases with the square root of the scan rate. The ratio of the reverse-to-forward peak current, $\boldsymbol{i_p/i_{pf}}$, is unity for a simple reversible couple. This peak ratio can be strongly affected by chemical reactions coupled to the redox process. The current peaks are commonly measured by extrapolating the preceding baseline current. The position of the peaks on the potential axis (E_p) is related to the formal potential of the redox process. The formal potential for a reversible couple is centered between E_{pa} and E_{pc}

$$E^\circ = (E_{pa} + E_{pc})/2 \qquad \textbf{(2.9)}$$

The separation between the peak potentials (for a reversible couple) is given by:

$$\Delta E_p = E_{pa} - E_{pc} = 59\text{mV}/n \qquad \textbf{(2.10)}$$

Thus, the peak separation can be used to determine the number of electrons transferred, and as a criterion for a Nernstian behavior. Accordingly, a fast one-electron process exhibits a ΔE_p of about 59 mV. Both the cathodic and anodic peak potentials are independent of the scan rate. It is possible to relate the half-peak potential ($E_{p/2}$, where the current is half of the peak current) to the polarographic half-wave potential, $E_{1/2}$

$$E_{p/2} = E_{1/2} \pm 29\text{mV}/n \qquad \textbf{(2.11)}$$

(The sign is positive for a reduction process.) For multielectron-transfer (reversible) processes, the cyclic voltammogram consists of several distinct peaks, if the E^o values for the individual steps are successively higher and are well separated. An example of such mechanism is the six-step reduction of the fullerenes C_{60} and C_{70} to yield the hexaanion products C_{60}^{6-} and C_{70}^{6-} where six successive reduction peaks

can be observed. The situation is very different when the redox reaction is slow or coupled with a chemical reaction. Indeed, it is these "nonideal" processes that are usually of greatest chemical interest and for which the diagnostic power of cyclic voltammetry is most useful. Such information is usually obtained by comparing the experimental voltammograms with those derived from theoretical (simulated) ones.

2.6.4 Square Wave Voltammetry (SWV)

The excitation signal in **SWV** consists of a symmetrical square-wave pulse of amplitude Esw superimposed on a staircase waveform of step height ΔE, where the forward pulse of the square wave coincides with the staircase step. The net current, ***i***net, is obtained by taking the difference between the forward and reverse currents (***i***for – ***i***rev) and is centered on the redox potential. The peak height is directly proportional to the concentration of the electroactive species and direct detection limits as low as 10^{-8} M is possible.

Square-wave voltammetry has several advantages. Among these are its excellent sensitivity and the rejection of background currents. Another is the speed (for example, its ability to scan the voltage range over one drop during polarography with the DME). This speed, coupled with computer control and signal averaging, allows for experiments to be performed repetitively and increases the signalto-noise ratio. Applications of square-wave voltammetry include the study of electrode kinetics with regard to preceding, following, or catalytic homogeneous chemical reactions, determination of some species at trace levels, and its use with

electrochemical detection in HPLC. Figure 2.9 shows an example of a square waveform.

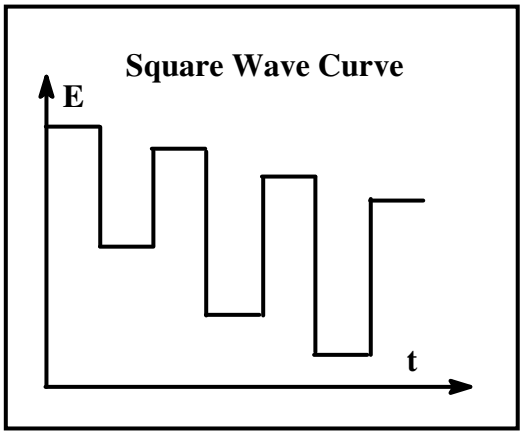

Fig.2.9 An example of Square wave form.

CHAPTER 3

EXPERIMENTAL

3.1 Materials

There was no further purification for all the chemicals used; some solvents were distilled according to the standard literature procedures (Armarego and Perrin, 1990). For spectroscopic analyses, pure spectroscopic grade solvents were used directly.

Reagents: Perylene-3,4,9,10-tetracarboxylic dianhydride, 1,4,5,8-naphthalenetetracarboxylic dianhydride, 1,4-bis(3-aminopropyl)piperazine, dehydroabietyl amine, zinc acetate, acetic acid, potassium hydroxide, phosphoric acid were obtained from Sigma Aldrich.

Solvents: Acetone, acetonitrile, chloroform, water**,** ethanol, isoquinoline, m-cresol were obtained from Sigma Aldrich.

3.2 Instruments:

Infrared Spectra

IR spectra were recorded with KBr pellets using a Mattson FT-IR spectrophotometer. IR analyses for the compounds produced gave consistent results for structural characteristics.

Elemental Analyses

Elemental analyses were performed on a Carlo Erba-1106 C, H and N analyzer.

Ultraviolet Absorption Spectra (UV)

UV absorption spectra of solutions were measured with a Varian Cary – 100 spectrophotometer and spectra of solid state were obtained in thin films using a Perkin – Elmer UV/VIS/NIR Lambda 19 spectrophotometer, equipped with solid state accessories.

Emission Spectra

Emission spectra and fluorescence quantum yield for the synthesized compounds were studied using Varian Cary Eclipse Spectrophotometer and measured at excitation, λ_{exc} = 360 nm & 485 nm.

Nuclear Magnetic Resonance Spectra (NMR)

^{1}H and ^{13}C NMR spectra were measured with a Bruker DPX-400 spectrometer operating at 400 and 100.6 MHz, respectively, in $CDCl_3$ with TMS as internal standard.

Mass Spectra

Mass spectra were measured on an Agilent 7500_A ICP-M instrument at Fragmentor 70 eV negative polarity. Data were presented in *m/z* values.

Differential Scanning Calorimetry (DSC)

Thermal analyses were measured using a Perkin Elmer, DSC Model, Jade DSC instrument. The samples were heated at 10 ^oC min^{-1} temperature increment in nitrogen atmosphere.

Thermogravimetric Analyses (TGA)

Thermogravimetic thermograms were obtained from a Perkin Elmer, TGA, Model, Pyris 1. The samples were heated at 10 ^oC min^{-1} in Oxygen.

.

3.3 Methods of Syntheses

This segment explained the synthesis of perylene diimide, synthesis of naphthalene monoimide and synthesis of the macromolecule.

The perylene diimide (PDI) was successfully synthesized via condensation of 1,4-Bis(3-aminopropyl)piperazine with perylene-3,4,9,10-tetrecarboxylic dianhydride (PDA) using m-cresol / isoquinoline mixture as solvent as shown below (Scheme 3.1). (Icil H., Arslan E. 2001).

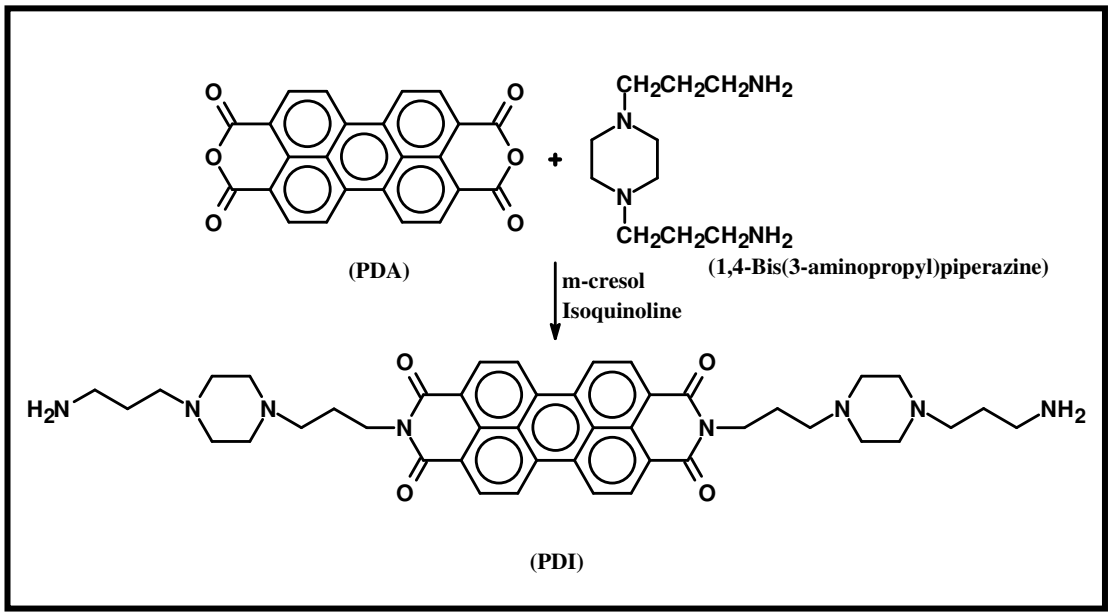

Scheme 3.1 Synthesis of N-N'-bis-{3-[4-(3-amino-propyl)-piperazin-1-yl]-propyl}-3,4,9,10-perylenebis(dicarboximide), PDI.

Another synthesis of naphthalene monoimide (NMI) was done using dehydroabietylamine with 1,4,5,8-naphthalenetetracaboxylic dianhydride (NDA) and water / KOH, H_3PO_4 as solvent (Scheme 3.2) (Pasaogullari N, Icil H et al. 2005).

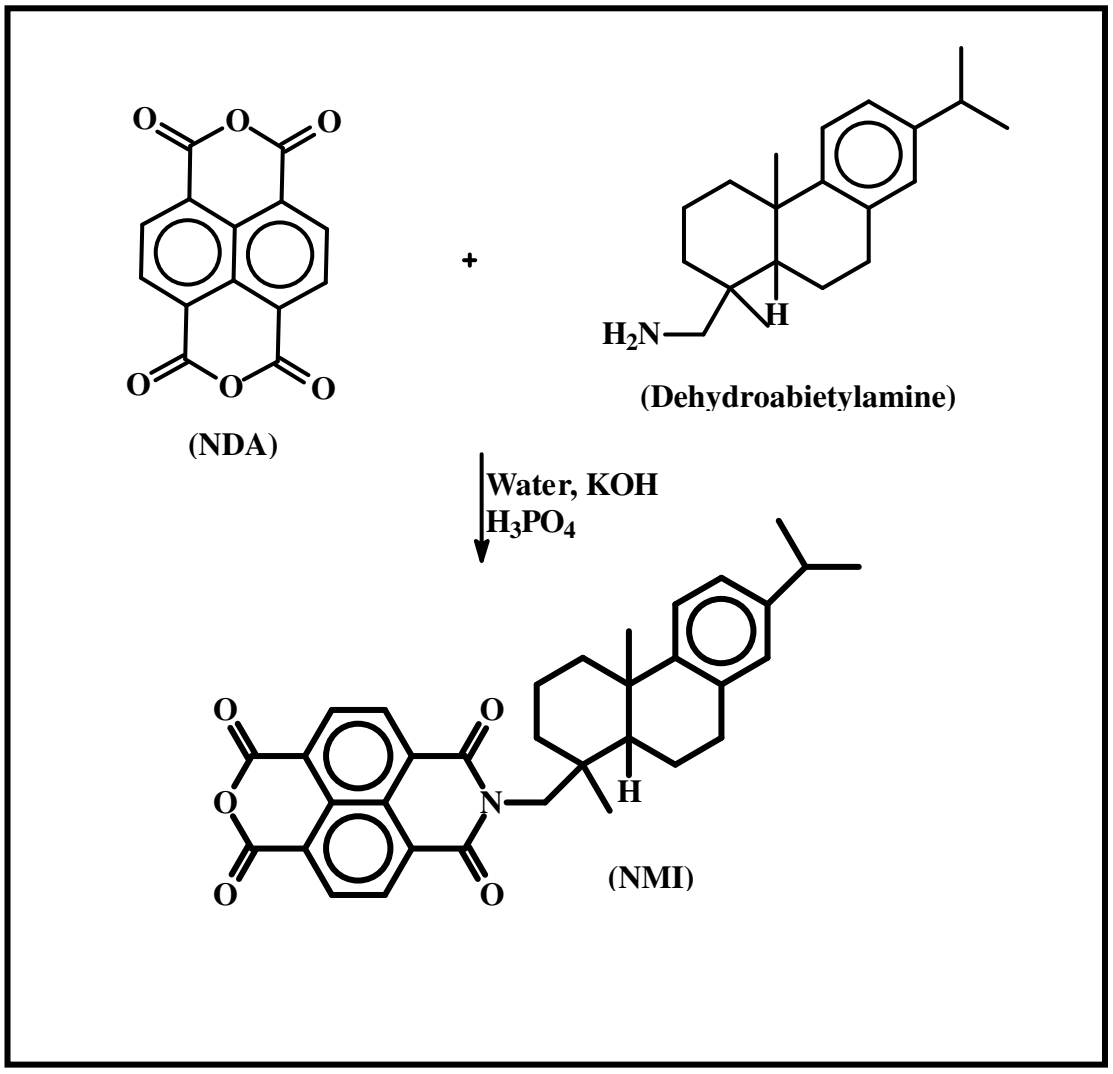

Scheme 3.2 Synthesis of N-(1-dehydroabietyl)-1,4,5,8-naphthalenetetracarboxylic-1,8-anhydride-4,5-imide, NMI.

Finally, a novel macromolecule (NPM) was synthesized from the perylene diimide and the naphthalene monoimide (Scheme 3.3) (Icil H, Arslan E. 2001).

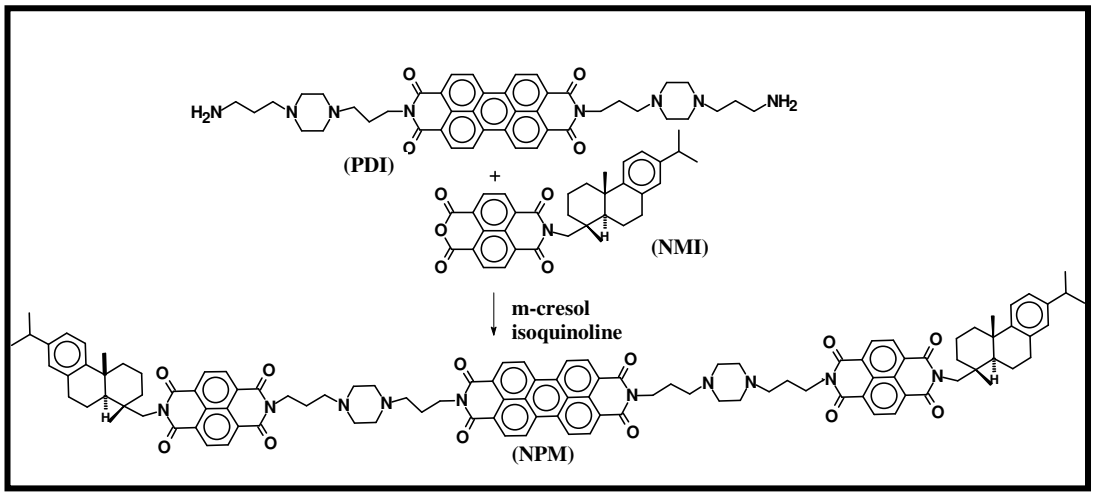

Scheme 3.3. Synthesis of N,N'-bis-{N-(3-[4-(3-amino-propyl)-piperazin-1-yl]-propyl)-N'-[1-dehdroabiety]-1,4,5,8-naphthalenetetracarboxydiimidly}-3,4,9,10-perylenebis(dicarboximide), (NPM).

3.4 Synthesis of N-N'-bis-{3-[4-(3-amino-propyl)-piperazin-1-yl]-propyl}-3,4,9,10-perylenebis(dicarboximide), PDI.

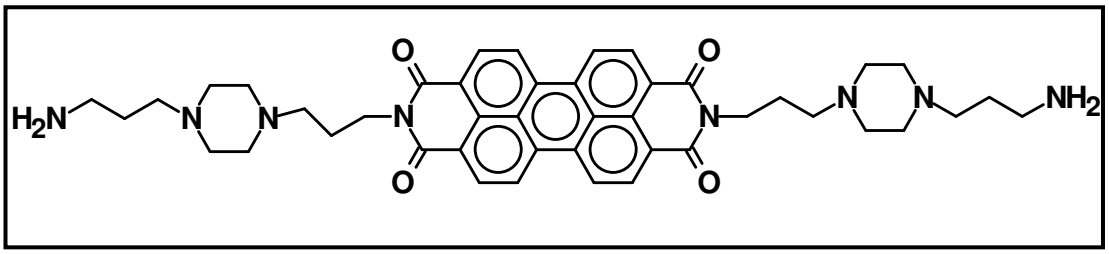

Perylene-3,4,9,10-tetracarboxylic dianhydride (1.00 g, 2.55 mmol), 1,4-bis(3-aminopropyl (2.10 g, 10.20 mmol) and $Zn(OAc)_2.2H_2O$ (0.55 g, 2.50 mmol) were heated in a carefully dried solvent mixture (60 mL m-cresol and 8 mL isoquinoline) under argon atmosphere at 80 ^oC for 4 h, 100 ^oC for 4 h, 120 ^oC for 4 h, 142 ^oC for 20 h and finally at 200 ^oC for 1 h. The solution was allowed to cool and then was poured into 300 mL acetone. The precipitate was filtered off and dried at 100 ^oC under vacuum. The product was treated with methanol in a Soxhlet apparatus for 1 day in order to remove the unreacted amine, the catalyst zinc acetate and high boiling solvents.

Yield: 1.68 g (88%), Color: Dark brown

IR (KBr, cm^{-1}): ν = 3441, 3083 2928, 2827, 2357, 1902, 1694, 1639, 1576, 1426, 1351, 1251, 1163, 976, 850, 813, 750, 640.

UV-vis ($CHCl_3$) (λ_{max} / nm) : 461, 490, 527.

Fluorescence ($CHCl_3$) (λ_{max} / nm): 534, 575, 626, Φ_f = 0.82

3.5 Synthesis of N-(1-dehydroabietyl)-1,4,5,8-naphthalenetetracarboxylic-1,8-anhydride-4,5-imide, NMI.

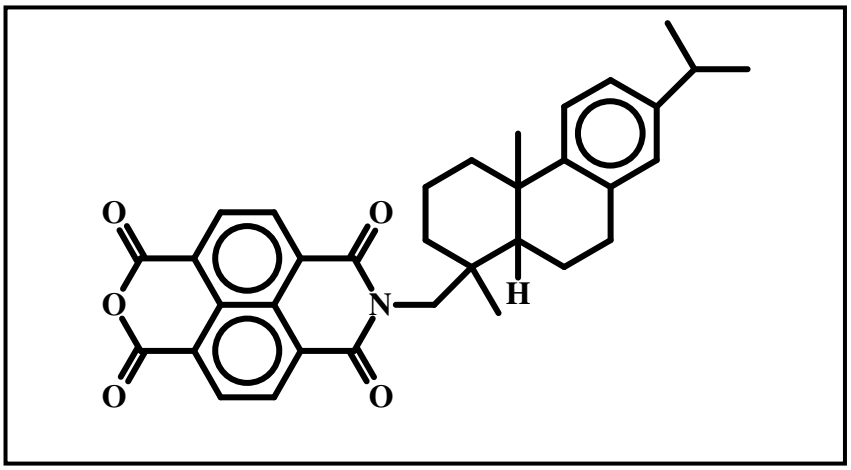

1,4,5,8-Naphthalenetetracarboxylic dianhydride (1.00 g, 3.7 mmol), KOH (1.0 M, 33 ml) and water (175 ml) were stirred at room temperature for 2 h, dehydroabietylamine (1.07 g, 3.7 mmol) was added and stirred for another 41 h at 80 ^{o}C. After acidification with acetic acid (10 %), the precipitate was collected by vacuum filtration, washed with water and dried in vacuum at 100 ^{o}C. The crude product was purified with simple purification techniques.

Yield: 0.50 g (24%), Color: Cream powder

IR (KBr, cm^{-1}): ν = 3075, 2940, 2866, 1701, 1651, 1585, 1439, 1376, 1340, 1238, 988, 775, 650.

UV-vis ($CHCl_3$) (λ_{max} / nm) : 351

Fluorescence ($CHCl_3$) (λ_{max} / nm) : 434, Φ_f = 0.019

MS, (*m/z*) = 536.2 (M+1), 525.0, 509.9, 509.2, 508.2, 480.2, 396.0, 395.1, 368.1, 367.0, 336.9, 336.0, 308.0, 222.9, 199.8, 199.7, 160.8, 113.0, 97.0.

3.6 Synthesis of N,N'-bis-{N-(3-[4-(3-amino-propyl)-piperazin-1-yl]-propyl)-N'-[1-dehdroabiety]-1,4,5,8-naphthalenetetracarboxydiimidly}-3,4,9,10-perylenebis(dicarboximide), (NPM).

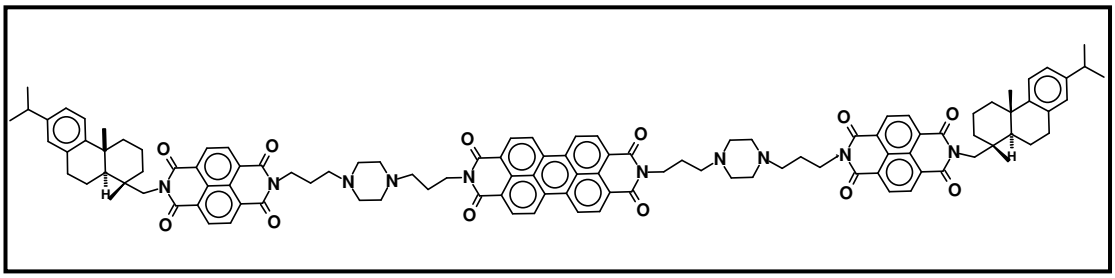

Perylene diimide (0.21 g, 0.285 mmol), Naphthalene monoimide (0.38 g, 0.713 g) and $Zn(OAc)_2.H_2O$ (0.55 g, 2.50 mmol) were heated carefully in a dried solvent mixture (60 mL m-cresol and 8 mL isoquinoline) under argon atmosphere at 100 ^oC for 10 h, 120 ^oC for 10 h, 140 ^oC for10 h and finally at 180 ^oC for 2 h.

The solution was allowed to cool and then poured into 300 mL acetone. The product was treated with methanol in a Soxhlet apparatus for 1 day in order to get the unreated compounds, the catalyst zinc acetate and high boiling solvents.

Yield: 0.26 g (50 %), Color: Dark brown

IR (KBr, cm^{-1}): ν = 3011, 2938, 2802, 1685, 1639, 1585, 1430, 1340, 1248, 1149, 1013, 804, 740, 577.

UV-vis ($CHCl_3$) (λ_{max} / nm) : 383**,** 397, 415, 460, 490, 526.

Fluorescence ($CHCl_3$) (λ_{max} / nm) : 433, 536, 576 626, Φ_f = 0.118

3.7 Reaction Mechanism of Macromolecule

STEP 1:

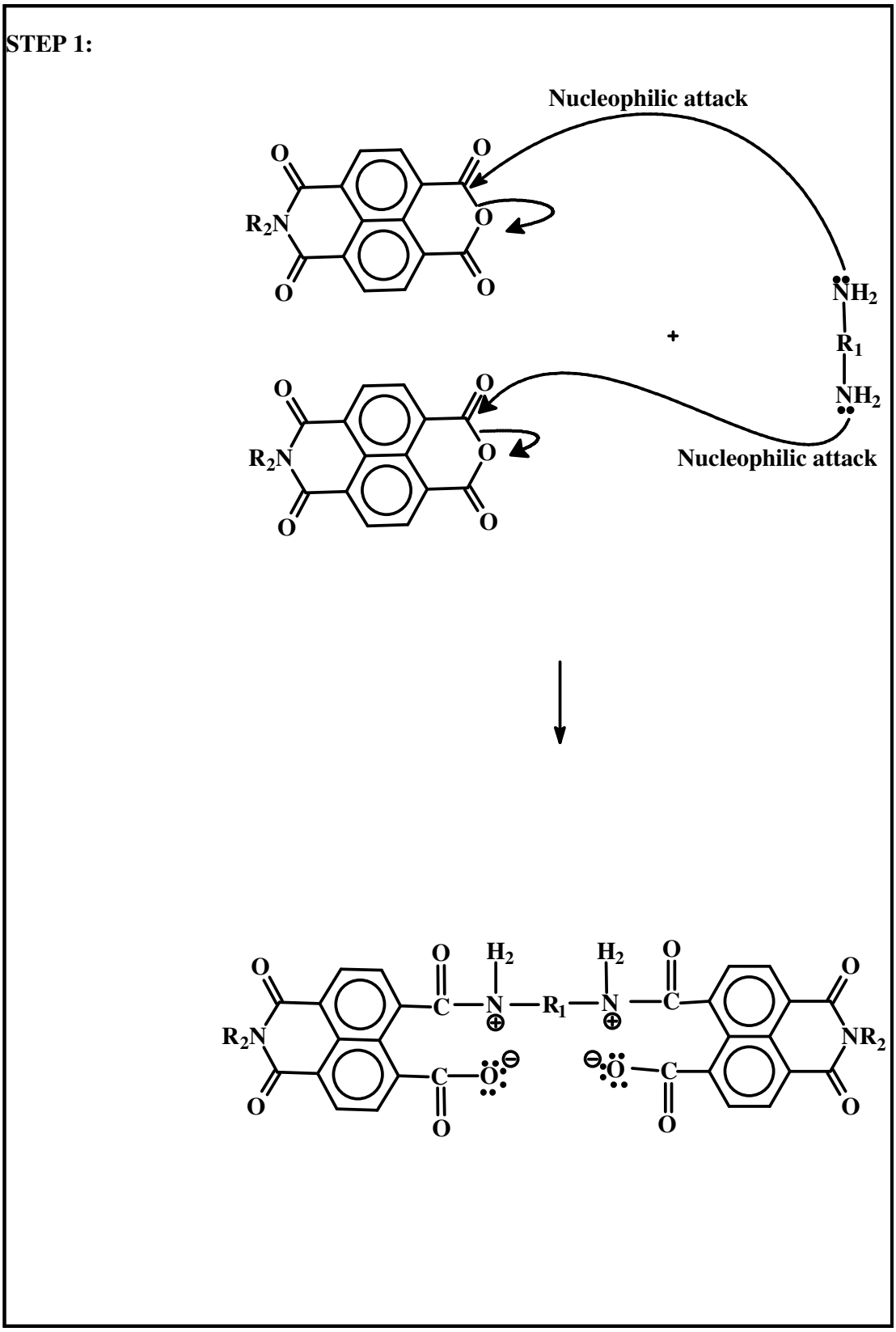

STEP 2:

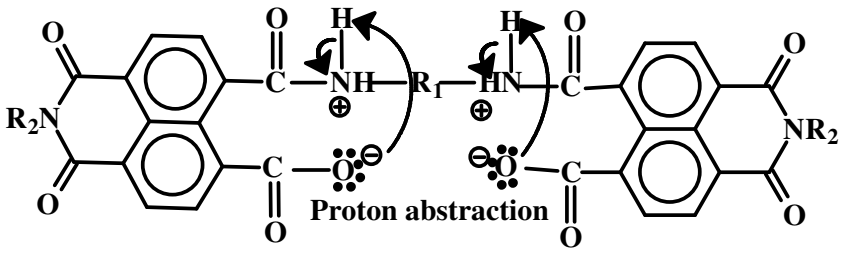

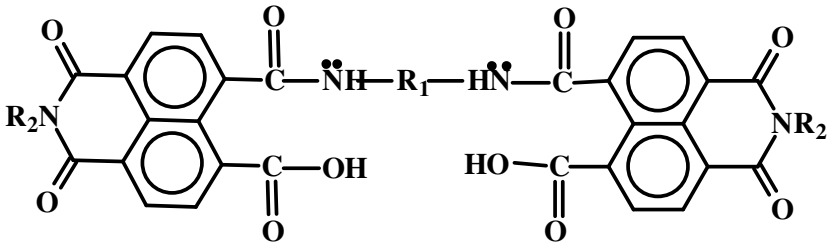

STEP 3:

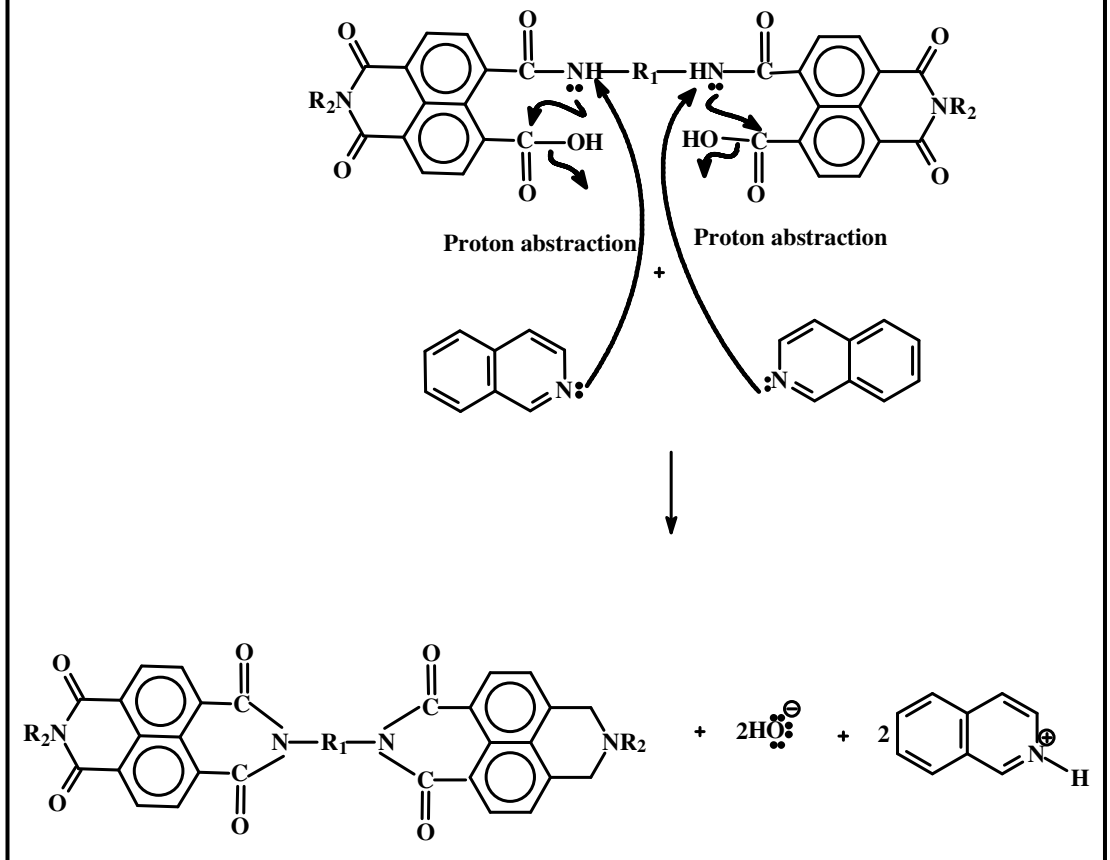

STEP 4:

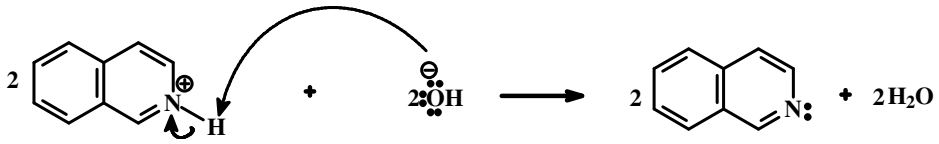

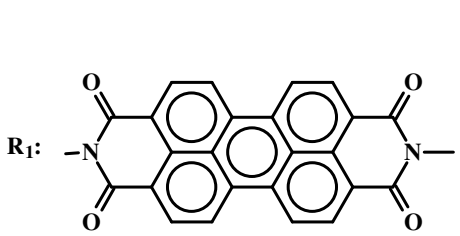

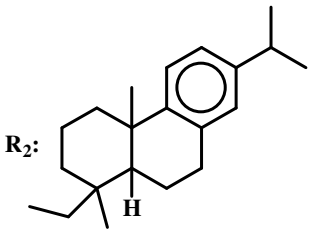

CHAPTER 4

DATA AND CALCULATIONS

4.1 Theoretical Aspect of Quantum Yields

The primary quantum yield of a photochemical reaction is the number of reactant molecules producing specified primary products per photon of light absorbed.

These primary products (atoms or ions) might serve as chain carriers and lead to more than one molecules of additional atoms or ions of product. The overall quantum yield '**Φ**' is the number of molecules reacting per photons absorbed.

$$\text{i.e. } \Phi = \frac{\text{number of moles (molecules) of product formed}}{\text{number of photons of radiation absorbed}}$$

The differential quantum yield is $\Phi = \dfrac{d[\chi] / dt}{n}$ **(4.1)**

Where $d[\chi] / dt$ is the rate of change of a measurable quantity, and 'n' the amount of photons (mol or its equivalent Einstein) absorbed per unit time. '**Φ**' can be used for photochemical reactions or photophysical processes.

High quantum yields are desirable for the application of photochemical reactions in organic syntheses. Quantum yield values fall in the range '0' to 1.0 although in some specific situations a higher value for chemical reaction may be observed. (J.C. Scaiano 1989).

4.2 Method of Measurement of Fluorescence Quantum Yields

When a fluorophore absorbs a photon of light, an energetically excited state is formed. The fate of this species is varied, depending on the exact nature of the fluorophore and its environment, but the end result is deactivation (loss of energy) and return to the ground state. The main deactivation processes which occur are fluorescence (loss of energy by emission of photon), internal conversion and vibrational relaxation (non-radiative loss of energy as heat to the environment), and intersystem crossing to the triplet manifold and subsequent non-radiative deactivation.

A common practice of measuring is to measure quantum yields relative to that of a standard compound, excited under identical conditions, whose quantum yield is known from previous determination (Zollinger H 1991). Given that the spectral response of the light detector is known, the most rapid and accurate way of determining emission efficiency is to measure the unknown quantum yield relative to that of some substance whose absolute emission quantum yield has already been accurately measured. It is only then necessary to determine, under identical conditions of cell geometry, incident light intensity and temperature, the fluorescence spectra of the dilute solutions of the unknown and of the standard. The solutions should have the same optical density at the wavelength of the exciting light so that they both capture the same number of photons. The quantum yield of the unknown relative to the standard is to ratio of the integrated band areas under the two fluorescence spectra after they have been corrected for the detector response function. Multiplying by the known quantum yield of the standard, then gives the absolute quantum yield of the unknown (Icil H, Uzun D et al. 1998).

$$\phi_f(U) = \frac{A_{std}}{A_u} \times \frac{S_u}{S_{std}} \times \left[\frac{n_u}{n_{std}}\right]^2 \times \phi_{std} \quad \textbf{(4.2)}$$

$\Phi_f(U)$: Fluorescence quantum yield of unknown

A_{std} : Absorbance of the reference at the excitation wavelength

A_u : Absorbance of the unknown at the excitation wavelength

S_{std} : The integrated emission area across the band of reference

S_u : The integrated emission area across the band of unknown

n_{std} : Refractive index of reference solvent

n_u : Refractive index of unknown solvent

Φ_{std} : Fluorescence quantum yield of reference (J. C. Scaiano, 1989)

The N,N'-bis(dodecyl)-3,4,9,10-perylenebis(discarboximide) in chloroform ($\mathbf{\Phi}_f$ = 1) (Icil, 1996) was used as reference for the fluorescence quantum yield measurements of PDI and NPM . The excitation wavelength, λ_{max} of both PDI and macromolecule was 485 nm. Since the solvents used are the same for both reference and sample, the refractive indexes can be ommited from the calculations of the fluorescence quantum yields. With this consideration the following equation is used for the calculation of fluorescence quantum yield.

$$\phi_f(U) = \frac{A_{std}}{A_u} \times \frac{S_u}{S_{std}} \times \phi_{std} \quad \textbf{(4.3)}$$

4.2.1 Fluorescence Quantum Yield (Φ_f) Calculations of PDI, NMI and NPM.

Φ_f Calculation of PDI :

N,N'-bis(dodecyl)-3,4,9,10-perylenebis(discarboximide) was used as reference (Icil 1996).

Φ_{std} = 1 when the solvent is chloroform

A_{std} = 0.1009

A_u = 0.1008

S_{std} = 10094 counts / (cm.sec)

S_u = 2896 counts / (cm.sec)

$$\Phi_f \text{ (PDI)} = \frac{0.1008}{0.1009} \times \frac{8300}{10094} \times 1$$

Φ_f = 0.822

Φ_f Calculation of NMI :

Anthracene was used as reference

Φ_{std} = 0.27 when the solvent is ethanol

A_{std} = 0.1020

A_u = 0.1019

S_{std} = 23615 counts / (cm.sec)

S_u = 1570 counts / (cm.sec)

n_{std} = 1.3614

n_u = 1.4458

Φ_f (NMI) $= \frac{0.1020}{0.1019} \times \frac{1570}{23615} \times \frac{1.4458}{1.3614} \times 0.27$

Φ_f = 0.019

Φ_f Calculation of NPM :

N,N'-bis(dodecyl)-3,4,9,10-perylenebis(discarboximide) was used as reference (Icil 1996).

Φ_{std} = 1 when the solvent is chloroform

A_{std} = 0.1015

A_u = 0.1018

S_{std} = 260 counts / (cm.sec)

S_u = 31 counts / (cm.sec)

Φ_f (NPM) $= \frac{0.1015}{0.1018} \times \frac{31}{260} \times 1$

Φ_f = 0.119

4.3 Calculation of Maximum Extinction Coefficients

The following equation 4.4 is used to calculate the extinction coefficients of the compounds. (J.C. Scaiano, 1989).

$$\varepsilon_{max} = \frac{A}{cl} \qquad \textbf{(4.4)}$$

Where ε_{max} : Maximum extinction coefficient at λ_{max}

A : Absorbance

C : Concentration and

l : Cell length.

ε_{max} calculation of PDI :

This was not calculated because of its poor solubility.

ε_{max} calculation of NMI :

c = 1.00 x 10^{-5} M in CHLOROFORM ; 1 = 1cm.

at λ_{max} = 351 nm, A = 0.4275

$$\varepsilon_{max} = \frac{0.4275}{1 \times 10^{-5}\ M \times 1\ cm} = 42750\ L\ mol^{-1}\ cm^{-1}$$

ε_{max} calculation of NPM :

c = M in CHLOROFORM ; 1 = 1cm.

at λ_{max} = 383 nm, A = 0.3756

$$\varepsilon_{max} = \frac{0.3756}{M \times 1cm} = \text{L mol}^{-1}\ \text{cm}^{-1}$$

at λ_{max} = 397 nm, A = 0.4015

$$\varepsilon_{max} = \frac{0.4015}{\text{M x 1 cm}} = \text{L mol}^{-1}\ \text{cm}^{-1}$$

at λ_{max} = 415 nm, A = 0.3639

$$\varepsilon_{max} = \frac{0.3639}{\text{M x 1 cm}} = \text{L mol}^{-1}\ \text{cm}^{-1}$$

at λ_{max} = 460 nm, A = 0.2679

$$\varepsilon_{max} = \frac{0.2679}{\text{M x 1 cm}} = \text{L mol}^{-1}\ \text{cm}^{-1}$$

at λ_{max} = 490 nm, A = 0.3447

$$\varepsilon_{max} = \frac{0.3447}{\text{M x 1 cm}} = \text{L mol}^{-1}\ \text{cm}^{-1}$$

at λ_{max} = 526 nm, A = 0.4095

$$\varepsilon_{max} = \frac{0.4095}{\text{M x 1 cm}} = \text{L mol}^{-1}\ \text{cm}^{-1}$$

4.4 Theoretical Radiative Lifetimes (τ_o) Calculations

The following equation 4.5 will be used to calculate the theoretical radiative lifetimes. (Bodapati J B 2005)

$$\tau_0 = \frac{3.5\times10^8}{\nu_{max}^2 \varepsilon_{max} \Delta\nu_{1/2}} = \frac{3.5\times10^8}{\lambda_{max}^2 \varepsilon_{max} \Delta\nu_{1/2}} \qquad \textbf{(4.5)}$$

Where

τ_o : Theoretical raditive lifetime in seconds

$\nu_{max} = \lambda_{max}$: Wavenumbers in cm^{-1}

ε_{max} : The maximum extinction coefficient at the selected absorption wavelength.

$\Delta\nu_{1/2}$: Half-width of the selected absorption in units of cm^{-1}

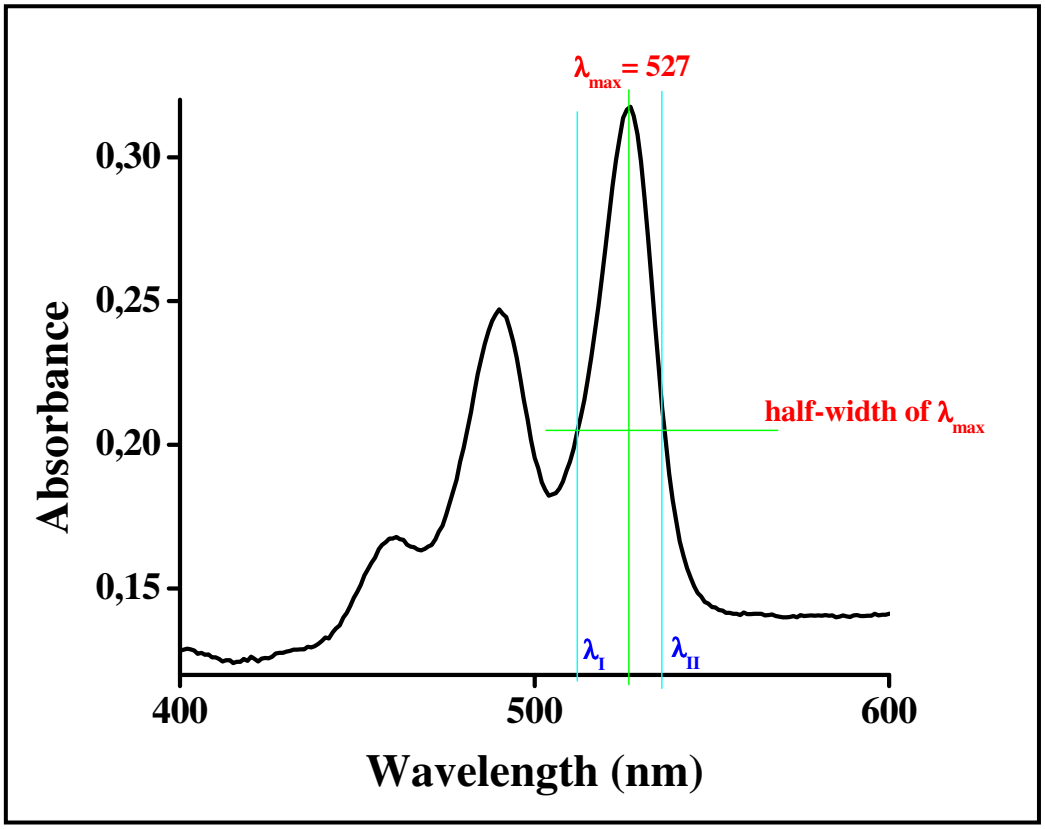

Figure 4.1. A representative figure to calculate the half-width of the selected absorption.

τ_o calculation of PDI :

λ_{max} = 527 nm

$$\lambda_{\max} = 527nm \times \frac{10^{-9}\,m}{1nm} \times \frac{100cm}{1m} = 5.27 \times 10^{-5}\,cm$$

$$\lambda_{max} = \frac{1}{5.27 \times 10^{-5}\,cm} = \textbf{18975.33 cm}^{-1}$$

ε_{max} = L mol^{-1} cm^{-1}

$$\Delta\nu_{1/2} = \upsilon_{II} - \upsilon_{I}$$

$$\lambda_{I} = 512.03nm \times \frac{10^{-9}\,m}{1nm} \times \frac{100cm}{1m} = 5.120 \times 10^{-5}\,cm$$

$$\upsilon_{I} = \frac{1}{5.120 \times 10^{-5}\,cm} = 19531 \text{ cm}^{-1}$$

$$\lambda_{II} = 536.98nm \times \frac{10^{-9}\,m}{1nm} \times \frac{100cm}{1m} = 5.370 \times 10^{-5}\,cm$$

$$\upsilon_{II} = \frac{1}{5.370 \times 10^{-5}\,cm} = 18622 \text{ cm}^{-1}$$

$$\Delta\nu_{1/2} = \upsilon_{II} - \upsilon_{I} = 18622 \text{ cm}^{-1} - 19531 \text{ cm}^{-1} = 909 \text{ cm}^{-1}$$

$\Delta\nu_{1/2}$ = 909 cm^{-1}

$$\tau_0 = \frac{3.5 \times 10^{8}}{\lambda_{\max}^{2}\,\varepsilon_{\max}\,\Delta\nu_{1/2}} = \frac{3.5 \times 10^{8}}{18975.33^{2} \times \varepsilon_{\max} \times 909} = \times 10^{-8} \text{ sec}$$

τ_0 = x 10^{-9} sec

$$\tau_0 = \times 10^{-9} \text{ sec} \times \frac{1ns}{10^{-9} \text{ sec}} \cong ns$$

τ_o calculation of NMI :

λ_{max} = 351 nm

$$\lambda_{\max} = 351nm \times \frac{10^{-9}\,m}{1nm} \times \frac{100cm}{1m} = 3.51 \times 10^{-5}\,cm$$

$$\boldsymbol{\lambda_{max}} = \frac{1}{3.51 \times 10^{-5}\,cm} = \mathbf{28490 \quad cm^{-1}}$$

ε_{max} = 42750 L mol^{-1} cm^{-1}

$$\Delta\nu_{1/2} = \upsilon_{II} - \upsilon_{I}$$

$$\lambda_{I} = 336.17nm \times \frac{10^{-9}\,m}{1nm} \times \frac{100cm}{1m} = 3.362 \times 10^{-5}\,cm$$

$$\upsilon_{I} = \frac{1}{3.362 \times 10^{-5}\,cm} = 29744 \text{ cm}^{-1}$$

$$\lambda_{II} = 368.85nm \times \frac{10^{-9}\,m}{1nm} \times \frac{100cm}{1m} = 3.689 \times 10^{-5}\,cm$$

$$\upsilon_{II} = \frac{1}{3.689 \times 10^{-5}\,cm} = 27107 \text{ cm}^{-1}$$

$$\Delta\nu_{1/2} = \upsilon_{II} - \upsilon_{I} = 27107 \text{ cm}^{-1} - 29744 \text{ cm}^{-1} = 2637 \text{ cm}^{-1}$$

$\Delta\nu_{1/2}$ = 2637 cm^{-1}

$$\tau_0 = \frac{3.5 \times 10^{8}}{\lambda_{\max}^{2}\,\varepsilon_{\max}\,\Delta\nu_{1/2}} = \frac{3.5 \times 10^{8}}{27322.4^{2} \times 42750 \times 2637} = 2.198 \times 10^{-8} \text{ sec}$$

τ_0 = 21.98 x 10^{-9} sec

$$\tau_0 = 21.98 \times 10^{-9} \text{ sec} \times \frac{1ns}{10^{-9} \text{ sec}} \cong 21.98ns$$

τ_o calculation of NPM :

λ_{max} = 526 nm

$$\lambda_{\max} = 526nm \times \frac{10^{-9}\,m}{1nm} \times \frac{100cm}{1m} = 5.26 \times 10^{-5}\,cm$$

$$\lambda_{max} = \frac{1}{5.26 \times 10^{-5}\,cm} = \textbf{19011.4 cm}^{-1}$$

ε_{max} = L mol^{-1} cm^{-1}

$$\Delta\nu_{1/2} = \upsilon_{II} - \upsilon_{I}$$

$$\lambda_{I} = 516.50nm \times \frac{10^{-9}\,m}{1nm} \times \frac{100cm}{1m} = 5.165 \times 10^{-5}\,cm$$

$$\upsilon_{I} = \frac{1}{5.165 \times 10^{-5}\,cm} = 19361.1 \text{ cm}^{-1}$$

$$\upsilon_{II} = 533.71nm \times \frac{10^{-9}\,m}{1nm} \times \frac{100cm}{1m} = 5.337 \times 10^{-5}\,cm$$

$$\lambda_{II} = \frac{1}{5.337 \times 10^{-5}\,cm} = 18737.1 \text{ cm}^{-1}$$

$$\Delta\nu_{1/2} = \upsilon_{II} - \upsilon_{I} = 18737 \text{ cm}^{-1} - 19361 \text{ cm}^{-1} = 624 \text{ cm}^{-1}$$

$\Delta\nu_{1/2}$ = 624 cm^{-1}

$$\tau_0 = \frac{3.5 \times 10^{8}}{\lambda_{\max}^{2}\,\varepsilon_{\max}\,\Delta\nu_{1/2}} = \frac{3.5 \times 10^{8}}{19011.4^{2} \times \times 624} = \times 10^{-8} \text{ sec}$$

τ_0 = x 10^{-9} sec

$$\tau_0 = \times 10^{-9} \text{ sec} \times \frac{1ns}{10^{-9} \text{ sec}} \cong ns$$

τ_o cannot be calculated because there's no ε_{max} due to poor solubility.

4.5 Calculations of Theoretical Fluorescence Lifetime (τ_f)

Fluorescence lifetimes were calculated using the formula 4.6 shown below (Turro, 1965).

$$\tau_f = \tau_0 . \Phi_f \qquad (4.6)$$

Where τ_f : Fluorescence lifetime

τ_0 : Theoretical radiative lifetime

Φ_f : Fluorescence quantum yield

τ_f calculation of PDI:

$\tau_f = \tau_0 . \Phi_f$

τ_0 = ns

Φ_f = 0.822

τ_f = ns x 0.822

τ_f calculation of NMI:

$\tau_f = \tau_0 . \Phi_f$

τ_0 = 21.98 ns

Φ_f = 0.019

τ_f = 21.98 x 0.019

τ_f = 0.42 ns

τ_f calculation of NPM:

$\tau_f = \tau_0 . \Phi_f$

τ_0 = ns

Φ_f = 0.119

τ_f = ns x 0.019

4.5.1 Calculations of Theoretical Fluorescence Rate Constant (k_f)

The fluorescence rate constant can be calculated by using Turro's equation 4.7 given below.

$$k_f = 1/\tau_0 \qquad (4.7)$$

k_f calculation of PDI:

$k_f = 1/\tau_0$

$\therefore \kappa_f = \frac{1}{\times 10^{-9}} =$ **sec^{-1}**

k_f calculation of NMI:

$k_f = 1/\tau_0$

$\therefore \kappa_f = \frac{1}{21.98 \times 10^{-9}} =$ **4.55 x 10^{-7} sec^{-1}**

k_f calculation of NPM:

$k_f = 1/\tau_0$

$\therefore \kappa_f = \frac{1}{\times 10^{-9}} =$ **sec^{-1}**

4.5.2 Calculations of Singlet Energy (E_s)

The following equation given by Turro can be used to calculate the singlet energy, Es.

$$E_s = \frac{2.86 \times 10^5}{\lambda_{max}} \qquad \textbf{(4.8)}$$

Where Es : Singlet energy in kcal/ mol

λ_{max} : Maximum absorption wavelength in Å

E_s calculation of PDI:

$$Es = \frac{2.86 \times 10^5}{\lambda_{max}}$$

at λ_{max} = 527nm i.e., $\lambda_{max} = 527nm \times \frac{10^{-9} m}{1nm} \times \frac{1A}{10^{-10} m} = 5270$ Å

$$\therefore E_s = \frac{2.86 \times 10^5}{5270} = \textbf{54.27 kcal/ mol}$$

E_s calculation of NMI:

$$Es = \frac{2.86 \times 10^5}{\lambda_{max}}$$

at λ_{max} = 351nm i.e., $\lambda_{max} = 351nm \times \frac{10^{-9} m}{1nm} \times \frac{1A}{10^{-10} m} = 3510$ Å

$$\therefore E_s = \frac{2.86 \times 10^5}{3510} = \textbf{81.48 kcal/ mol}$$

E_s calculation of NPM:

$$Es = \frac{2.86\times10^5}{\lambda_{max}}$$

at λ_{max} = 526nm i.e., $\lambda_{max} = 526nm \times \frac{10^{-9}m}{1nm} \times \frac{1A}{10^{-10}m} = 5260$ Å

$$\therefore E_s = \frac{2.86\times10^5}{5260} = \textbf{54.37 kcal/ mol}$$

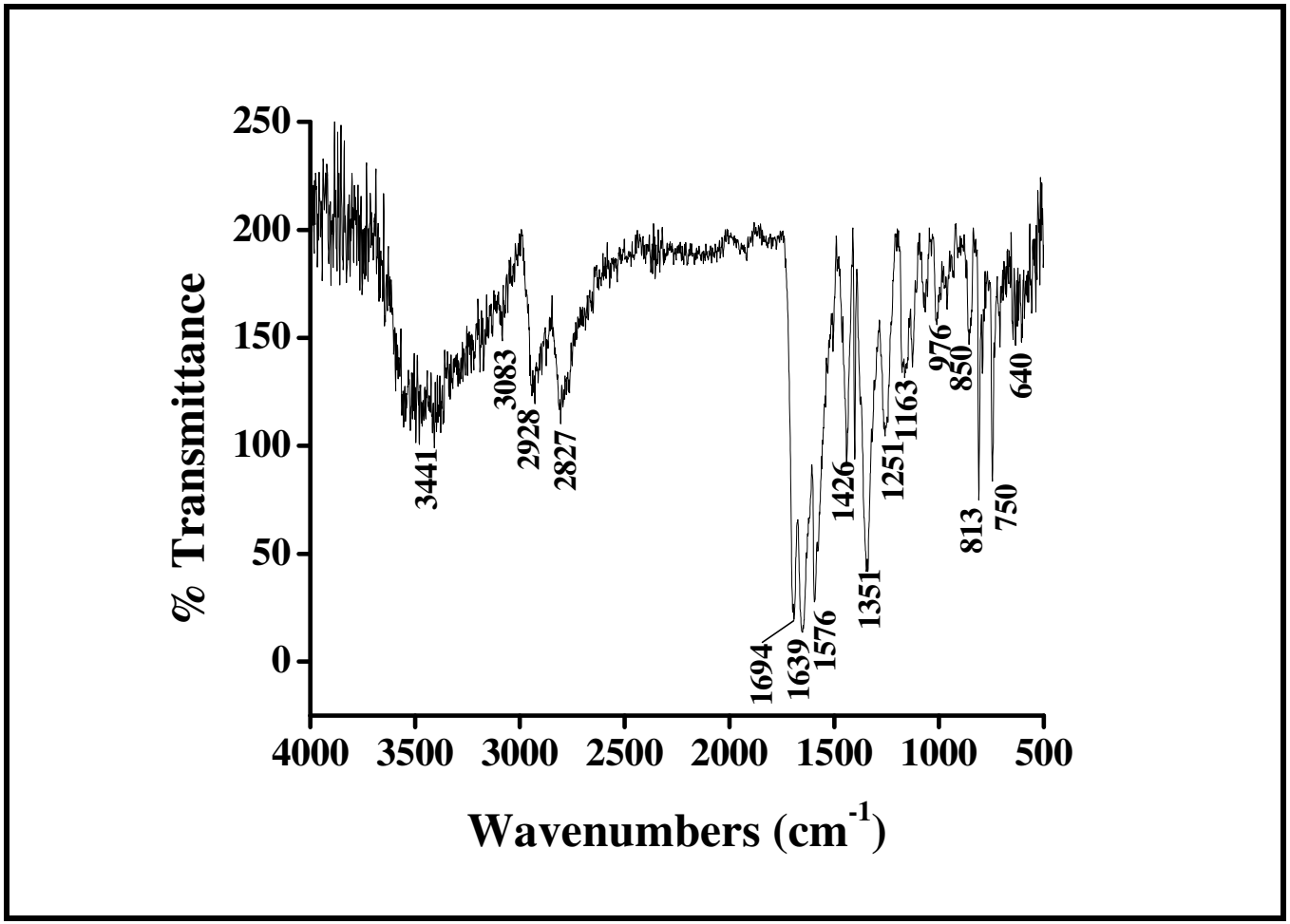

Figure 4.2 IR spectrum of N-N'-bis-{3-[4-(3-amino-propyl)-piperazin-1-yl]-propyl}- 3,4,9,10-perylenebis(dicarboximide), PDI, at solid state (KBr).

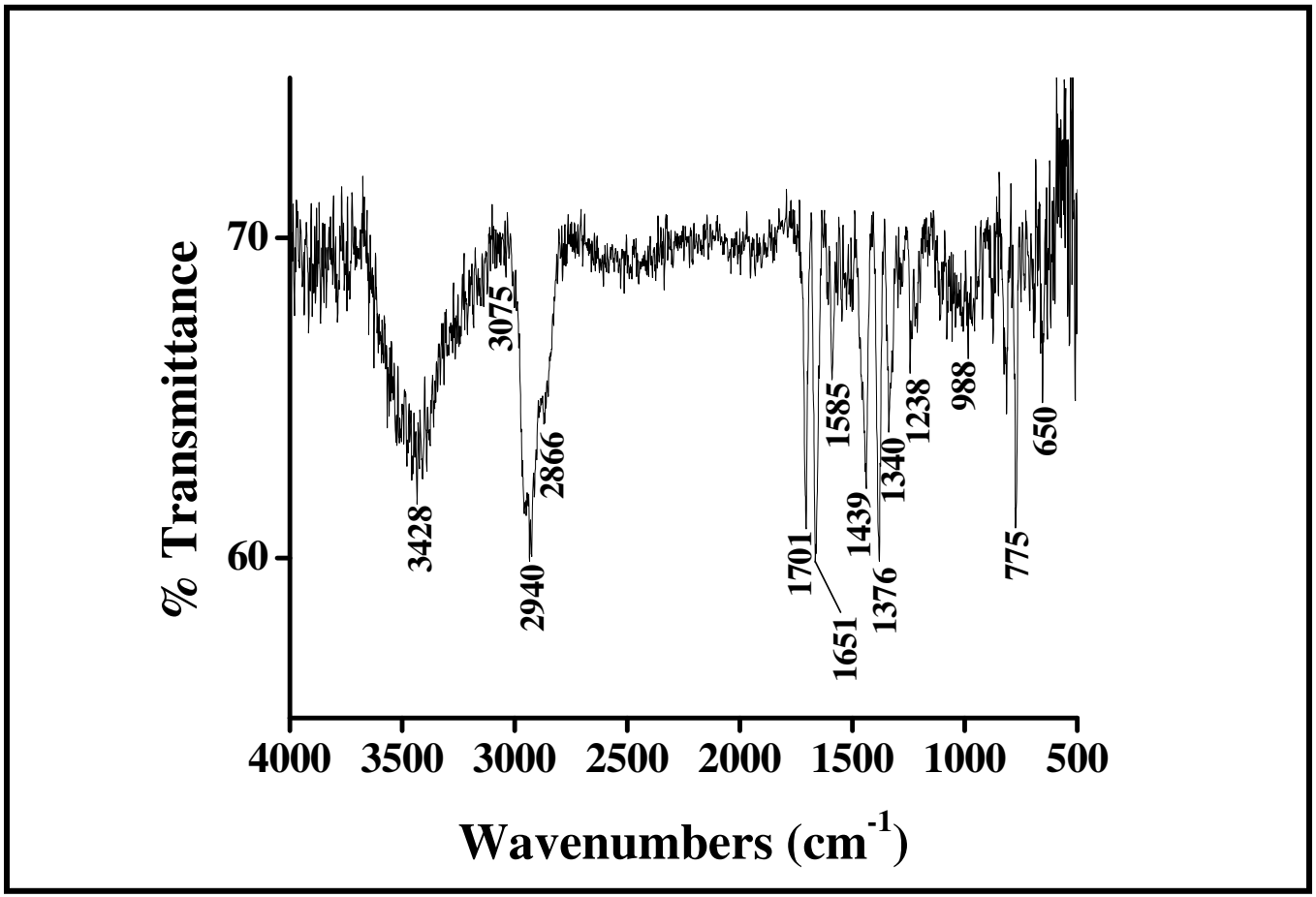

Figure 4.3 IR spectrum of N-(1-dehydroabietyl)-1,4,5,8-naphthalenetetracarboxylic-1,8-anhydride-4,5-imide, NMI, at solid state (KBr).

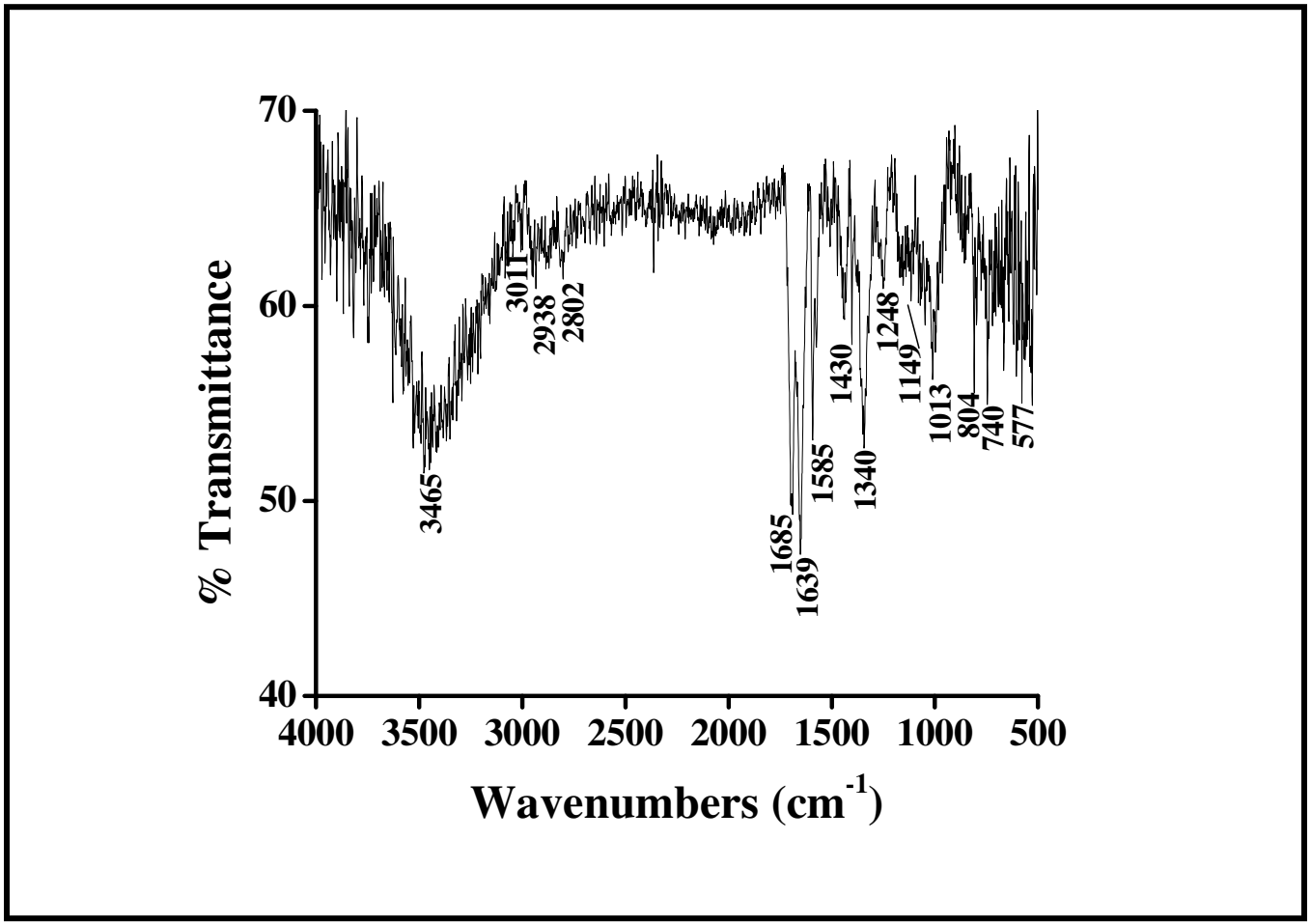

Figure 4.4 IR spectrum of N,N'-bis-{N-(3-[4-(3-amino-propyl)-piperazin-1-yl]-propyl)-N'-[1-dehdroabiety]-1,4,5,8-naphthalenetetracarboxydiimidly}-3,4,9,10-perylenebis(dicarboximide), (NPM), at solid state (KBr).

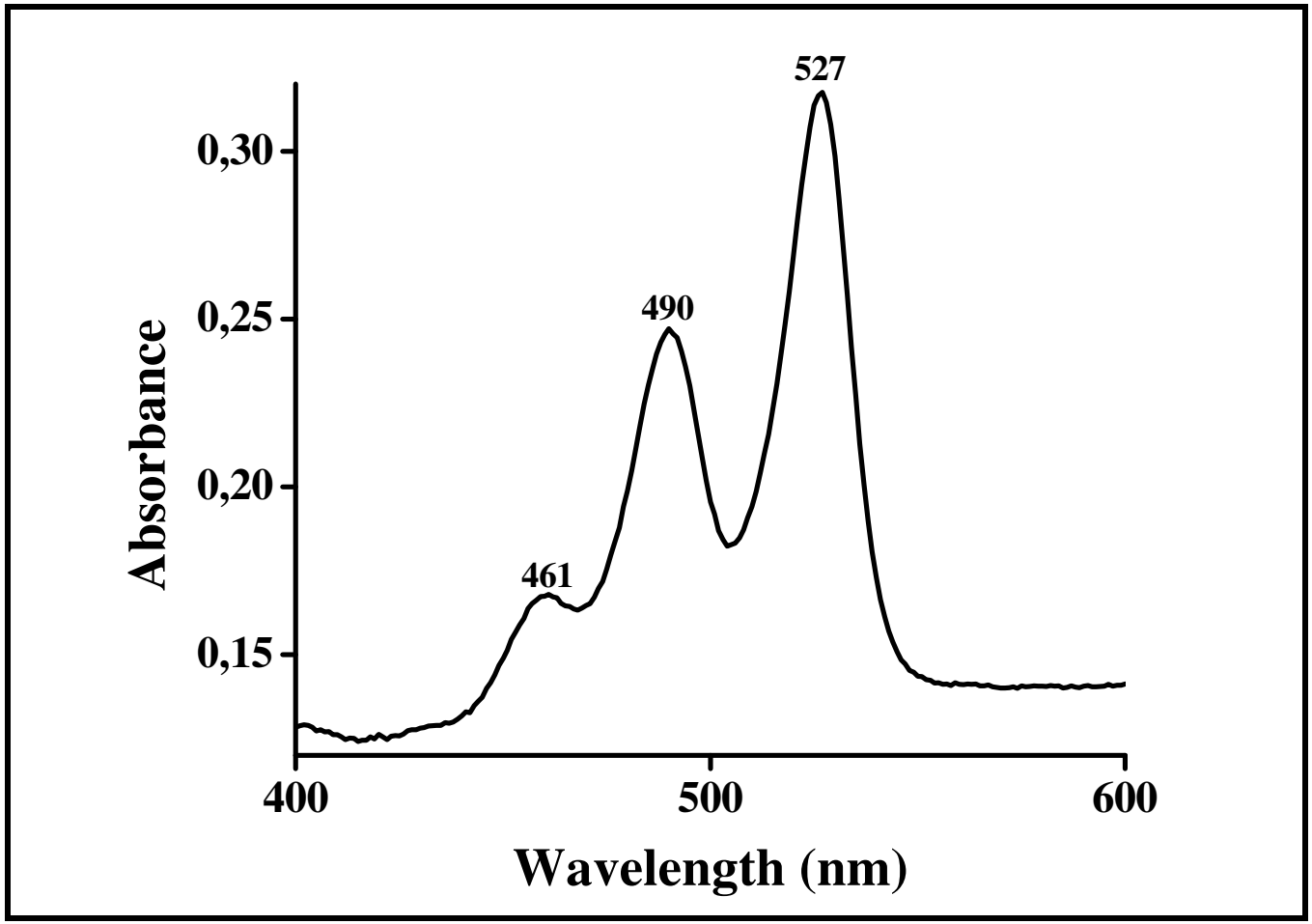

Figure 4.5 UV-vis absorption spectrum of N-N'-bis-{3-[4-(3-amino-propyl)-piperazin-1-yl]-propyl}- 3,4,9,10-perylenebis(dicarboximide), PDI in $CHCl_3$.

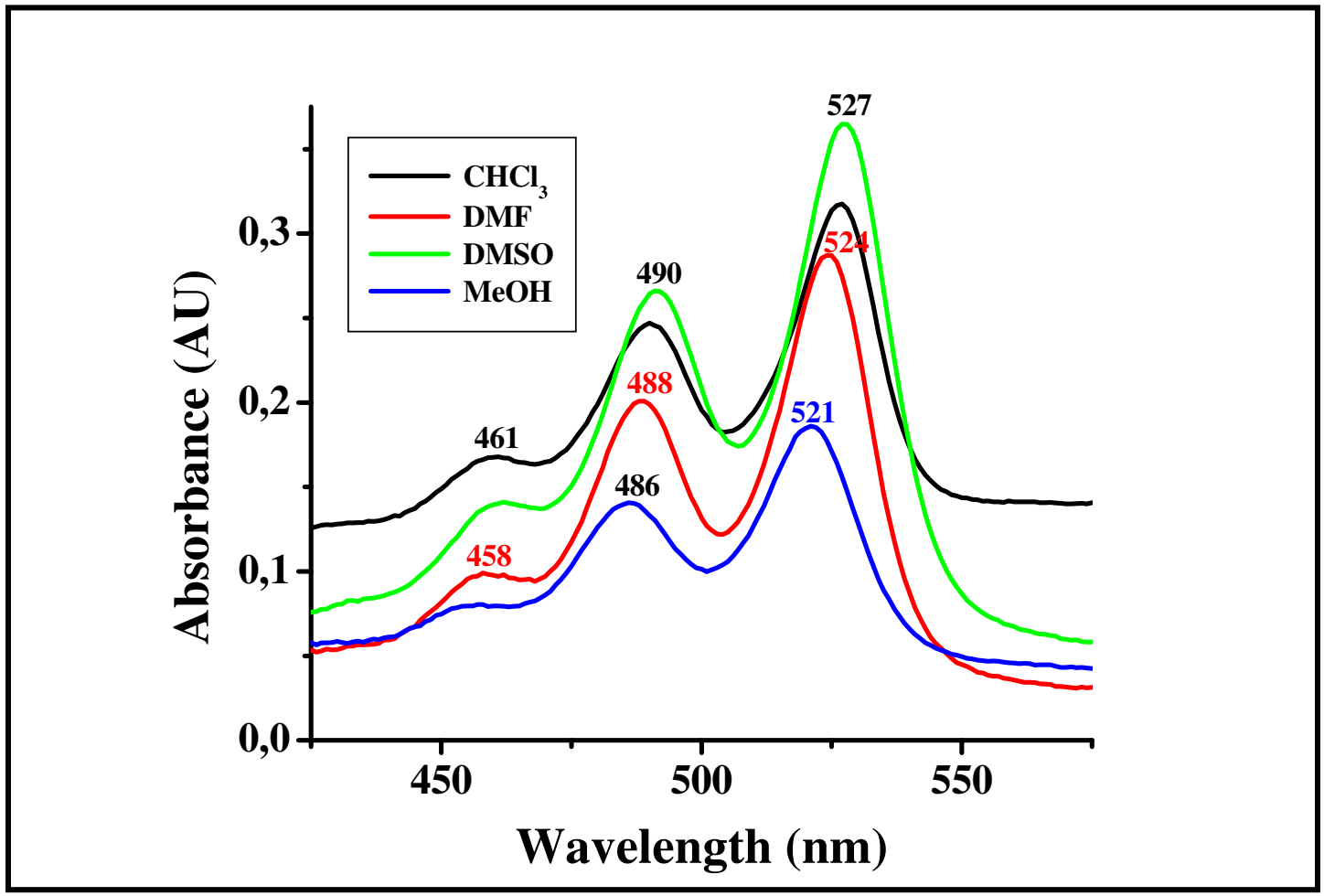

Figure 4.6 UV-vis absorption spectra of N-N'-bis-{3-[4-(3-amino-propyl)-piperazin-1-yl]-propyl}- 3,4,9,10-perylenebis(dicarboximide), PDI in $CHCl_3$, DMF, DMSO and MeOH.

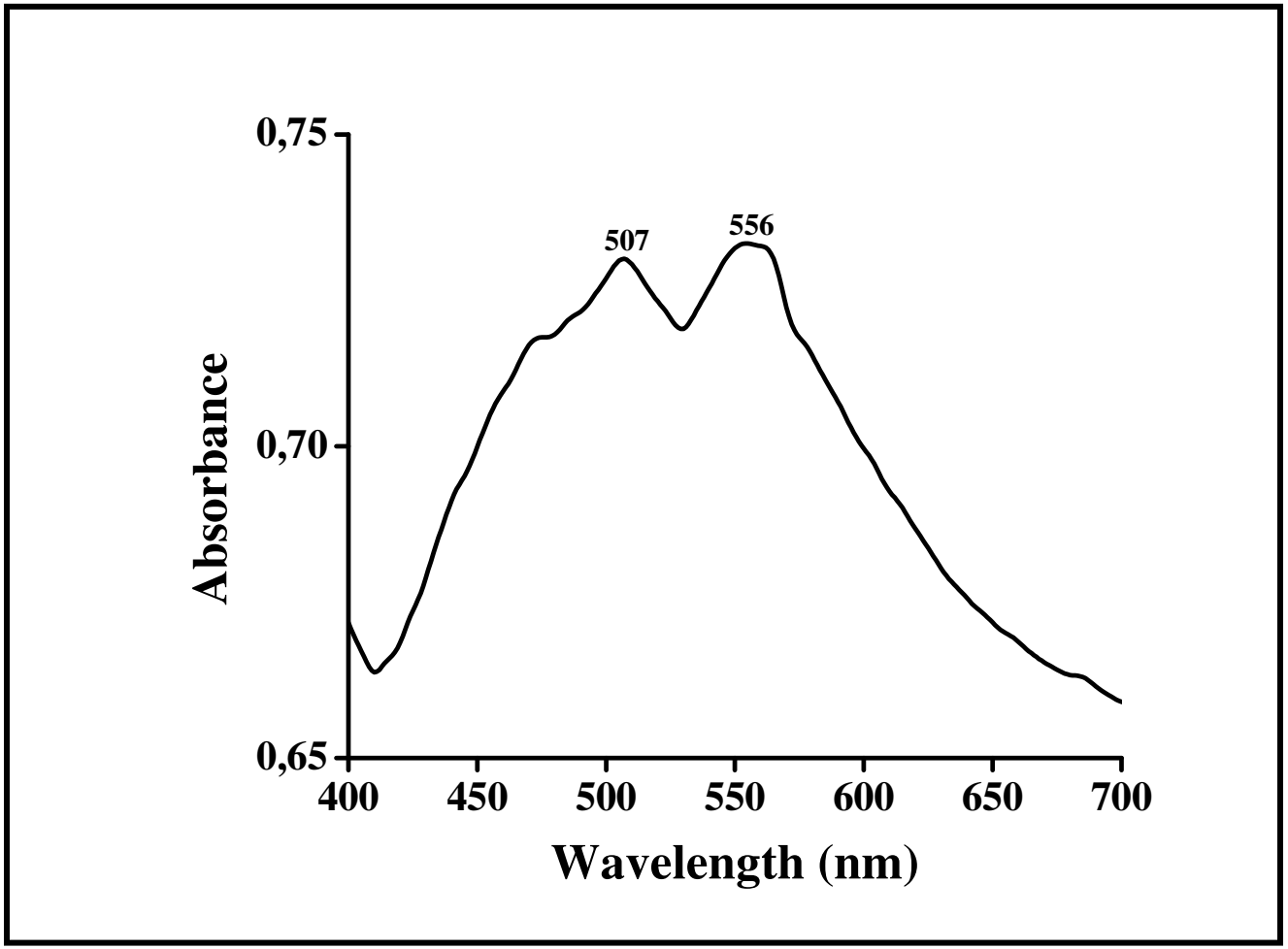

Figure 4.7 Solid state UV-vis absorption spectrum of N-N'-bis-{3-[4-(3-amino-propyl)-piperazin-1-yl]-propyl}- 3,4,9,10-perylenebis(dicarboximide), PDI.

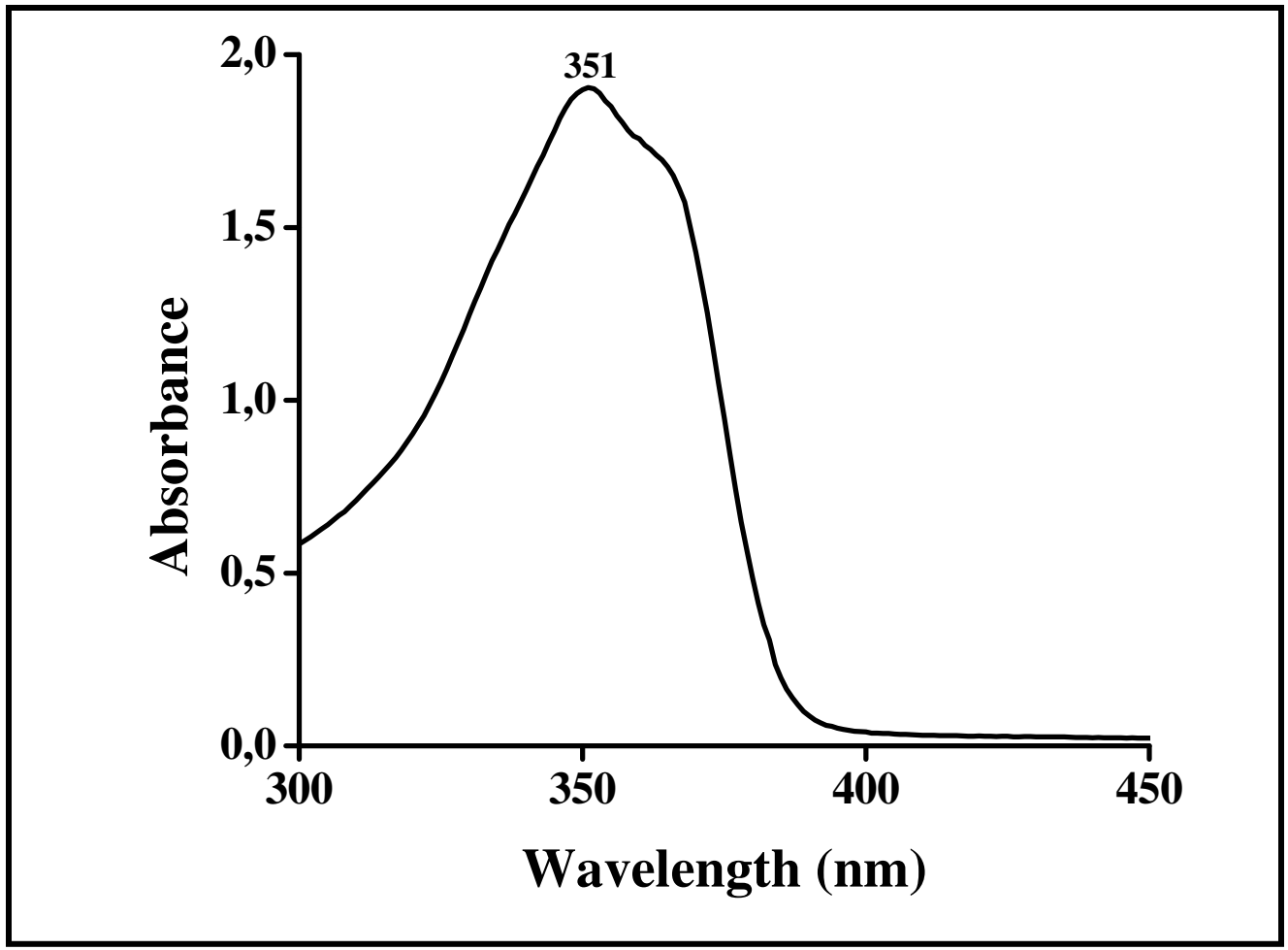

Figure 4.8 UV-vis absorption spectrum of N-(1-dehydroabietyl)-1,4,5,8-naphthalenetetracarboxylic-1,8-anhydride-4,5-imide, NMI in $CHCl_3$.

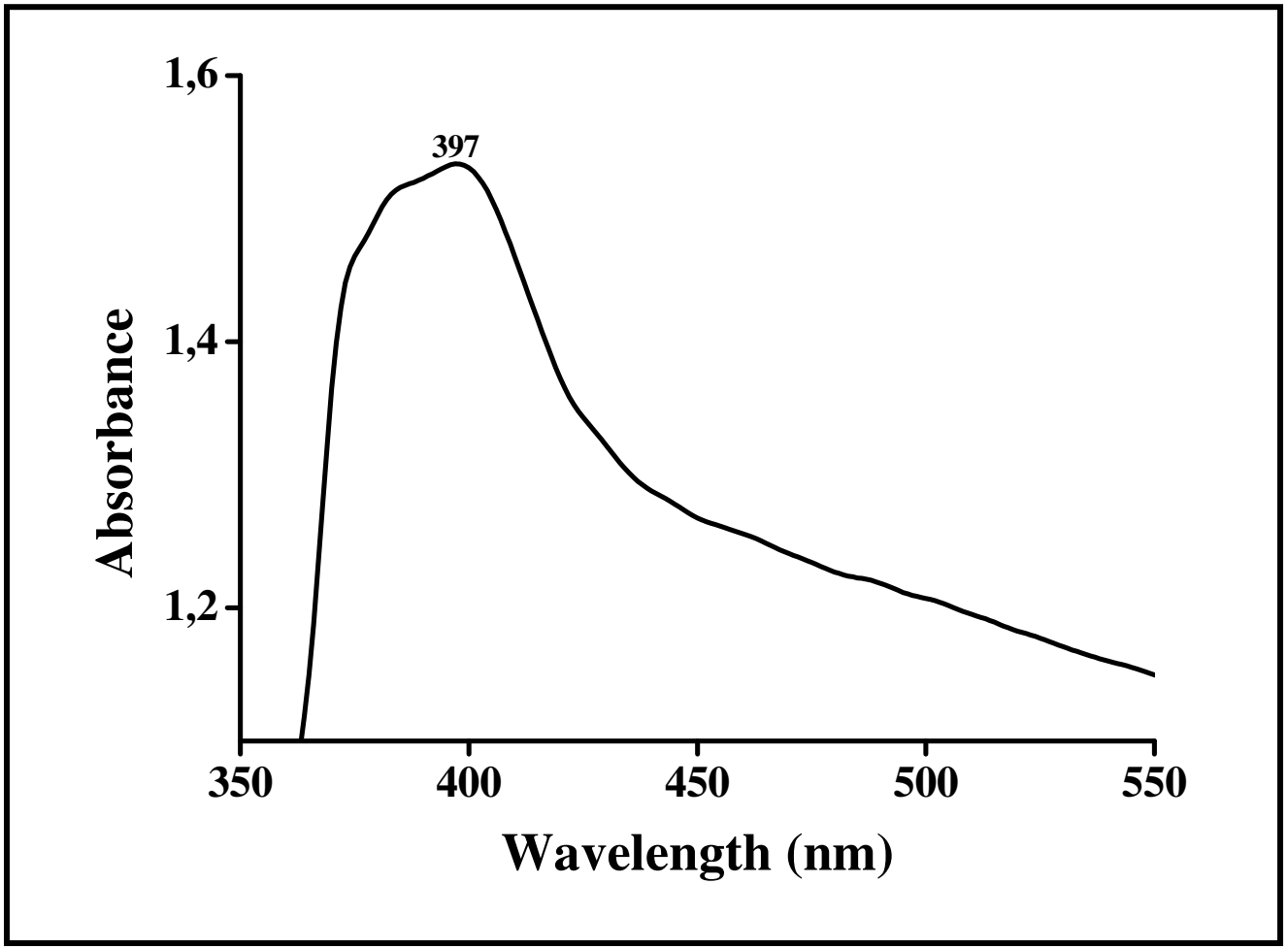

Figure 4.9 Solid state UV-vis absorption spectrum of N-(1-dehydroabietyl)-1,4,5,8-naphthalenetetracarboxylic-1,8-anhydride-4,5-imide, NMI.

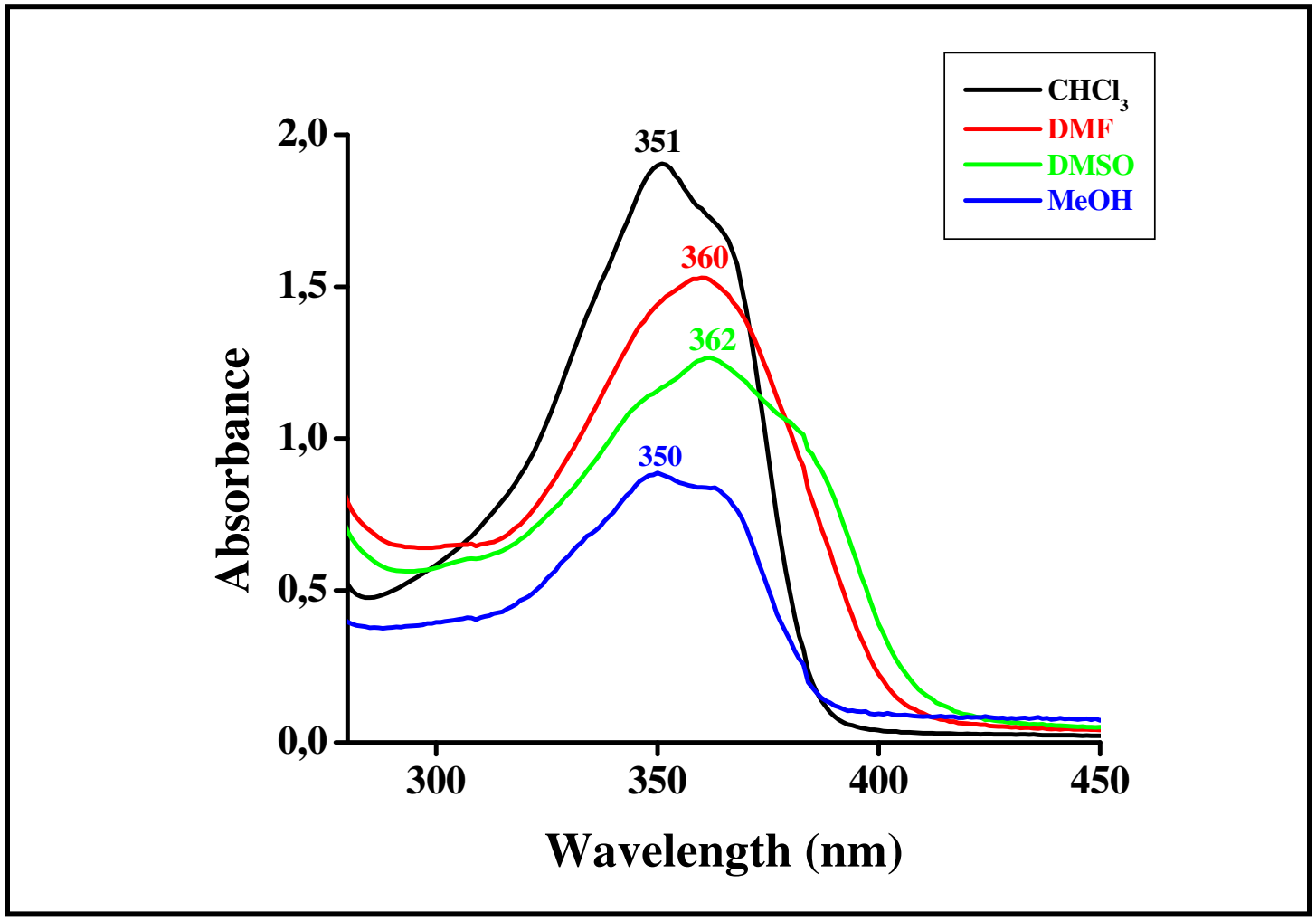

Figure 4.10 UV-vis absorption of N-(1-dehydroabietyl)-1,4,5,8-naphthalenetetracarboxylic-1,8-anhydride-4, 5-imide, NMI in $CHCl_3$, DMF, DMSO and MeOH.

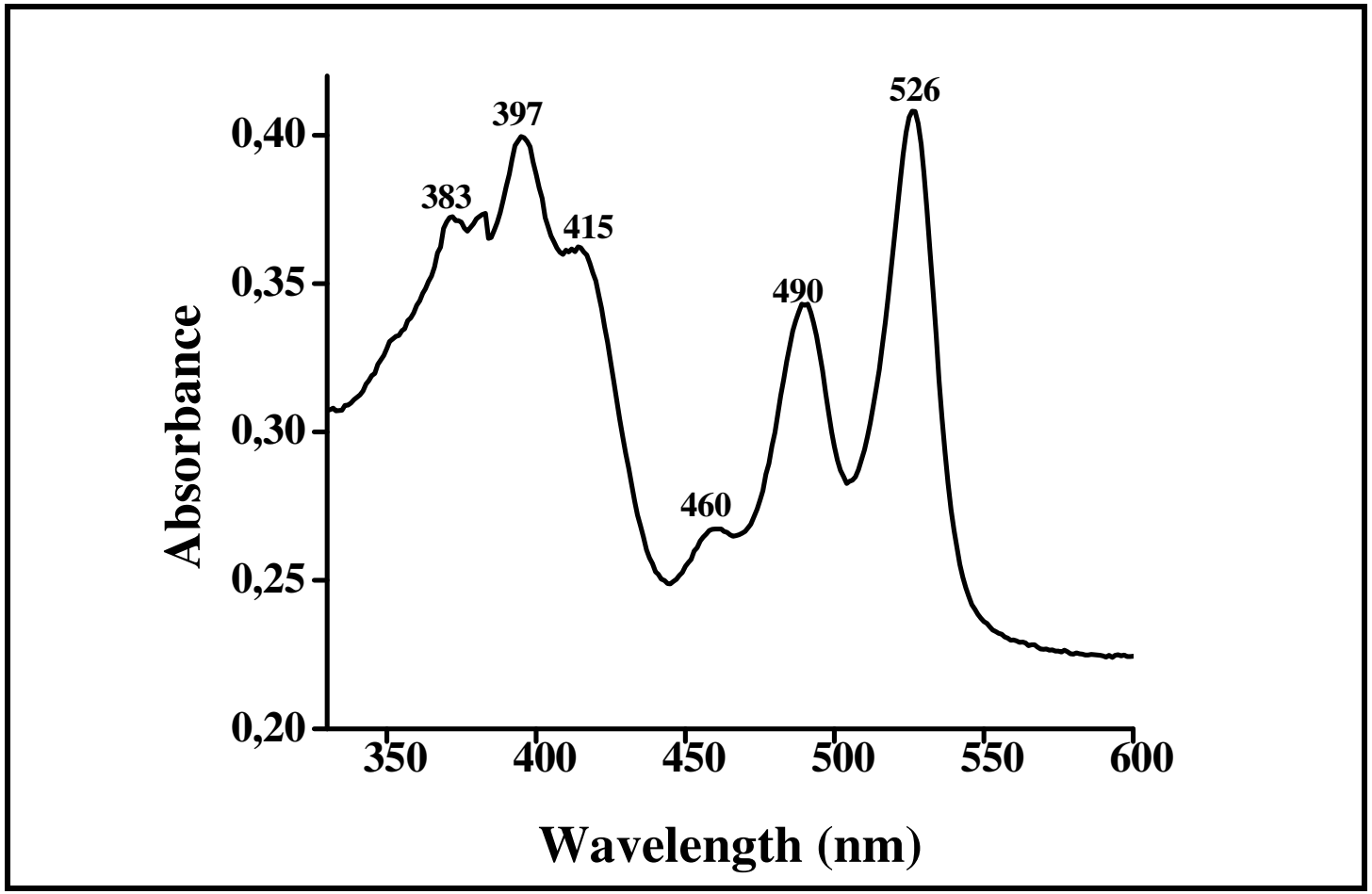

Figure 4.11 UV-vis absorption spectrum of N,N'-bis-{N-(3-[4-(3-amino-propyl)-piperazin-1-yl]-propyl)-N'[1dehdroabiety]-1,4,5,8-naphthalenetetracarboxydiimidly}-3,4,9,10-perylenebis(dicarboximide), (NPM) in$CHCl_3$.

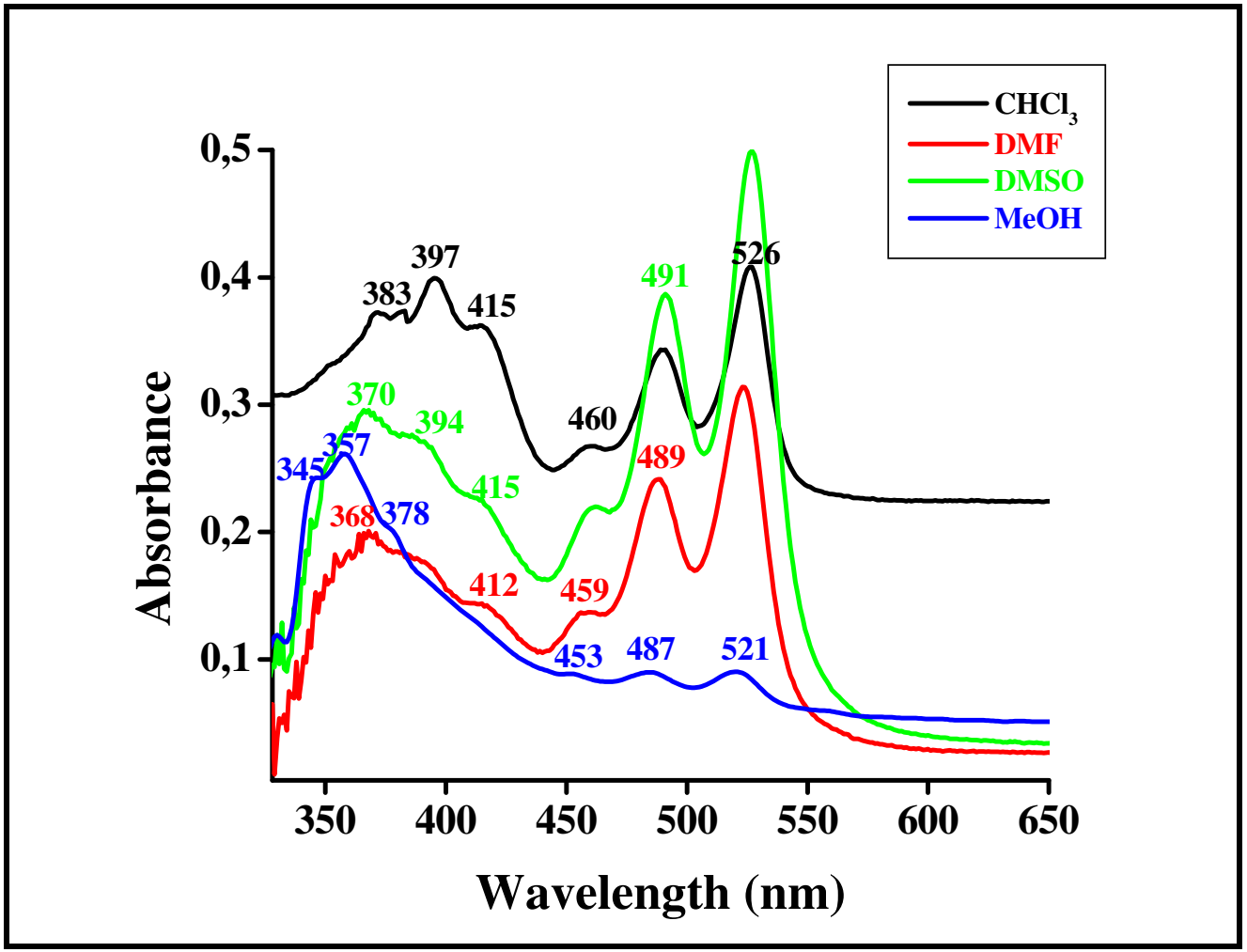

Figure 4.12 UV-vis absorption of NPM in $CHCl_3$, DMF, DMSO and MeOH.

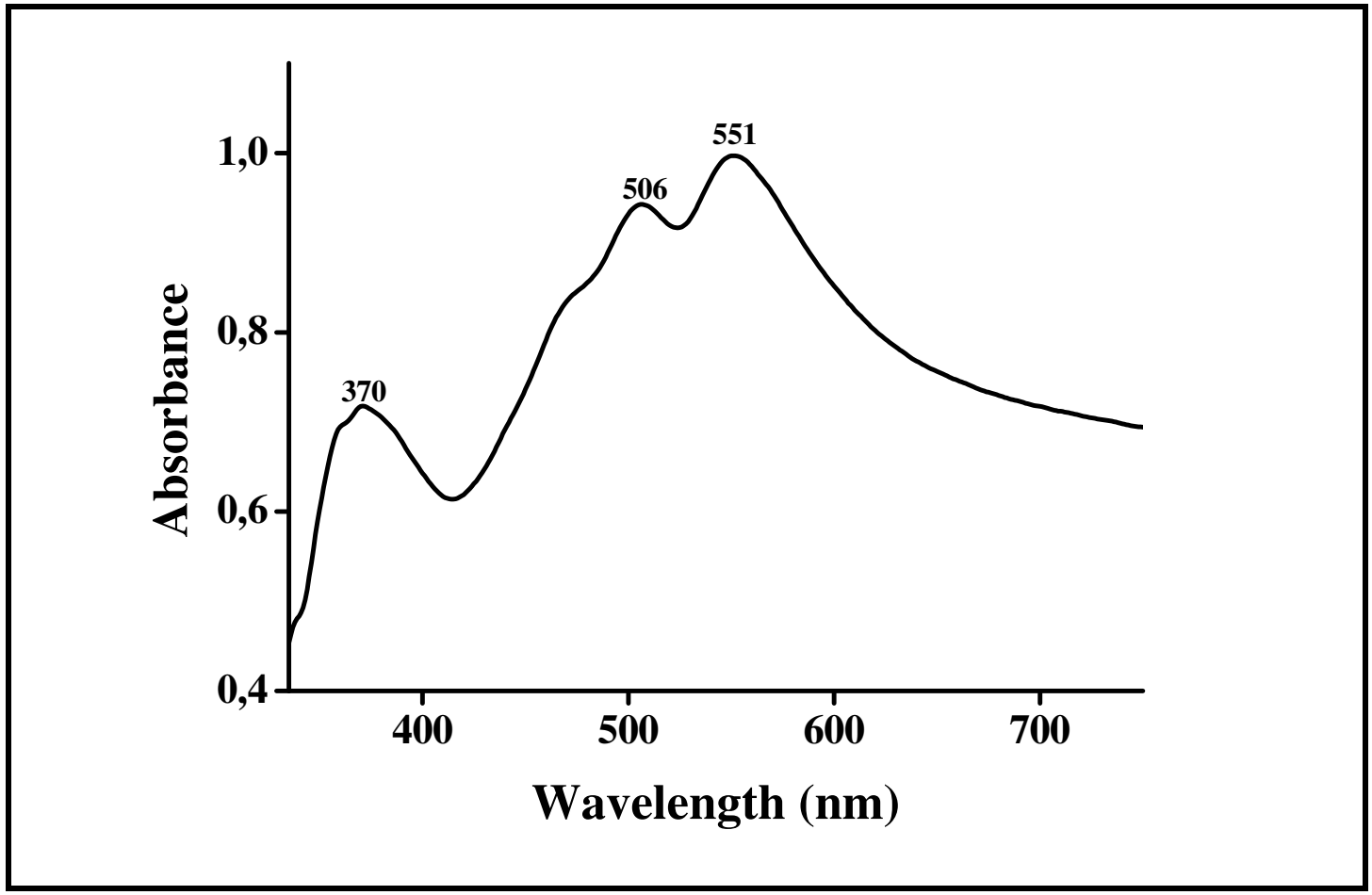

Figure 4.13 Solid state UV-vis absorption spectrum of NPM.

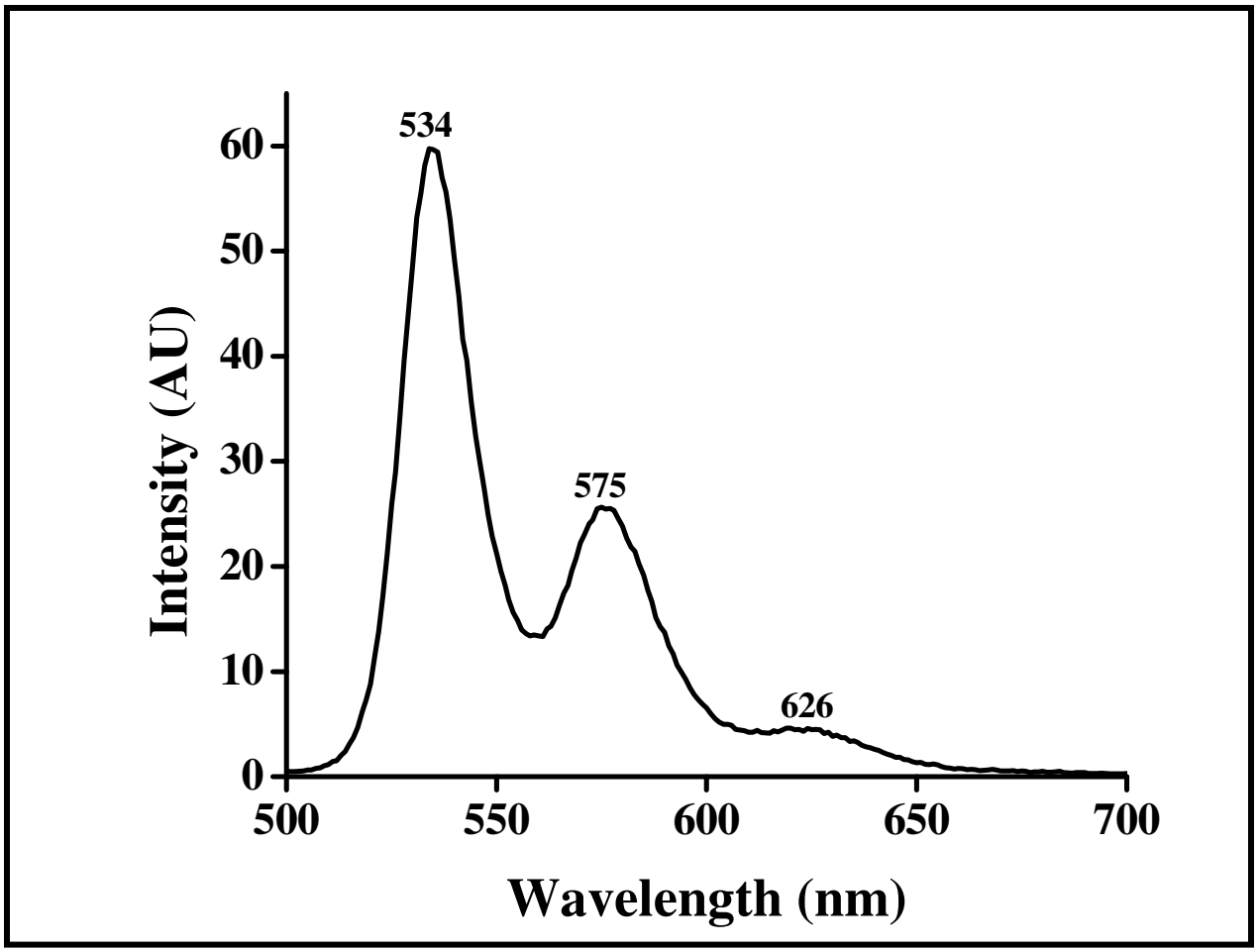

Figure 4.14 Emission spectrum of PDI in $CHCl_3$.

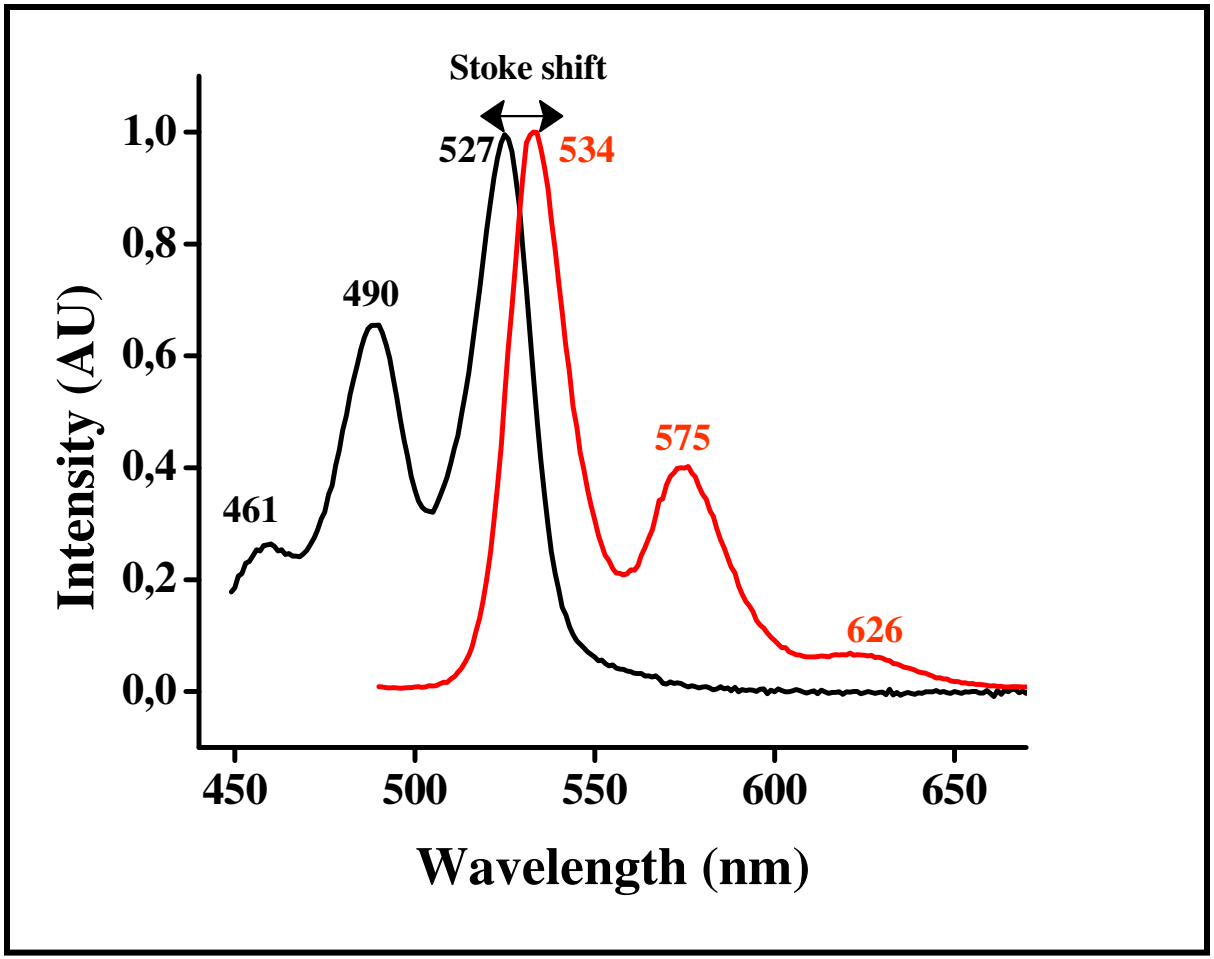

Figure 4.15 UV-vis absorption and emission spectra of PDI, λ_{exc} = 485 nm in $CHCl_3$

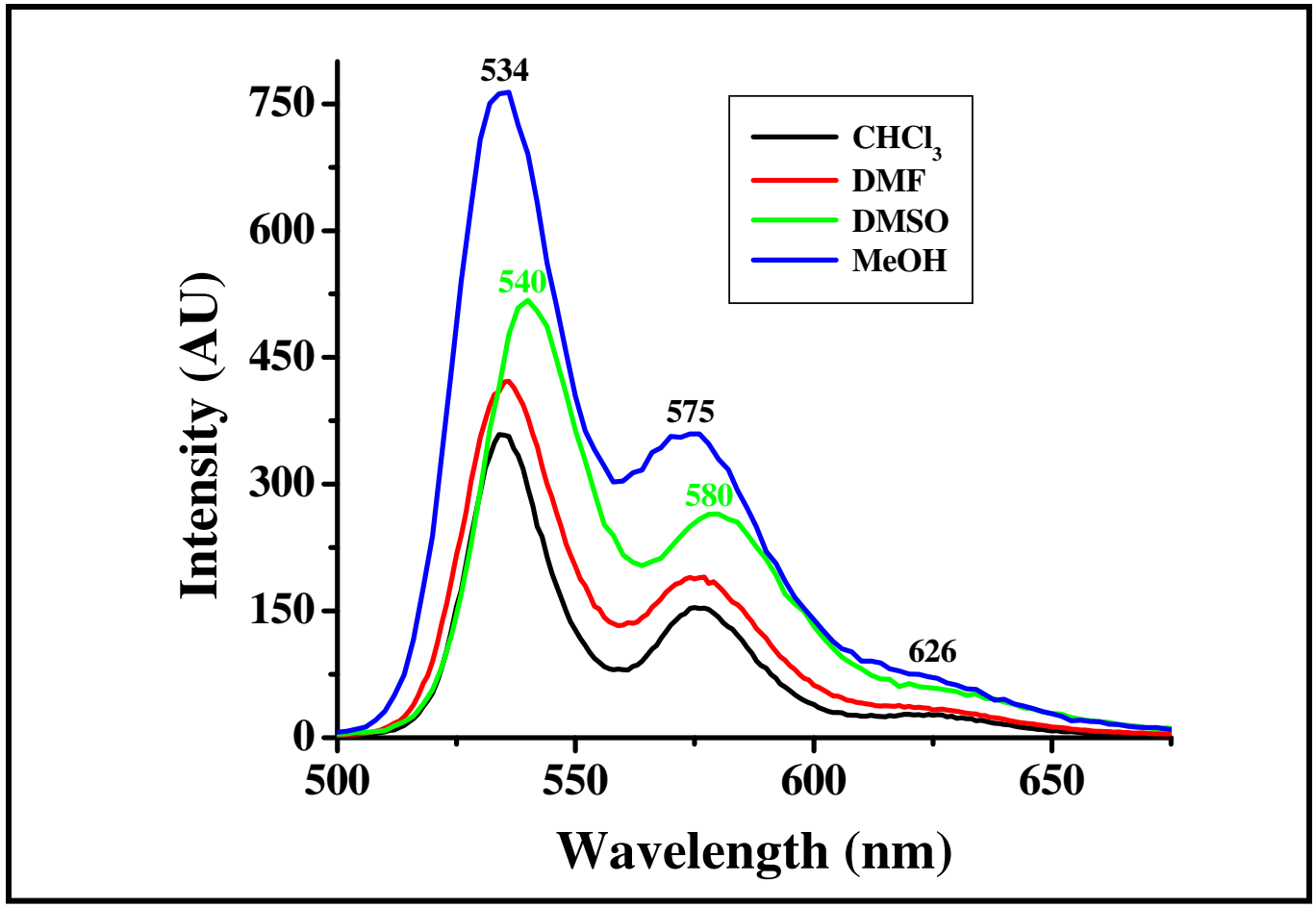

Figure 4.16 Emission spectra of PDI in CHCl3, DMF, DMSO and MeOH

.

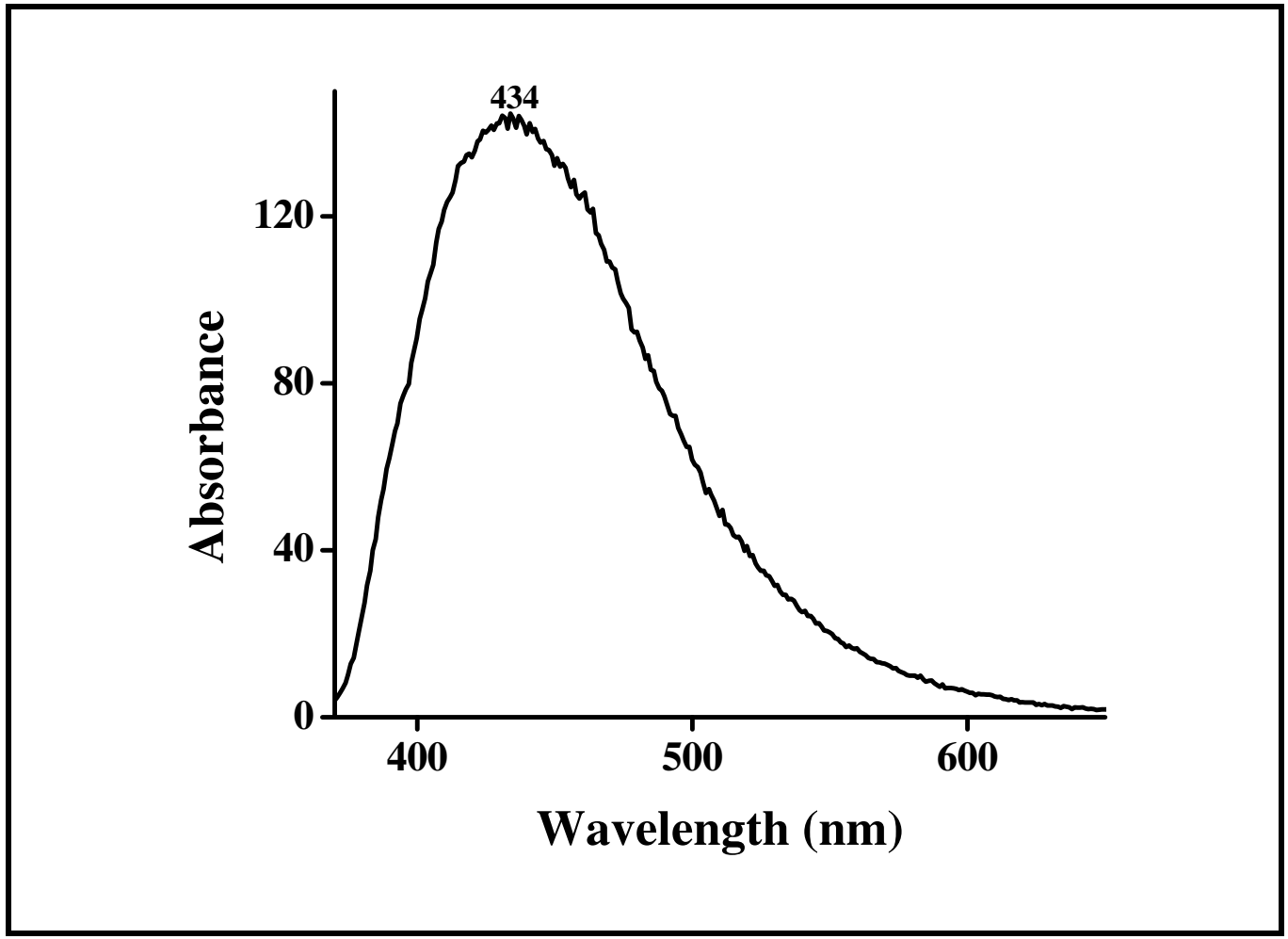

Figure 4.17 Emission spectrum of NMI in $CHCl_3$.

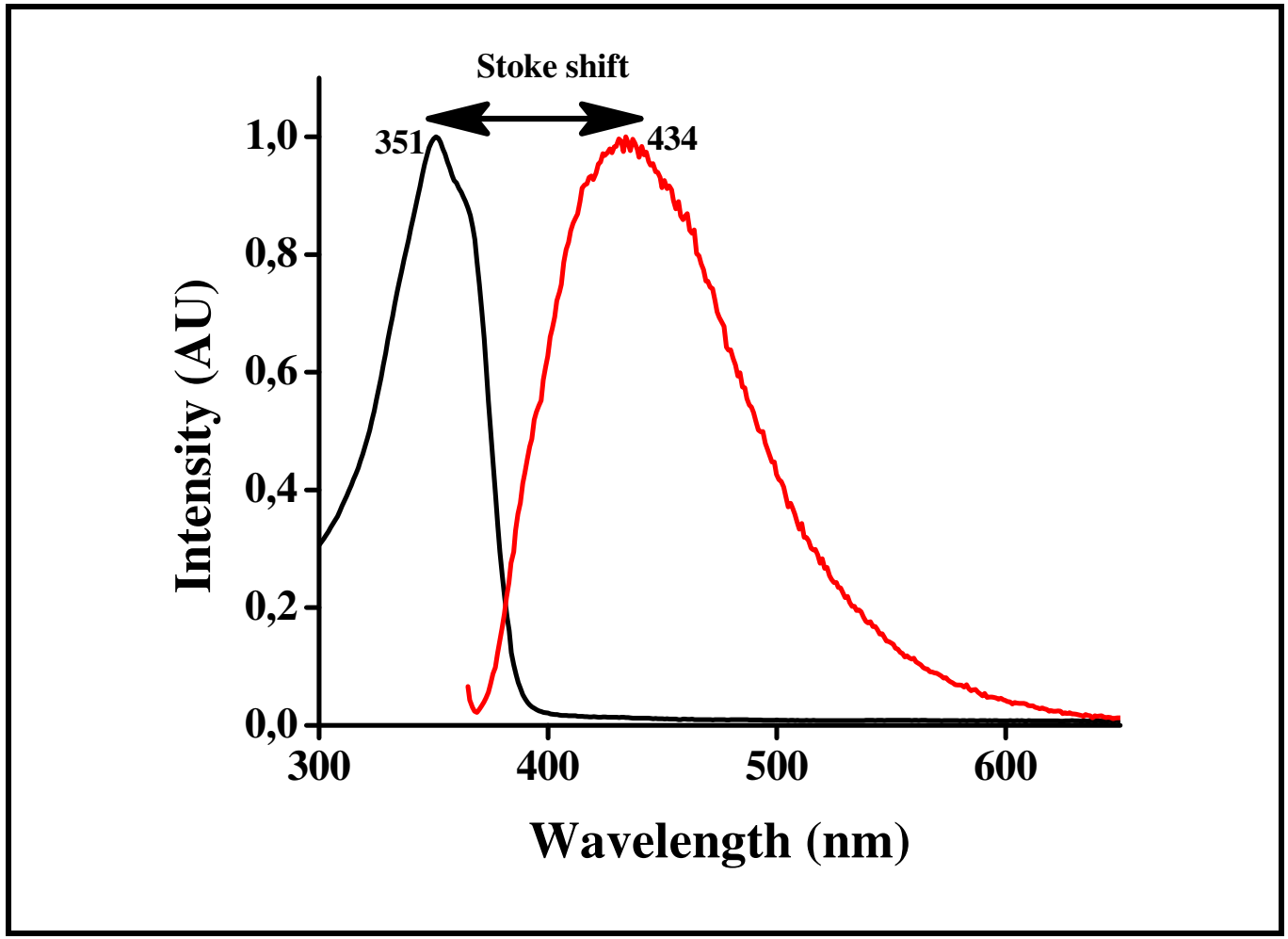

Figure 4.18 UV-vis absorption and emission spectra of NMI, λ_{exc} = 360 nm in $CHCl_3$

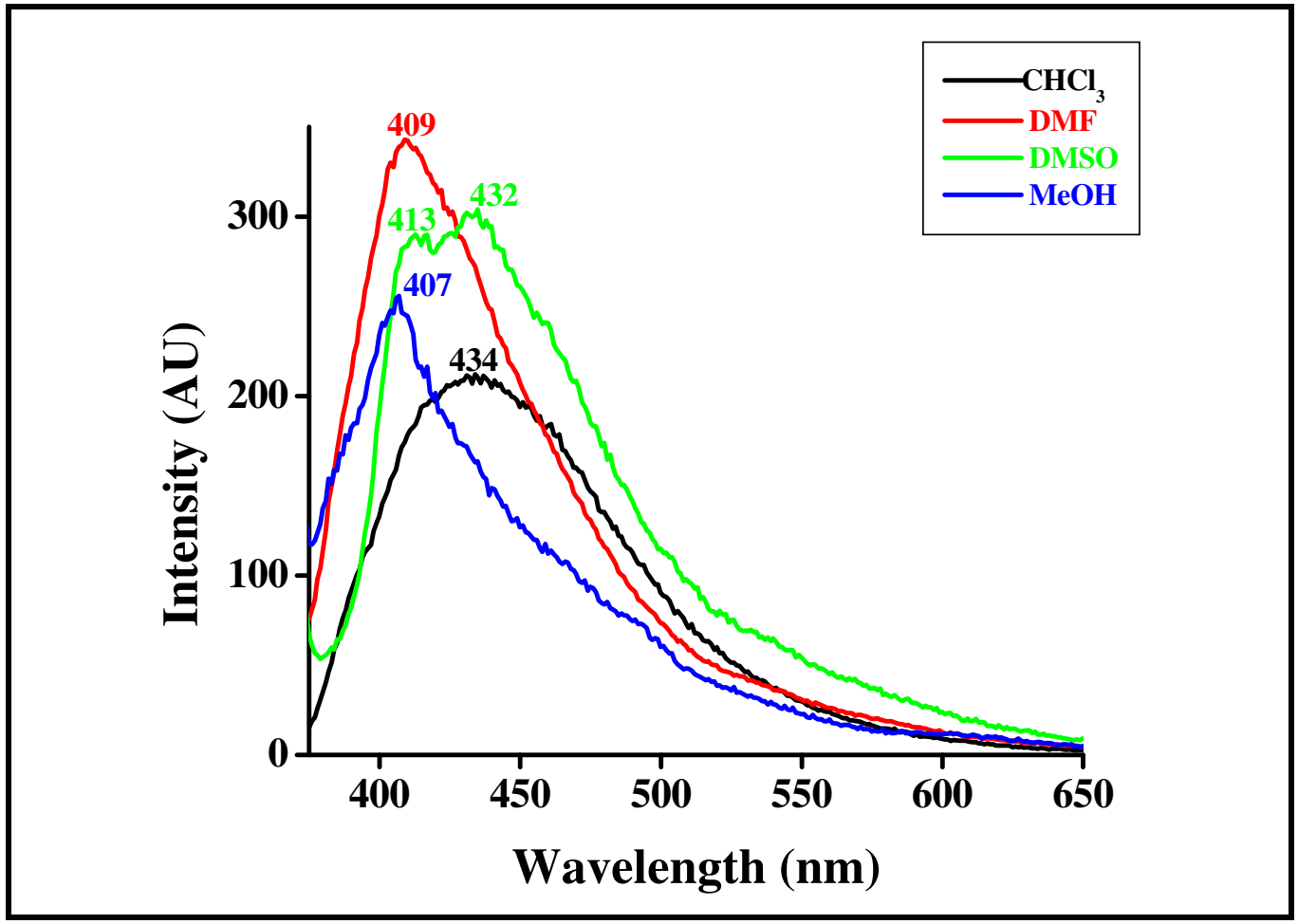

Figure 4.19 Emission spectra of NMI in $CHCl_3$, DMF, DMSO and MeOH.

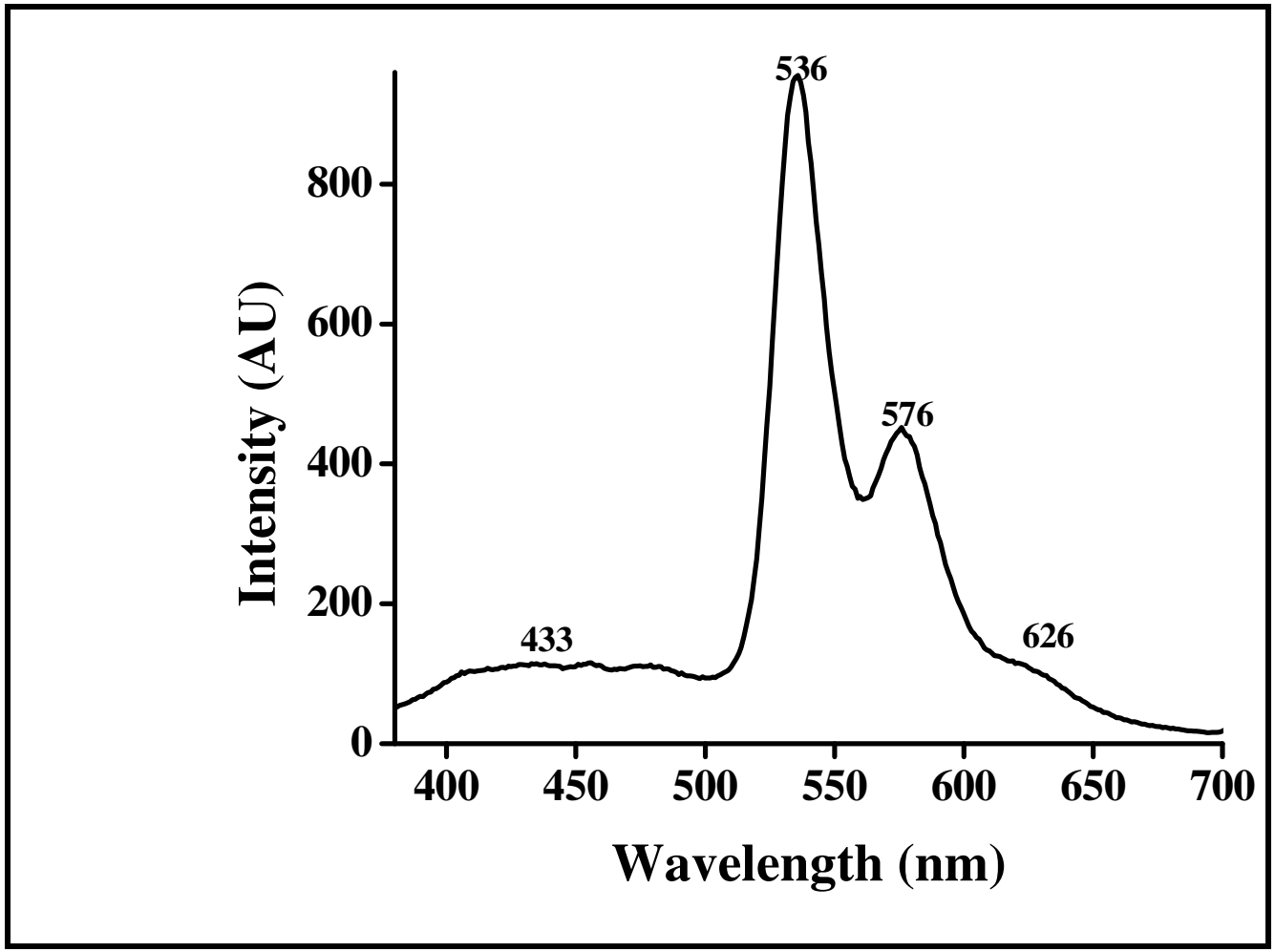

Figure 4.20 Emission spectrum of NPM in $CHCl_3$.

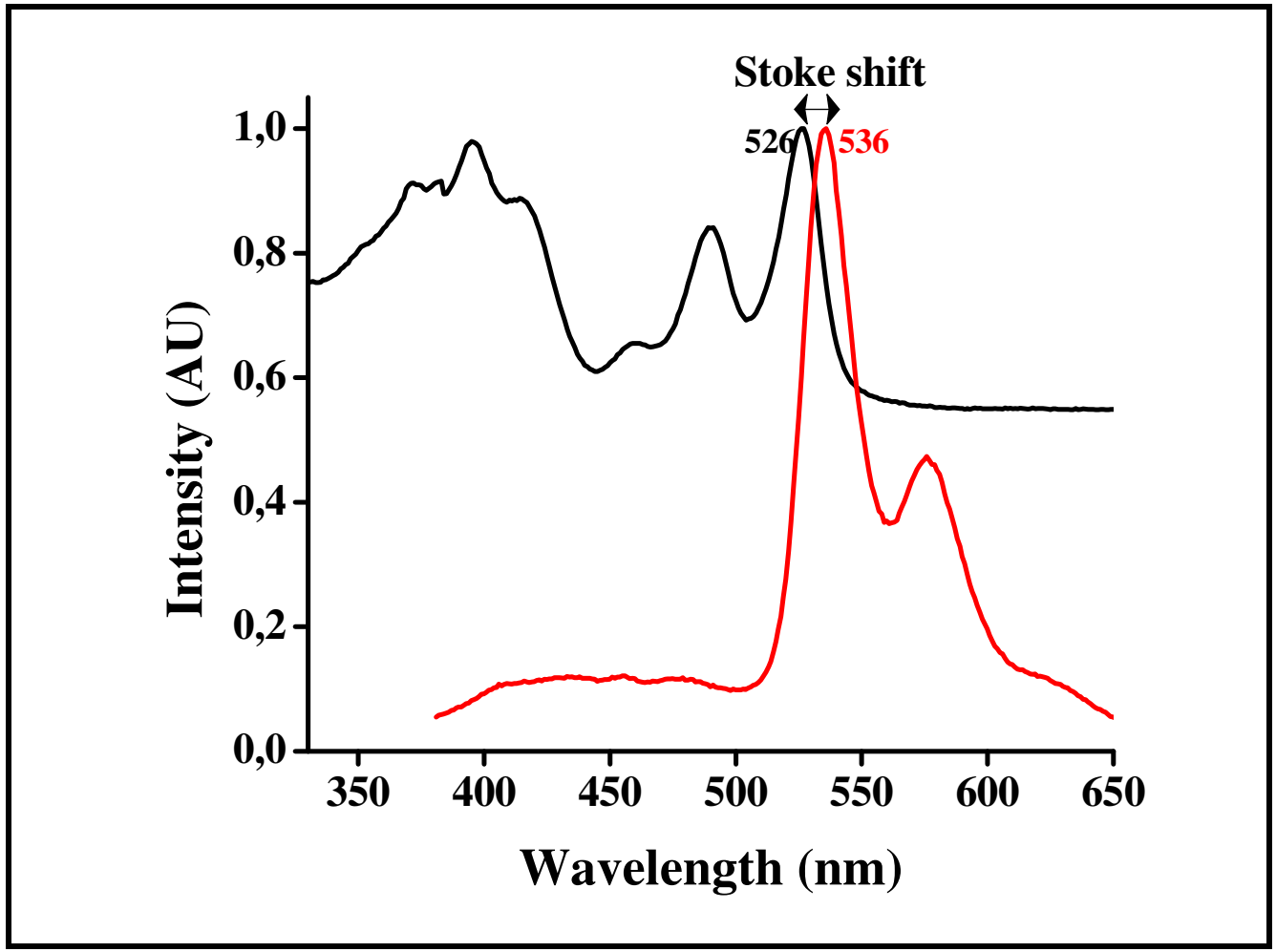

Figure 4.21 UV-vis absorption and emission spectra of NPM, λ_{exc} = 485 nm in $CHCl_3$.

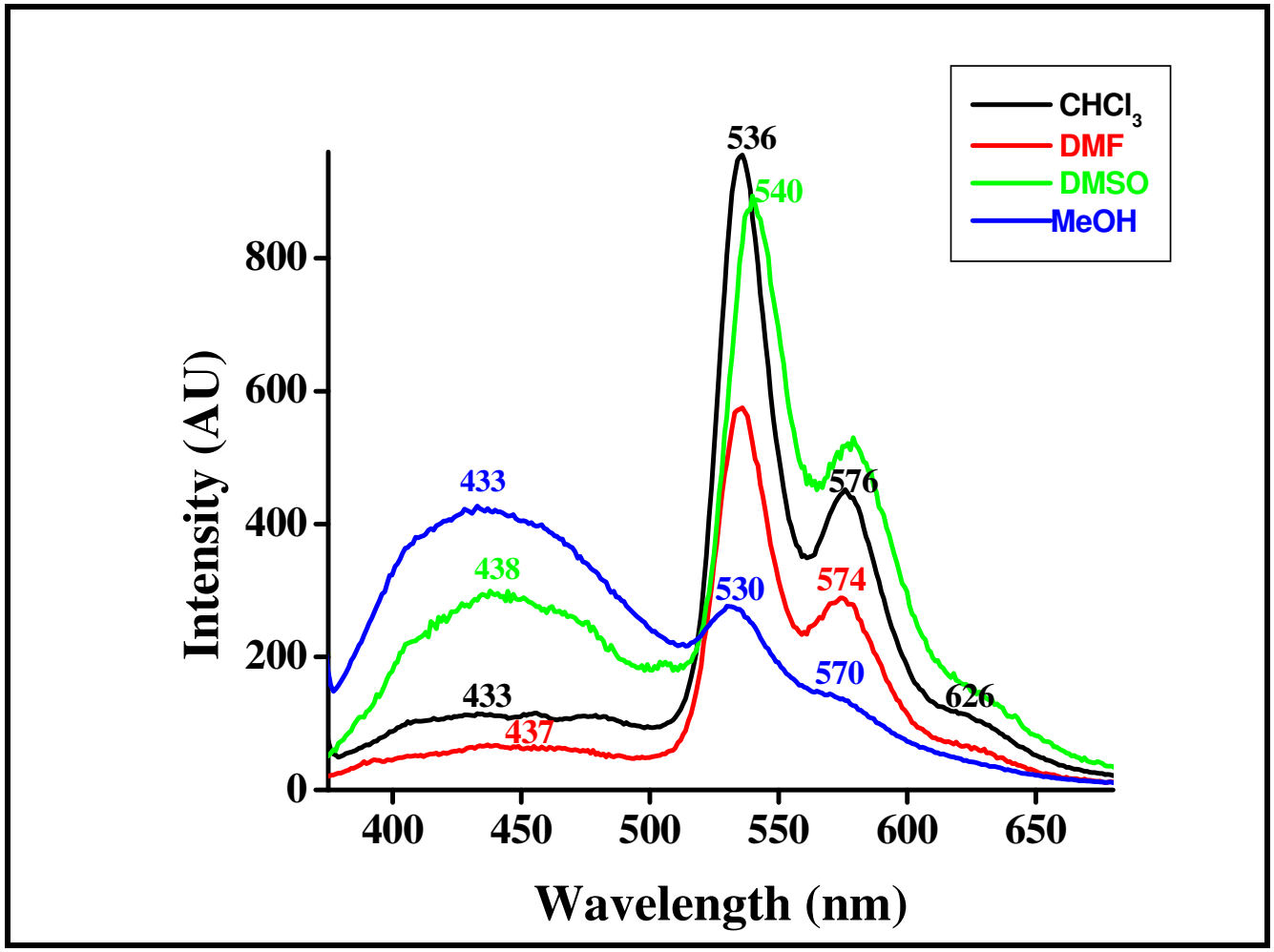

Figure 4.22 Emission spectra of NPM in $CHCl_3$, DMF, DMSO and MeOH.

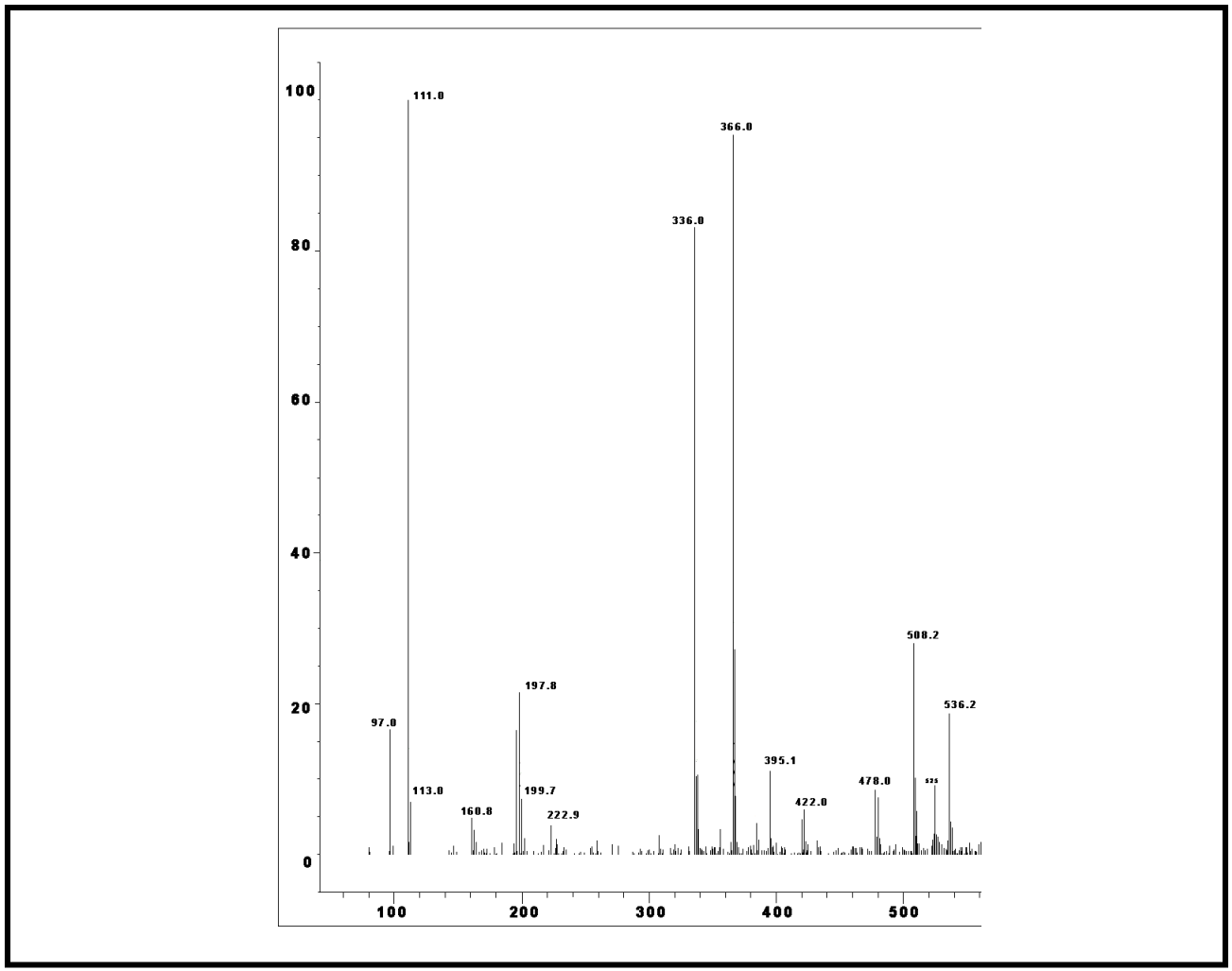

Figure 4.23 Mass Spectrum of NMI.

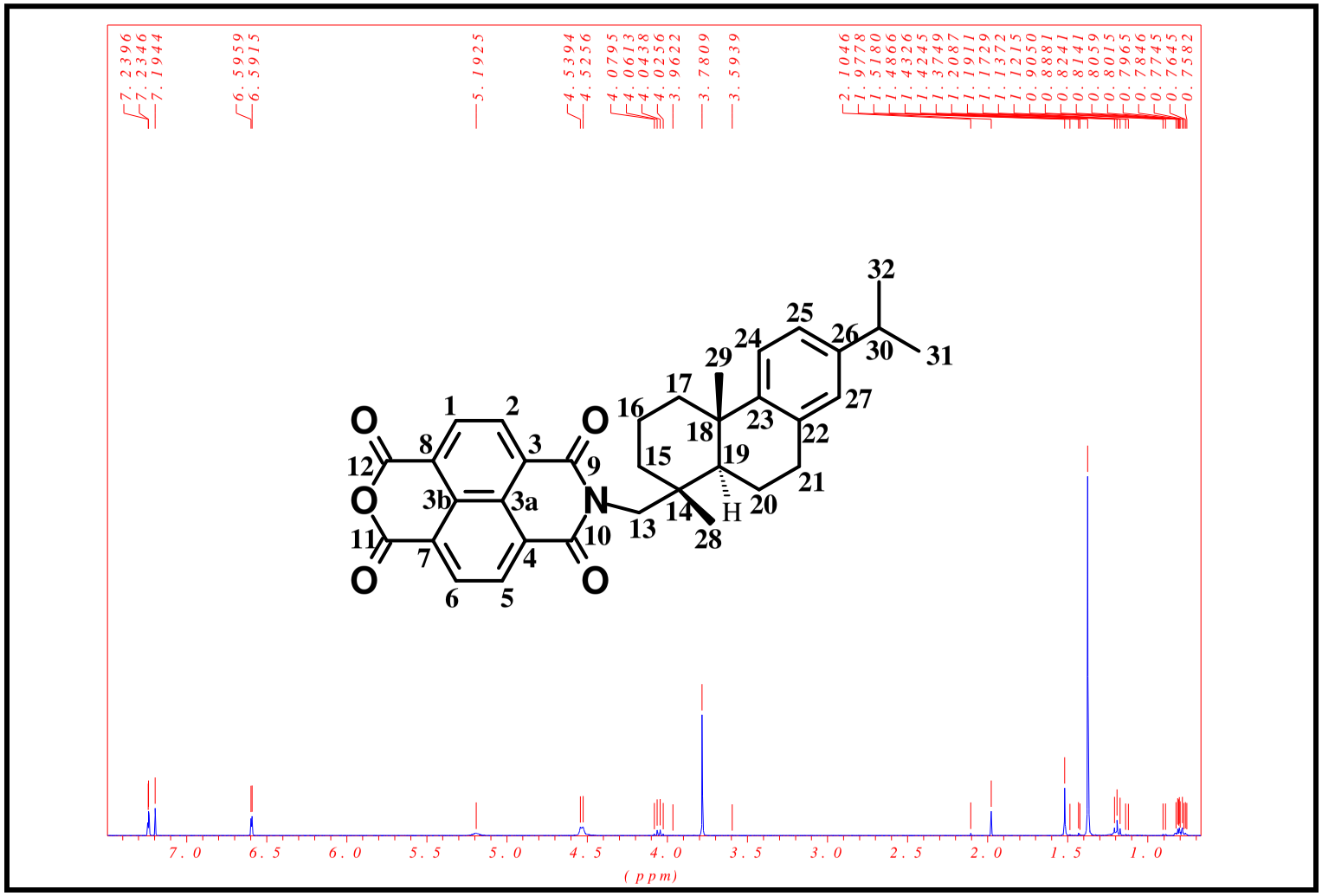

Figure 4.24 ^{1}H NMR spectrum of NMI in $CDCl_3$.

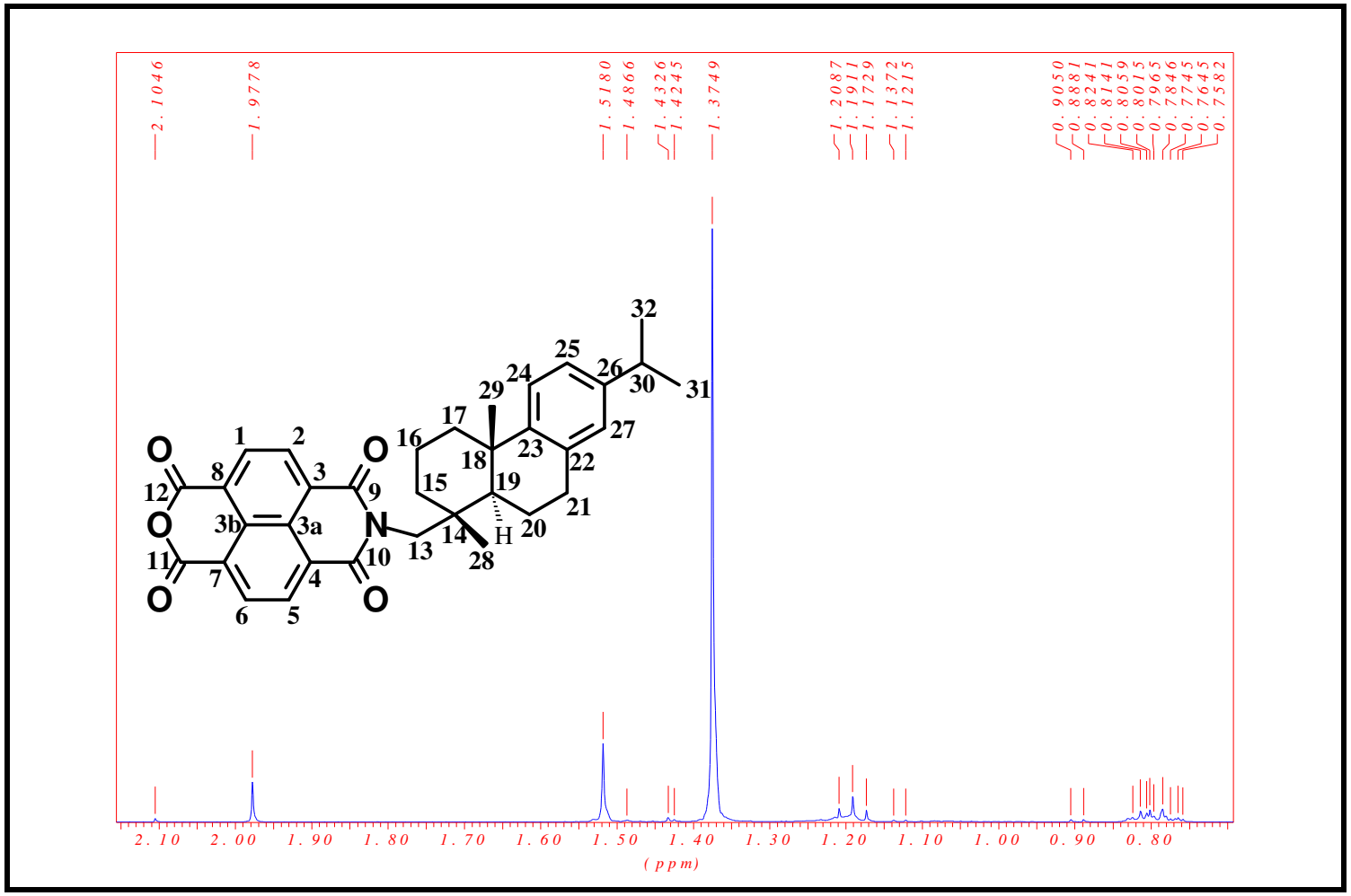

Figure 4.25 ^{1}H NMR spectrum of NMI, in $CDCl_3$.

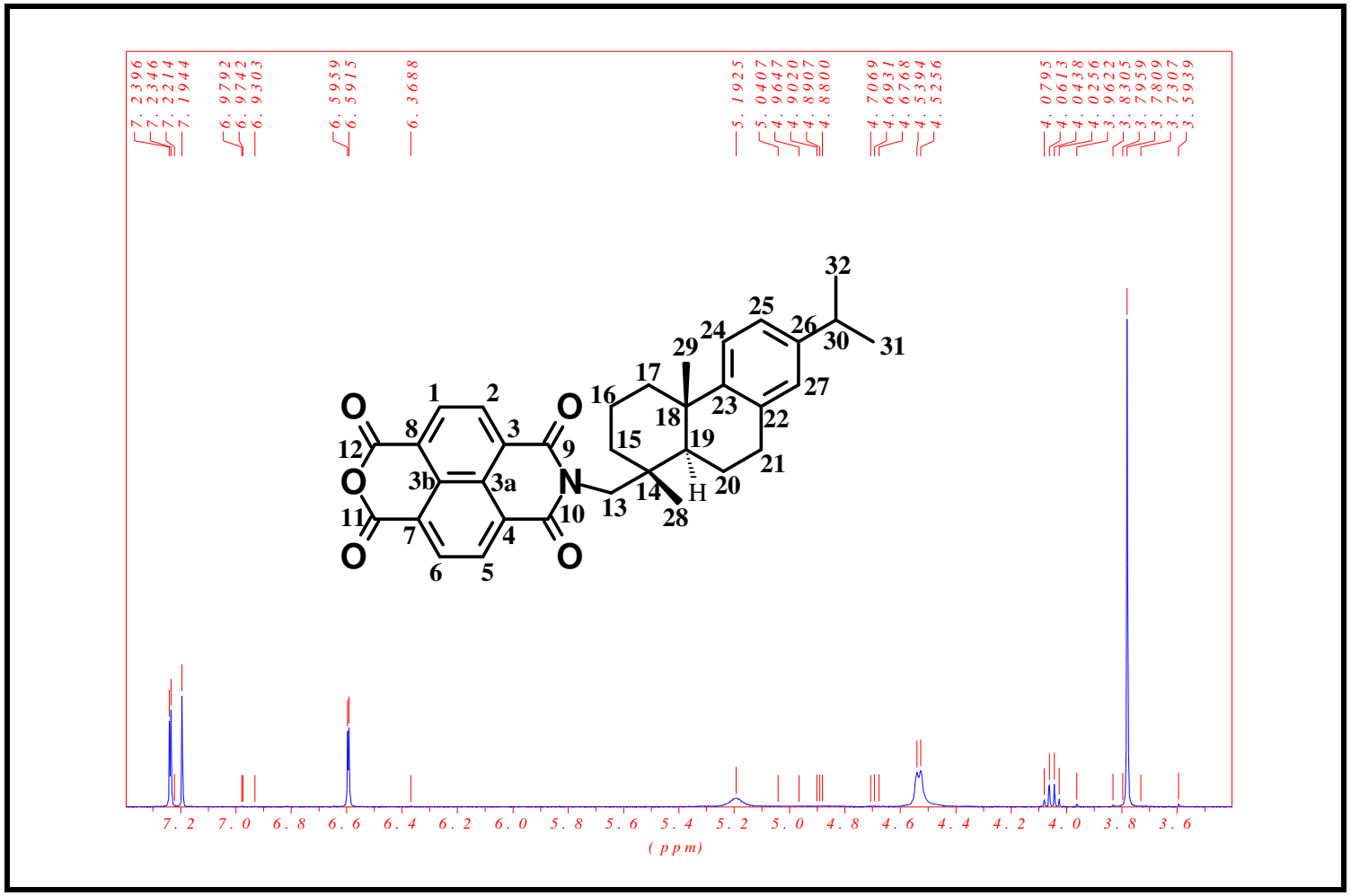

Figure 4.26 ^{1}H NMR spectrum of NMI, in $CDCl_3$.

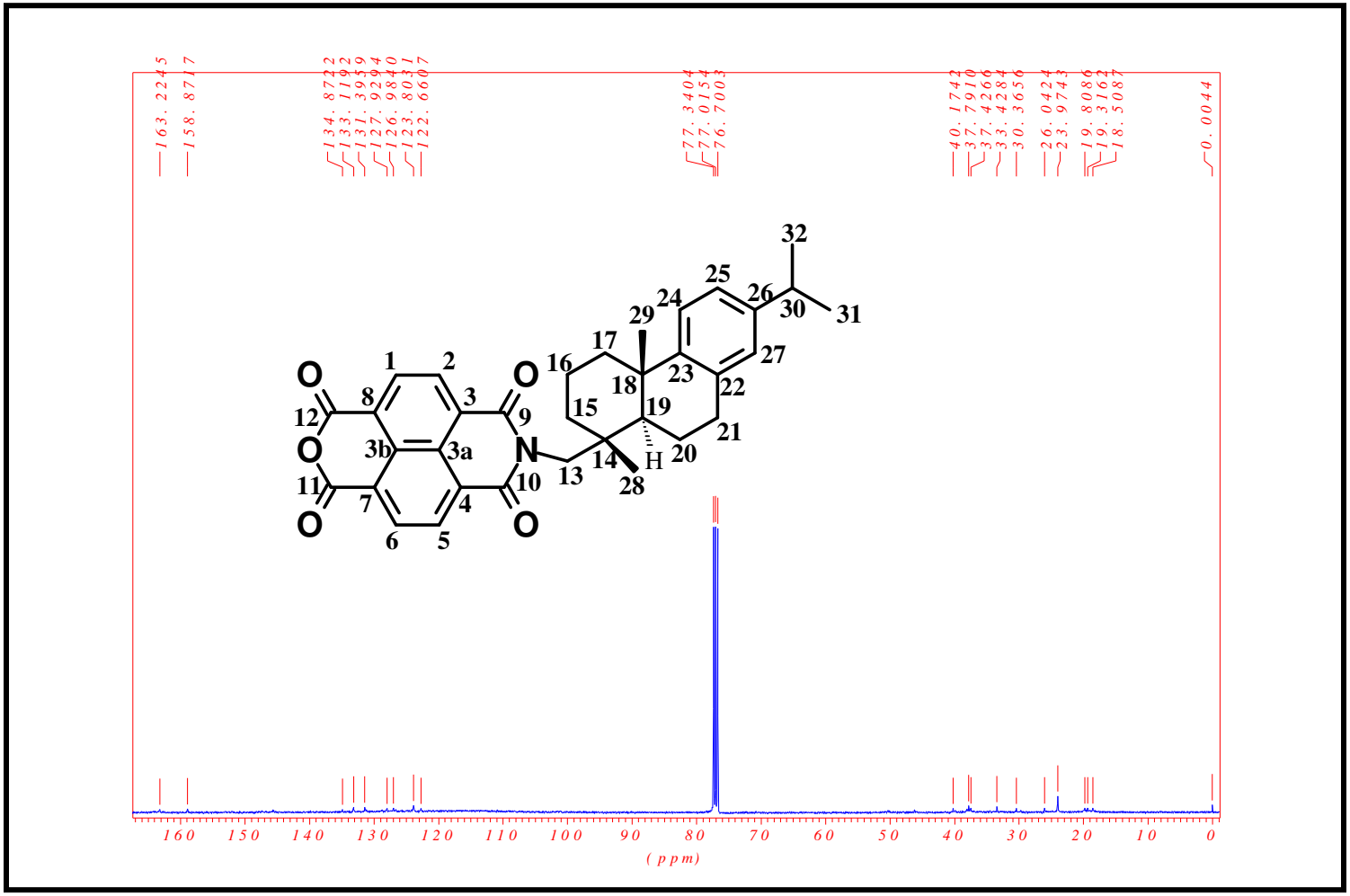

Figure 4.27 ^{13}C NMR spectrum of NMI, in $CDCl_3$.

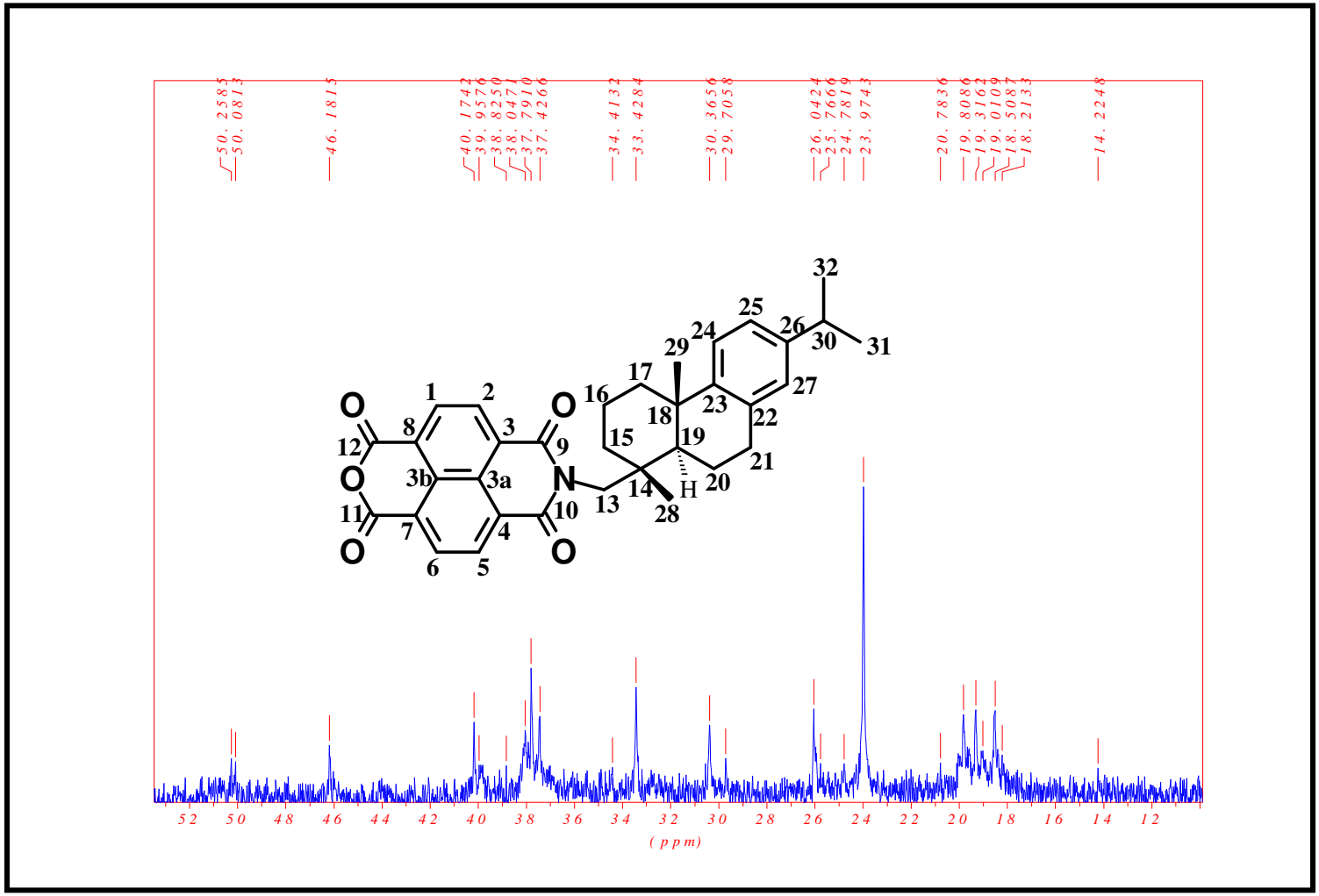

Figure 4.28 ^{13}C NMR spectrum of NMI, in $CDCl_3$.

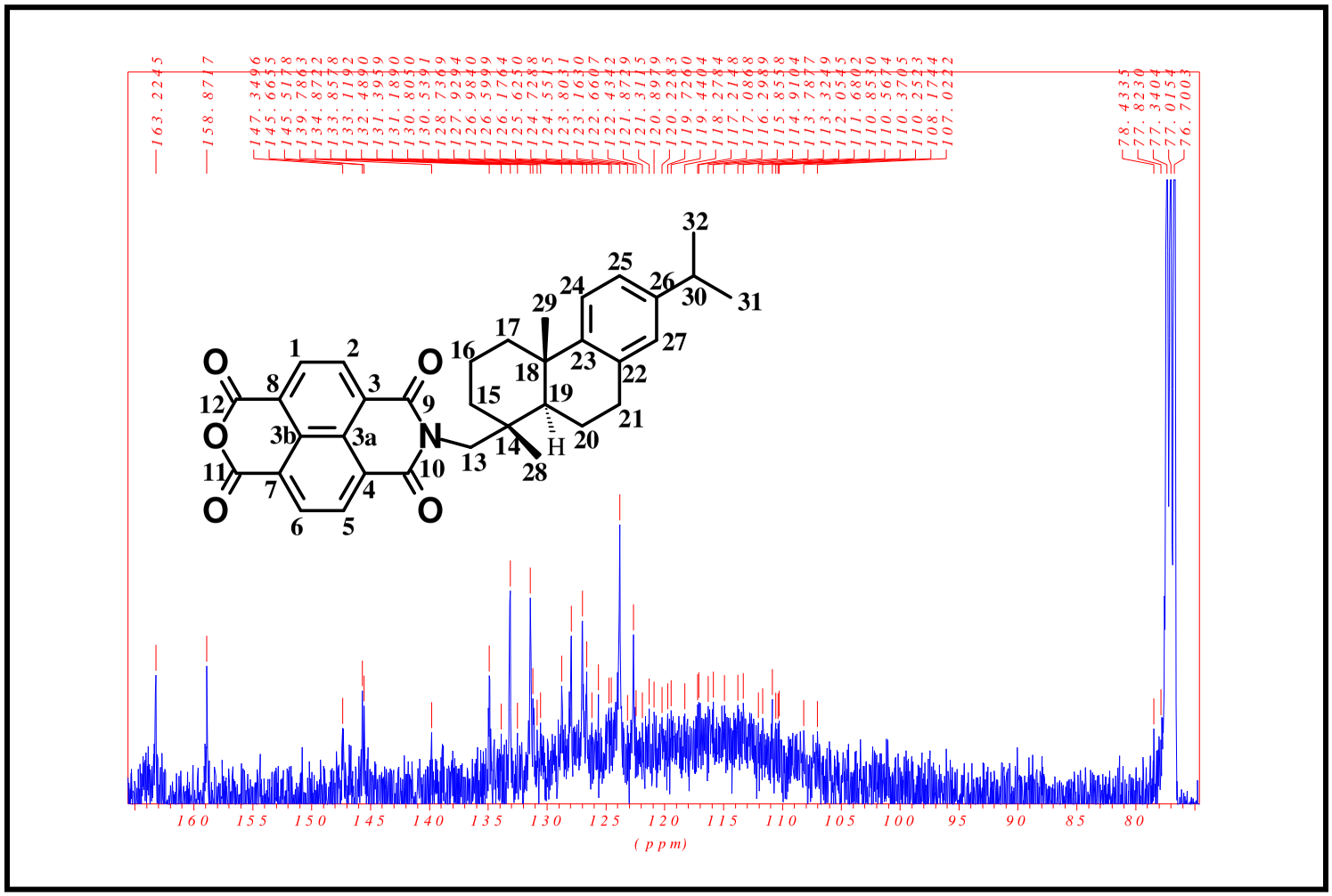

Figure 4.29 ^{13}C NMR spectrum of NMI, in $CDCl_3$.

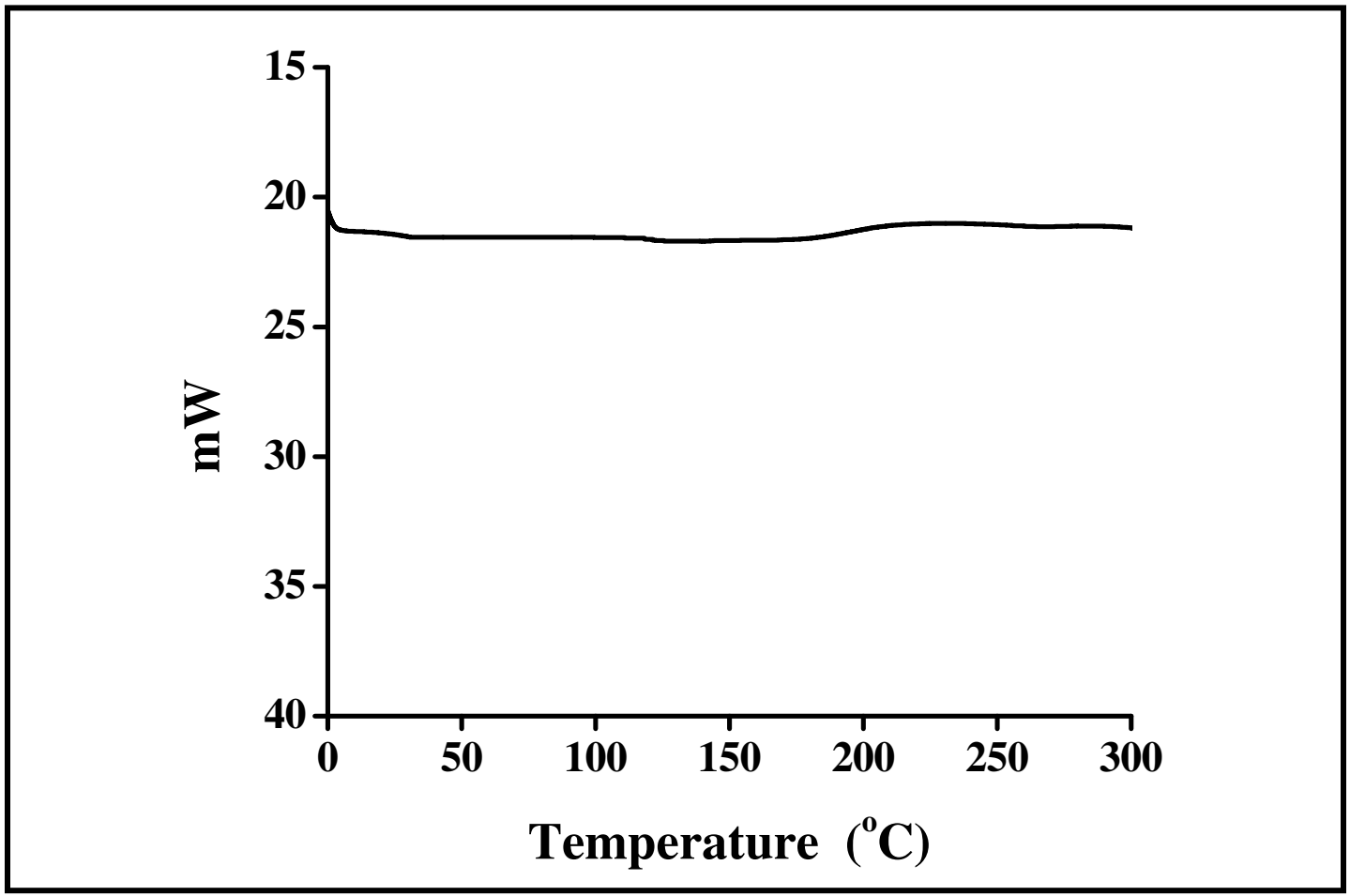

Figure 4.30 DSC curve of PDI at a heating rate of 10 ^{0}C / min in nitrogen.

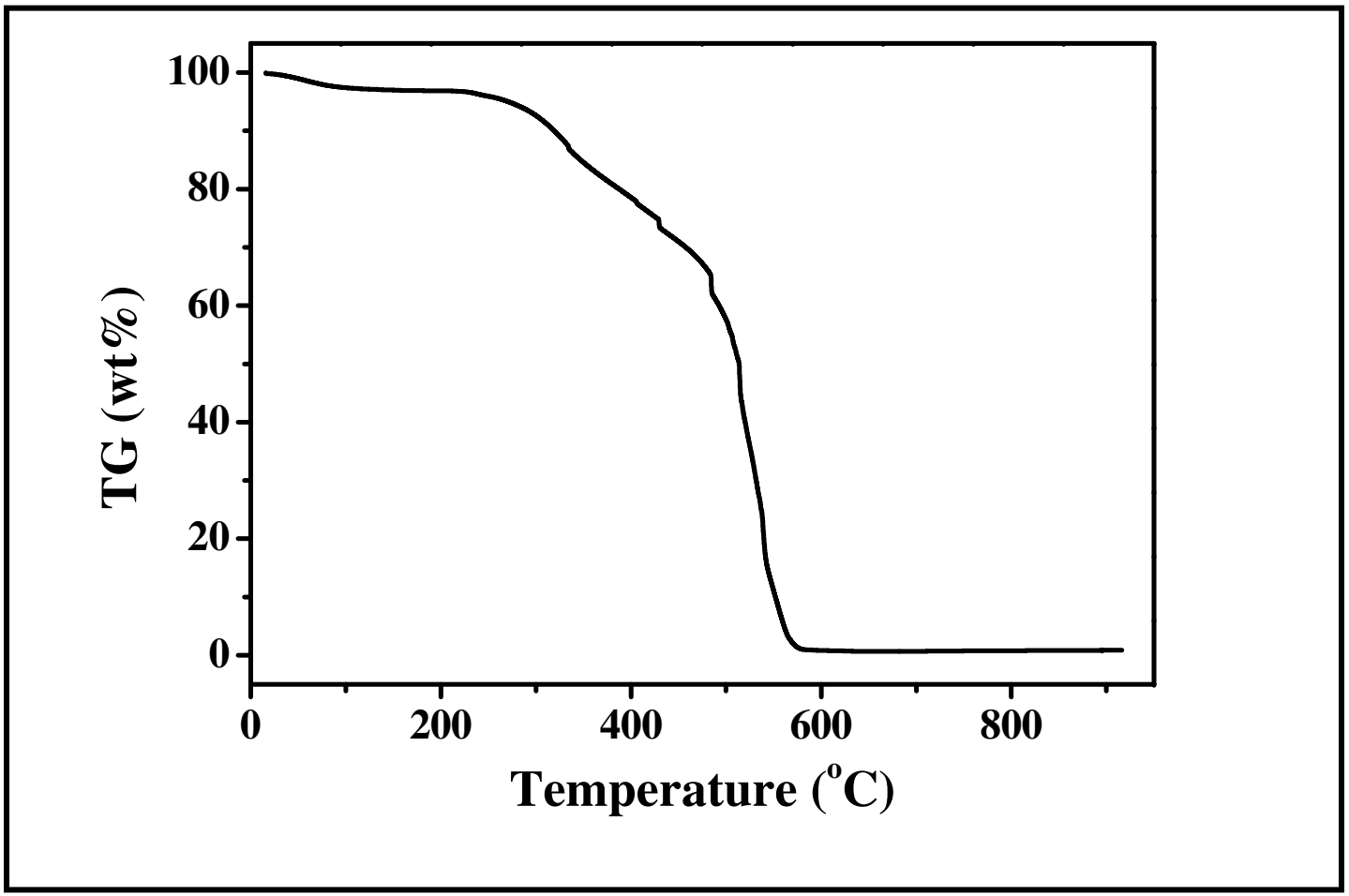

Figure 4.31 TGA thermogram of PDI at heating rate of 10 °C / min in oxygen.

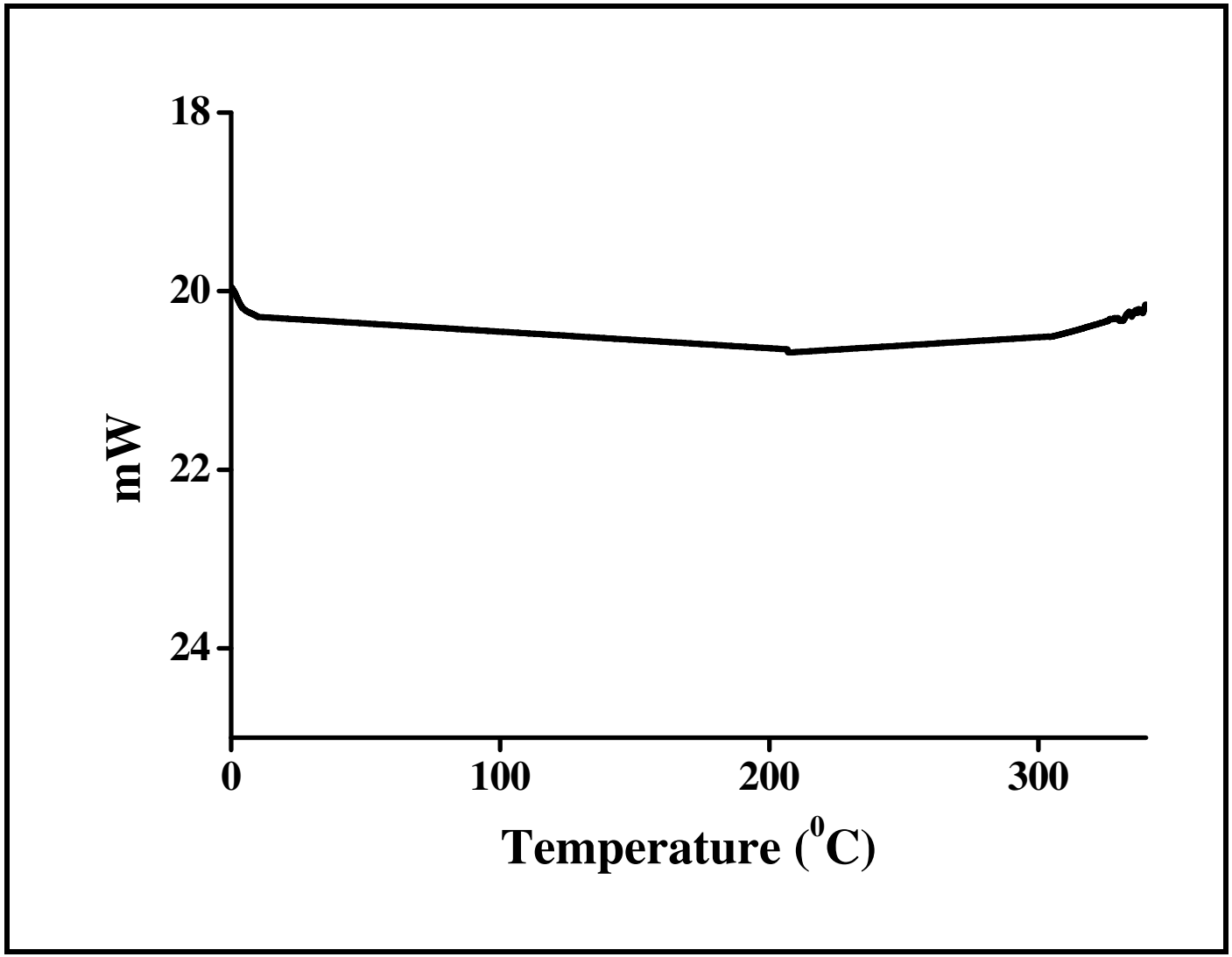

Figure 4.32 DSC curve of NMI at a heating rate of 10 ^{0}C / min in nitrogen.

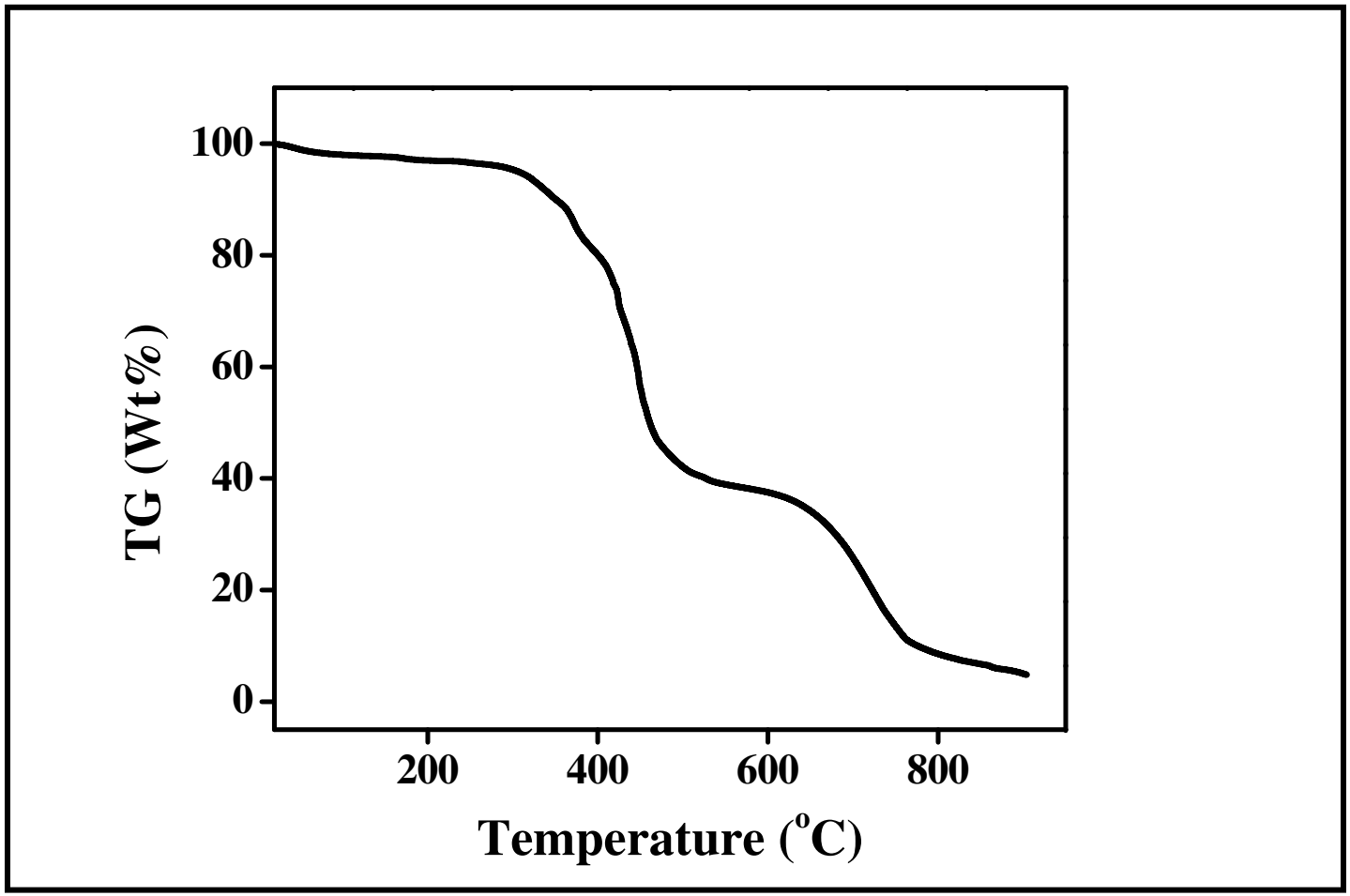

Figure 4.33 TGA thermogram of NMI at heating rate of 10 °C / min in oxygen.

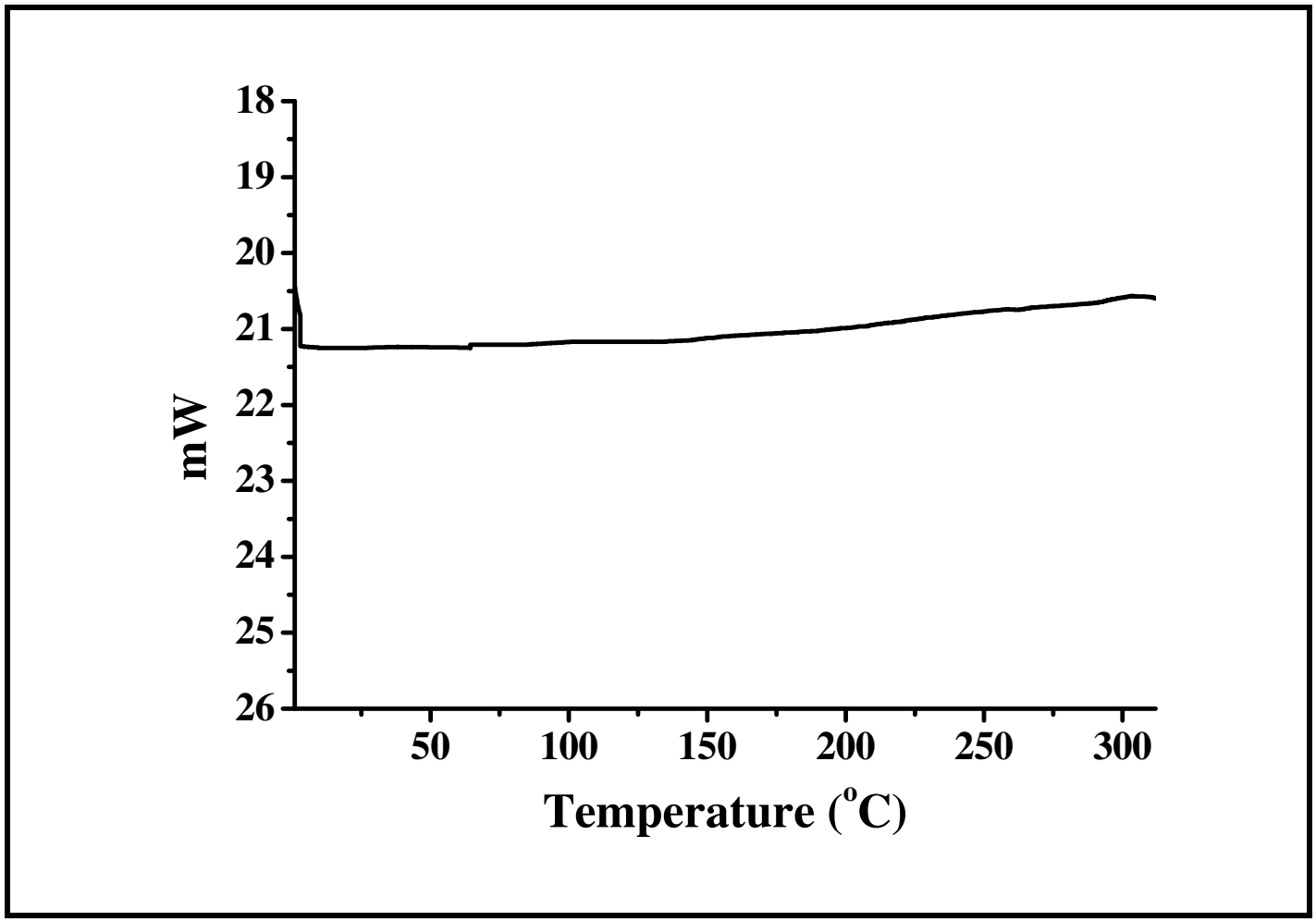

Figure 4.34 DSC curve of NPM at a heating rate of 10 ^{0}C / min in nitrogen.

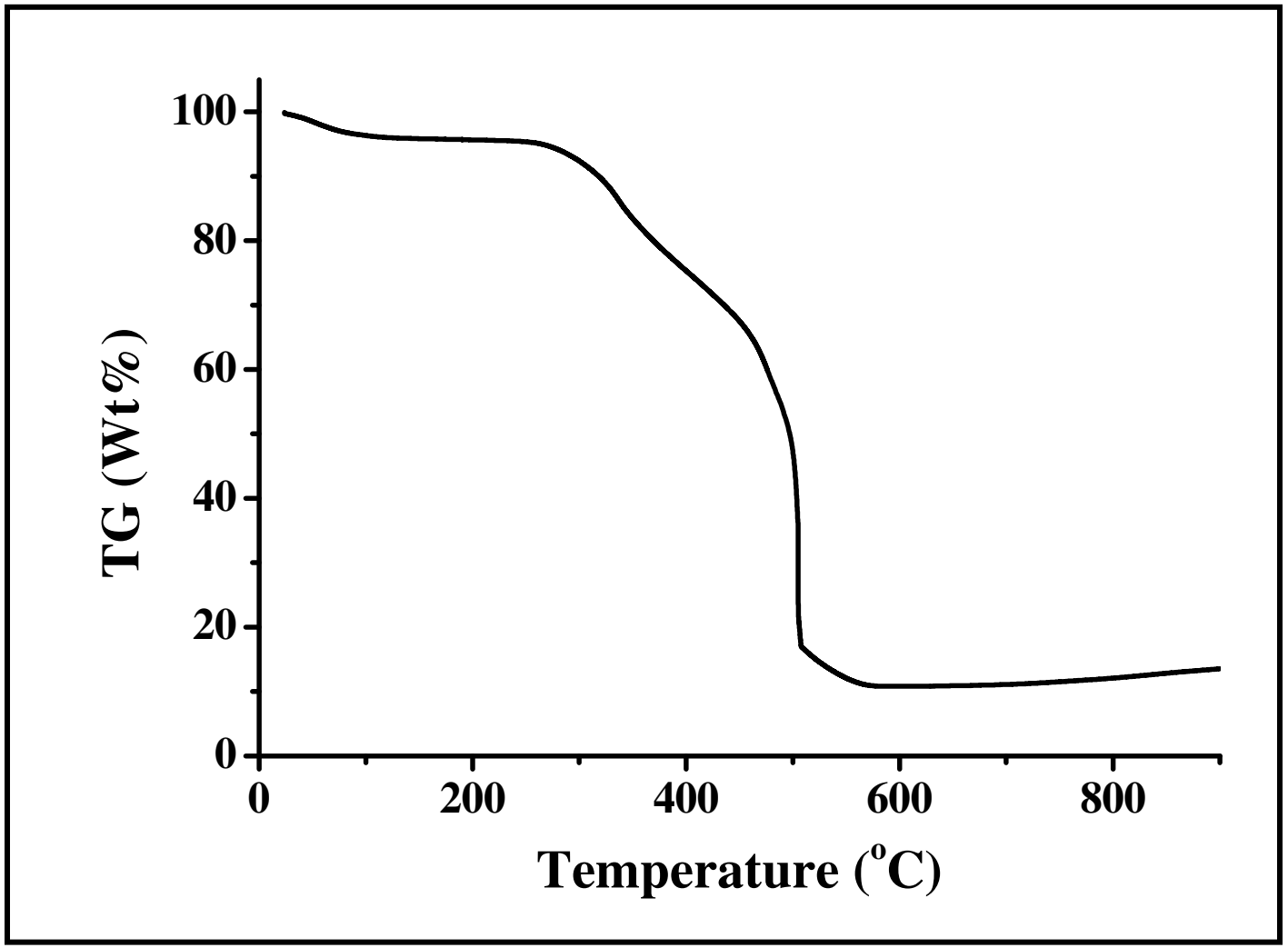

Figure 4.35 TGA thermogram of NPM at heating rate of 10 °C / min in oxygen.

CHAPTER 5

DISCUSSION

The synthesis and spectral analysis results of PDI, NMI and the NPM are discussed below.

5.1 Synthesis Analyses and IR Spectra

The structural characteristics of the products were checked with solid state IR spectra (Fig.4.2 - 4.4) of KBr pellets. The IR Spectrum of PDI, has shown characteristic bands at 3441 cm^{-1} (N-H stretch); 3083 cm^{-1} (aromatic C-H stretch); 2928 cm^{-1}, 2827 cm^{-1} (aliphatic C-H stretch); 1694 cm^{-1},1639 cm^{-1} (imide C=O stretch); 1576 cm^{-1} (C=C stretch); 1351 cm^{-1} (C-N stretch); 813 cm^{-1} and 750 cm^{-1} (C-H bend).

The IR Spectrum of NMI has shown characteristic bands at 3075 cm^{-1} (aromatic C-H stretch), 2940 cm^{-1}, 2866 cm^{-1} (aliphatic C-H stretch), 1701 cm^{-1} (anhydride C=O stretch), 1651 cm^{-1} (imide C=O stretch), 1585 cm^{-1} (aromatic C=C stretch), 1340 cm^{-1} (C-N stretch), 1238 cm^{-1} (C-O-C stretch), 775 cm^{-1} (C-H bend).

The IR Spectrum of NPM, has shown characteristics bands at 3011 cm^{-1} (aromatic C-H stretch); 2938 cm^{-1}, 2802 cm^{-1} (aliphatic C-H stretch); 1685 cm^{-1}, 1639 cm^{-1} (imide C=O stretch); 1585 cm^{-1} (aromatic C=C stretch), 1340 cm^{-1}, 1248 cm^{-1} (C-N stretch); 804 cm^{-1} and 740 cm^{-1} (C-H bend).

5.2 Analysis of UV Spectra

The UV-vis absorption spectrum of PDI shows three characteristic bands at 527, 490 and 461 nm in $CHCl_3$ (Fig.4.5).

UV spectra of PDI in various solvents (DMSO, DMF, $CHCl_3$ and MeOH) are shown in Fig.4.6. PDI showed a red shifted absorption peaks (461, 490 and 527 nm) in polar aprotic solvent DMSO. It is expected that, protic and non-protic solvents should have different solvations and specific interactions with PDI, due to their polarity and possibly intramolecular and intermolecular interactions. The absorption spectra of PDI in solution and in solid state showed differences in terms of spectral shape which is attributed to different π-π stacking interaction in the solid state (Fig.4.6 and Fig.4.7).

The UV spectrum of NMI showed one band at 351 nm in $CHCl_3$ (Fig.4.8). UV spectra of the monoimide in different solvents (DMSO, DMF, $CHCl_3$ and MeOH) are shown in Fig.4.10. In all the solvents, one broad peak was observed which is attributed to charge transfer complex. Similarly, the solid state absorption spectrum of NMI (Fig.4.9) showed one broad absorption peak with an enhanced absorption band up to 550 nm. This happened due to the respective π-π stacking interactions in solid state (Fig.4.8 and Fig.4.9).

The UV-vis absorption spectrum of macromolecule, NPM, has shown six absorption peaks at 526,490, 460, 414, 397 and 383 nm in $CHCl_3$ (Fig.4.11) with an enhanced absorption range from 325 to 550 nm. This successful result was the main objective of the work.

UV spectra of the macromolecule in different solvents are shown in Fig.4.12. Characteristically six absorption bands are observed which the first three are belonging to naphthalene and the rest to perylene chromophores. Interestingly, in

polar aprotic solvents (DMF, DMSO), the bands related to naphthalene chromophore showed blue shift (370, 394 and 415 nm), however the bands related to perylene chromophore remained same (460, 491 and 526 nm).

Notably, in polar protic solvent methanol, NPM showed diminished absorption bands at 453, 487 and 521 nm which are belonging to perylene chromophore. This result is attributed to possible hydrogen bonding and charge transfer complex. Although the peak shapes of solid state absorption spectrum were not very different from the absorption peaks in solution, a much broader range of absorption was noticed in solid state. The broad band indicated the strong π-π stacking interactions in solid state (Fig.4.13).

5.3 Analysis of Emission Spectra

The emission spectrum of PDI (λ_{exc} = 485 nm) shows three characteristic emission bands at 535 nm, 575 nm and 626 nm with about 9 nm Stoke shift in $CHCl_3$ (Fig.4.14 – 4.15) and the emission peaks intensities decrease respectively. Surprisingly, the emission peak values of PDI remain nearly the same in all of the solvents reported except a little red shift in DMSO (Fig.4.16). Remarkably, the small redshift in polar aprotic solvents is an indication of better solvation of the excited state than of the polar ground state of PDI.

The emission spectrum of NMI (λ_{exc} = 360 nm) in $CHCl_3$ solution shows a broad structureless emission at 434 nm (Fig.4.17) representing an excimer like emission.

The emission spectra in different solvents ($CHCl_3$, DMF, DMSO and MeOH) are shown in Fig.4.19. In different solvents used, a broad structureless, excimer like emission were observed.

The emission spectrum of NPM which was taken at λ_{exc} = 360 nm shows four characteristic emission bands at 433 nm, 536 nm, 576 nm, 626 nm with about 10 nm Stoke shift in $CHCl_3$ (Fig.4.20 – 4.21). Similar to the absorption spectra of NPM (Fig.4.11- Fig.4.13), emission spectra include both the naphthalene core (at 433 nm) and perylene core (at 536, 576, and 626 nm) emissions.

The emission spectra of macromolecule in different solvents ($CHCl_3$, DMF, DMSO and MeOH) are shown in Fig.4.22. In $CHCl_3$, and DMF, the emission maxima (at 433 nm, 437 nm) intensity for naphthalene chromophore were very low comparing to the perylene chromophore emission maxima intensities. On the other hand, the observed results occurred in a completely opposite manner in DMSO. Notice that the emission bands of naphthalene chromophore were intensified in DMSO whereas the emission bands related to perylene chromophore diminished in methanol.

5.4 Analysis of MS Spectra

The mass spectrum of PDI, NPM have not been taken due to poor solubility of the compounds.

Fig.4.23 shows the LC-MS spectrum of NMI. The mass spectrum confirmed the structure. The molecular ion peak of NMI has been detected at 536 m/z (M-1).

5.5 Analysis of NMR

The NMR spectra of PDI and NPM could not be obtained due to the poor solubility.

The NMR spectrum of NMI confirms its structure and purity. Complete analyses of the compound have been given below (Fig.4.24 – 4.29).

N-(1-dehydroabietyl)-1,4,5,8-naphthalenetetracarboxylic-1,8-anhydride-4,5-imide, NMI

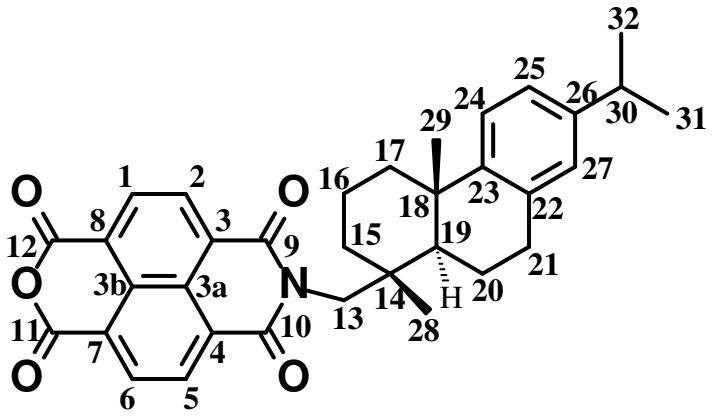

NMI

^{1}H NMR, δ_H (ppm) (400 MHz, $CDCl_3$): 7.24 (d, *J* = 2.00 Hz, 4Ar-H, H-C(1), H-C(2), H-C(5), H-C(6)), 6.59 (d, *J* = 1.76 Hz, 3Ar-H, H-C(24), H-C(25), H-C(27)), 3.78 (s, 2CH, H-C(30), H-C(19); 1CH_2, H_2-C(13)), 1.97 (s, 1CH_2, H_2-C(21)), 1.52-1.17 (4CH_3, H_3-C(28), H_3-C(29), H_3-C(31), H_3-C(32); 3CH_2, H_2-C(16), H_2-C(17), H_2-C(20)), 0.83-0.76 (m, 1CH_2, H_2-C(15)).

^{13}C NMR, δ_C (ppm) (100 MHz, $CDCl_3$): 163.226 (4(C), C(9)-C(12)), 158.869 (4CH, C(1), C(2), C(5), C(6)), 145.66 (2(C), C(3a), C(3b)), 145.52 (3(C), C(22), C(23), C(26), 134.87-131.40 (4(C), C(3), C(4), C(7), C(8)), 128.74-125.63 (3CH, C(24), C(25), C(27)), 123.80 (1CH, C(19)), 122.66 (1CH_2, C(13)), 121.31-110.85 (2

CH, C(15), C(17); $2CH_2$, C(14), C(18)), 46.18 (1CH, C(30)), 40.17 ($1CH_2$, C(21)), 33.43-26.04 ($2CH_3$, C(28), C(29)), 23.98 ($2CH_3$, C(31), C(32)), 19.81-18.51 ($2CH_2$, C(16), C(20)).

5.6 Analysis of DSC Curves And TGA Thermograms

Thermal analyses of the compounds were studied by differential scanning calorimetry (DSC) and thermogravimetry (TGA).

No glass transitions and melting point were observed for PDI, NMI and NPM in the DSC runs up to 300 ^{o}C in nitrogen atmosphere (Fig.4.30-Fig.4.35).

TGA thermogram of PDI shows only a 16 % weight loss of the compound until 400 ^{o}C and 25 % weight loss until 450 ^{o}C in Fig.4.31. The starting decomposition temperature was 300 ^{o}C where all these prove the high thermal stability of the compound.

The weight loss starting temperature of NMI was 315 ^{o}C. Furthermore, the temperature of 37 % weight loss was 600 ^{o}C as shown in Fig.4.33.

Similarly, NPM has shown high thermal stability as shown in Fig.4.35. The weight loss starting temperature was 300 ^{o}C. The temperature of 20 % weight loss was 400 ^{o}C. Macromolecule is as thermally stable as the PDI and also it holds important potential for photonic technologies.

CHAPTER 6

CONCLUSION

The synthesis and characterization of a macromolecule that contains two naphthalene and one perylene chromophores is main objective in this project.

The results were:

(i) One naphthalene monoimide (NMI), perylene diimide (PDI) and macromolecule (NPM) were successfully synthesized. The synthesized products were characterized using the data from NMR, IR, MS, UV-vis, DSC, TGA and elemental analysis.

(ii) The optical, photophysical and thermochemical properties of the compounds were investigated in detail.

(ii) NMI showed highest solubility. On the other hand NPM showed higher solubility compared to PDI.

(iii) In polar aprotic solvents (DMF, DMSO), the bands related to naphthalene chromophore showed blue shift (370, 394 and 415 nm), however the bands related to perylene chromophore remained same (460, 491 and 526 nm).

(iv) The absorption maxima of PDI in different solvents are almost the same except in DMSO where a little red shift was observed.

(v) The absorption spectra measured for NMI in different solvents were broad indicating charge transfer complex.

(vi) The emission maxima of NPM in different solvents are almost same expect in DMSO.

(vii) The emission spectra measured for PDI were mirror images to their absorption spectra in various solvents however NMI showed structureless and broad excimer like emission.

(viii) The fluorescence quantum yields of NMI and NPM were low.

(ix) Macromolecule is as thermally stable as the PDI and also it holds important potential for photonic technologies.

REFERENCES:

Bodapati, J B (2005), Ms Thesis, Eastern Mediterranean University.

Burzynski, R and Prasad, P. N (1994), Vol. 1, No.4.

Christoph, Thalacher et al. (2005), Org. Biomol. Chem., 3, 414-422.

Danielle, L. Aubela, (2004), PhD Thesis, University of Pittsburgh.

Frank Würthner, (2004), The Royal Society of Chemistry, Chem. Commun., 1564–1579.

Frank Würthner, (2006), Pure Appl. Cem., Vol. 78, no. 12, pp. 2341-2349,

Frank Würthner, Volume Editor, Supramolecular Dye Chemistry; 258.

H. Langhals, (2005), Helvetica Chimica Acta Vol. 88.

Icil, H and Arslan, (2001), Spectrosc.Lett., 34(3), 355–363.

Icil, H and Icil S. (1996), Spectrosc.Lett., 29(7),1253-1257.

Icil, H et al. (2003), Photochem. Photobiol. Sci., 2, 218–223.

Icil, H Pasaogullari, N. and Martin Demuth, (2006), Dyes and Pigments 69, 118-127.

Icil, H Uzun, et al. (1998), Spectrosc.Lett., 31(3), 667–671.

J. C. Scaiano, (1989) (Ed.), Handbook of Organic Photochemistry, CRC Press.

J.K. Sugden, (2004), Biotechnic and Histochemistry, 79; 2, 71–90.

Lang,Ying Yang et al. (2008), Chinese Chem. Lett., 19, 1260–1263.

Liu Z, Rill R.L, (1996), Analytical Biochemistry, 236(0142), 136-145.

New J. Cem. (2003), 27:1277.

Nicholson, R. S and Shain I., (1964), Anal. Chem., 36, 706.

P. N. Theresa, (2000), PhD Thesis, Tulane University.

Pasaogullari N, (2005), PhD Thesis, Eastern Mediterranean University.

Posch, H E, Wolfbeis O S, (1998), Sensors and Actuators, Vol. 15, Issue 1,77–83.

Rodrigues, M A, Petri D.F. et al. (200) Rio de Janeiro-Brasil, v. 72, p. 75-78.

Ruland, G E, (1997), PhD Thesis, State University of New York.

Stephen David, (2007), PhD Thesis, Arizona State University.

Turro, N J, (1965), Molecular Photochemistry, Benjamin, London, 44.

Zollinger, H, (1991), Color Chemistry, 2_{nd} Revised (Ed.).